DESIGN AND OPTIMIZATION OF SINGLE-PARTICLE IMPACT DAMPER

MUHAMMAD AYAZ AKBAR

PhD

THE HONG KONG POLYTECHNIC UNIVERSITY

2024

The Hong Kong Polytechnic University

Department of Mechanical Engineering

Design and Optimization of Single-particle Impact Damper

Muhammad Ayaz Akbar

A thesis submitted in partial fulfilment of the requirements for the
degree of Doctor of Philosophy

October 2023

CERTIFICATE OF ORIGINALITY

I hereby declare that this thesis is my own work and that, to the best of my knowledge and belief, it reproduces no material previously published or written, nor material that has been accepted for the award of any other degree or diploma, except where due acknowledgement has been made in the text.

_____ (Signed)

 Muhammad Ayaz Akbar (Name of Student)

II

Abstract

Particle impact damper (PID) is a type of passive nonlinear vibration damper that offers easy installation, durability, and operation in harsh environments. They can be categorized as single-particle impact dampers (SPID) or multiple-particle impact dampers (MPID). SPID has a simpler design process and enhanced momentum transfer with the primary mass, while MPID exhibits complex nonlinear behaviour and generates more noise. Designing optimal PID is challenging due to nonlinear phenomena. MPID faces challenges in satisfying design parameters and suffers energy loss. SPID, on the other hand, has easier design parameters and simplified numerical modelling. Overall, PID shows promise in many vibration control applications.

In light of these considerations, it becomes essential to analyse and compare the performance of SPID and MPID. The study reveals that MPID exhibits more complex nonlinear behaviour, making it challenging to develop an optimal design approach. The higher number of particles generating impacts in MPID also results in increased noise during operation. Additionally, the unpredictability of particle positioning makes it difficult to satisfy design parameters. In contrast, SPID with its single-particle mass offers enhanced momentum transfer with the primary mass and simpler design and analysis processes. To further enhance the design of SPID, an optimal design methodology is established using a numerical approach. This research study focuses on ensuring both non-chaotic responses and optimal damping performance of the system. A range of design parameters is identified through extensive numerical simulations, and a statistical approach is employed to identify the optimal solution with the minimum vibration amplitude. The influence of internal friction is also analysed, revealing that higher friction degrades damping performance. Experimental validation is conducted to confirm the optimal design combinations obtained from numerical simulations.

Moreover, the impact force generated by the single-particle mass during impact raises concerns about potential risks to vulnerable structures or the induction of dangerous stresses over multiple impact cycles. To address this concern, an alternative design of the SPID is investigated, combining viscoelastic materials at the impact point between the particle and the primary mass. The study also compares the impact characteristics of soft and hard impacts on the damping performance of SPID. It is found that soft impacts contribute to slightly improved

III

damping performance by enhancing energy dissipation. The clearance magnitude of the SPID design is identified as a significant parameter that plays a crucial role in the design process.

Furthermore, a new hybrid damper design is proposed by combining the SPID with a friction damper (FD). Previous findings indicate that SPID alone cannot achieve vibration suppression comparable to the conventional tuned mass damper (TMD), while FD is ineffective at resonance but can generate significant damping forces. A mathematical model is developed for the hybrid damper, and optimal combinations of SPID and FD are estimated. The predicted results are validated through experimental tests on a prototype. A parametric analysis of the proposed hybrid damper demonstrates its ability to reduce the maximum vibration amplitude of a single-degree-of-freedom (SDOF) primary structure. The hybrid damper exhibits effectiveness over a wide range of excitation frequencies and achieves comparable vibration suppression performance to a TMD with a similar mass ratio. Unlike the TMD, the hybrid damper does not require optimally tuned natural frequency and damping, eliminating the detuning problem associated with TMD. Numerical simulations using random earthquake excitation data further confirm the performance of the hybrid damper as a passive vibration control solution.

In summary, this research has focused on a single-particle impact damper (SPID) and has provided practical design strategies to optimize its damping performance. The study emphasizes the advantages of SPID, including its simplicity, ease of installation, and effectiveness over a wide frequency range. The findings of this research contribute valuable insights and open up new possibilities for the practical application of SPID in the field of structural vibration control.

List of Publications

Journal Papers:

- **Muhammad Ayaz AKBAR**, Waion Wong, Emiliano Rustighi, (2024) "Design optimization of a single-mass impact damper", Journal *of Sound and Vibration*, 570 118019. **(Published)**

- **Muhammad Ayaz AKBAR**, Waion Wong, Emiliano Rustighi, (2023) "A hybrid damper with tunable particle impact damping and Coulomb friction", *Machines*, 11, 545. **(Published)**

- **Muhammad Ayaz AKBAR**, Waion Wong, "Single-particle impact damper with soft impact design." *Mechanical Systems and Signal Processing*. **(Under Review)**

Conference Papers:

- **Muhammad Ayaz AKBAR**, Waion Wong. (2023). A Hybrid Damper with Particle Impact Damper and Coulomb Friction Designed for Free Vibration Damping. *Experimental Vibration Analysis for Civil Engineering Structures. EVACES 2023*. Lecture Notes in Civil Engineering, vol 432. Springer, Cham.

- **Muhammad Ayaz AKBAR**, Waion Wong, (2021). "A Pendulum Type Particle Impact Damper," Jing X., Ding H., Wang J.(eds) *Advances in Applied Nonlinear Dynamics, Vibration and Control -2021. ICANDVC 2021*. Lecture Notes in Electrical Engineering, vol 799. Springer, Singapore

Acknowledgement

Table of Contents

List of Figures

List of Tables

List of Symbols and Abbreviations

Symbols

$\ddot{x}$	Acceleration of primary structure; m/s^2
$\ddot{y}$	Acceleration of particles; m/s^2
Z	Amplitude of support motion; m
d	Clearance; m
e	Coefficient of restitution;
c	Damping coefficient; Ns/m
z	Displacement of support; m
y	Displacement of particle; m
x	Displacement of primary structure; m
F(t)	Excitation force; N
x_0	Initial position of primary structure; m
y_0	Initial position of particle; m
$\dot{x}_0$	Initial velocity of primary structure; m/s
$\dot{y}_0$	Initial velocity of particle; m/s
M	Mass of primary structure; kg
m	Mass of primary structure; kg
k	Spring constant; N/m
E_s	Storage modulus; MPa
E_l	Loss modulus; MPa
E_c	Complex modulus; MPa
η	Loss factor
ν	Shape factor; 1/m
$\dot{z}$	Velocity of support; m/s
$\dot{y}$	Velocity of particle; m/s
$\dot{x}$	Velocity of primary structure; m/s
$\dot{y}_n^+$	Velocity of particle after n^{th} impact; m/s
$\dot{y}_n^-$	Velocity of particle before n^{th} impact; m/s

$\dot{x}_n^+$ Velocity of primary structure after n^{th} impact; m/s

$\dot{x}_n^-$ Velocity of primary structure before n^{th} impact; m/s

Greek Symbols

μ_e Coefficient of friction (External friction);

μ_i Coefficient of friction (Internal Friction friction);

ω Frequency of excitation force; rad/s

γ_F Friction force ratio related to harmonic excitations;

γ_g Friction force ratio related to ground disturbance;

ω_n Natural frequency of primary structure; rad/s

β Mass ratio; m/M

ζ Damping ratio

Abbreviations

PID   Particle impact damper

SPID   Single-particle impact damper

MPID   Multi-particle impact damper

FFT   Fast Fourier transform

MDOF   Multi degree of freedom

TMD   Tuned mass damper

RMS   Root Mean Square.

COR   Coefficient of Restitution

SDOF   Single degree of freedom

FD   Friction damper

Chapter 1

Introduction

1.1. Motivation

Vibrations play a crucial role in structures, machines, and processes. However, they often cannot be prevented, especially in scenarios like wind-excited structures or vehicles travelling on rough roads. These unwanted vibrations can result in increased noise, decreased comfort, and potential structural failure. Additionally, there is a growing interest in lightweight designs to conserve energy and natural resources. However, lightweight structures are more prone to vibrations. Consequently, the development of structural vibration control methods has become essential in engineering applications to ensure optimal performance and safety. Indeed, over the past few decades, significant efforts have been made to explore various structural vibration control approaches aimed at enhancing the vibration attenuation of several types of structures. These control approaches seek to minimize the effects of vibrations, such as structural damage, discomfort, and reduced functionality. The concept of resonance is critical in the study of structural vibration control. The structure is excited by a continuous external force with an excitation frequency (ω). Resonance occurs when the frequency of the excitation force (ω) is closer to the natural frequency of the vibrating structure (ω_n) in many systems. The actual resonance frequency might change when damping is higher. At resonance, the displacement of the structure increases after each cycle and reaches its highest value. Hence, resonance imposes the highest strains and stresses on the structure due to the maximum displacement of structural elements. Usually, vibration control technologies are employed to mitigate the vibration energy of the structure at resonance.

Several techniques have been investigated in structural vibration control, including passive, active, and semi-active control methods. Passive control strategies involve the use of passive devices, such as tuned mass dampers (TMDs), viscoelastic materials, and particle impact damper, to absorb or dissipate vibration energy. Active control methods, on the other hand, employ sensors, actuators, and control algorithms to actively counteract the vibrations in real-time. Semi-active control techniques combine elements of both passive and active control, providing a balance between effectiveness and energy consumption. The goal of these control

approaches is to achieve improved vibration attenuation, reduce dynamic responses, mitigate resonance effects, and enhance overall structural performance. By implementing these control strategies, structures can exhibit increased resistance to dynamic loads, improved occupant comfort, enhanced functionality, and extended service life.

Ongoing research and development continue to focus on advancing structural control approaches, exploring new materials, optimizing control algorithms, and integrating smart technologies. The aim is to further enhance the effectiveness, efficiency, and applicability of structural control methods for a wide range of structures, including buildings, bridges, offshore platforms, and aerospace systems. Vibration control encompasses both active and passive technologies. Active control offers precision but requires external power, controllers, and sensors, making it expensive and unreliable during power outages or natural disasters. On the other hand, passive vibration control has gained importance as it operates without active power supply or control circuits. It utilizes the vibration energy of the primary structure.

Due to the various benefits mentioned, passive vibration control systems are widely utilized in structural vibration control applications (Casciati & Faravelli, 2009; Djemal et al., 2019; Jaisee et al., 2021; Mead & Mead, 1999; Salvi et al., 2018; Titirla, 2023). Passive vibration absorbers can be further grouped into friction dampers, viscous dampers, viscoelastic dampers, particle impact dampers, tuned mass dampers, tuned liquid dampers, etc. Particle impact dampers also referred to as single-particle impact dampers, granular dampers, and impact mass dampers are passive vibration dampers. Particle impact dampers are easy to make and install; a cavity made in the primary structure, or a container attached to the primary structure is filled with different particles. The particles are usually made of metallic materials. When the primary structure vibrates, momentum is transferred to the particles and the energy dissipation occurs due to impacts and frictional effects. The entire process leads to the reduction of structural vibration.

Particle impact dampers show numerous advantages over other passive absorbers because of their simple concept and easy design and installation process. They are cost-effective devices and degradation over time is less likely (Butt, 1995). This makes them an alternate choice where high durability is required or where permanent maintenance is not or hardly feasible. Particle impact dampers can even operate in extreme conditions (Johnson & Simonian, 1995; Lu et al., 2017; Panossian, 2002) including extreme temperatures like in space

applications (Moore et al., 1995; Panossian, 1992), and extreme pressures (Bannerman et al., 2011; Sack et al., 2013) using appropriate materials for particles, e.g. steel, and tungsten. It has been reported also that particle impact dampers are less sensitive to the direction of the excitation (Wang & Wu, 2015) and can work in multiple directions (Michon et al., 2013). In addition, particle impact damper adds little mass to the primary structure causing no significant changes (Saeki, 2002).

Besides all these advantages and the potential of particle impact damper, the development is still in early stages due to the complex nonlinear phenomena associated with them. The lack of analytical methods leads to no optimal design methods available for other passive vibration absorbers such as TMD. Most of the literature available is based on trial and error or specific to one application studied. Therefore, this study aims to study the performance of particle impact dampers in structural vibration control applications. Furthermore, this work will focus on finding a general method to formulate an optimum design strategy for a single-particle impact damper.

1.2. Literature Review

The first-ever study on particle impact damper can be traced back to (Paget, 1937). Paget observed that an unrestrained mass on a shaking structure can be utilized for vibration suppression and a single-particle impact damper was proposed to be employed in a turbine blade. Such a damper was classified as an impact damper and later particle impact damper became a derivative of impact damper. Afterwards, (Lieber & Jensen, 1945) investigated a single-particle impact damper where a single mass is moving between the walls of a container to suppress the structural vibrations. In the following years, impact damper has been investigated due to their simplicity and robust properties against various severe environmental conditions (Grubin, 1956; Masri & Caughey, 1966; Sami Faiz, 1965). Afterwards, (Masri, 1969) introduced the multi-unit impact damper. Masri replaced the single unit with multiple units of single particle impact damper operating in parallel. He reported that the overall performance of the multi-unit single-particle impact damper stays unaffected, however, lower impact forces can be achieved due to the distributed mass of the single-particle. Since the introduction of impact dampers, various designs have been studied. These designs can be grouped into single-unit single-particle impact damper (SPID), multi-unit single-particle

impact damper, single-unit impact damper, and multi-unit impact damper as shown in Figure 1-1 (Lu et al., 2018). Each design or configuration has its specific advantages and properties. Initially, these designs of particle impact dampers had been studied without an underlying structure. The researchers directly used a shaking force on the container of particles and measured the response of the container with different configurations (single-particle, multi-particles, single-unit, multi-unit) and no real change in performance was reported (Araki et al., 1986; Masri, 1969, 1970; Paget, 1937).
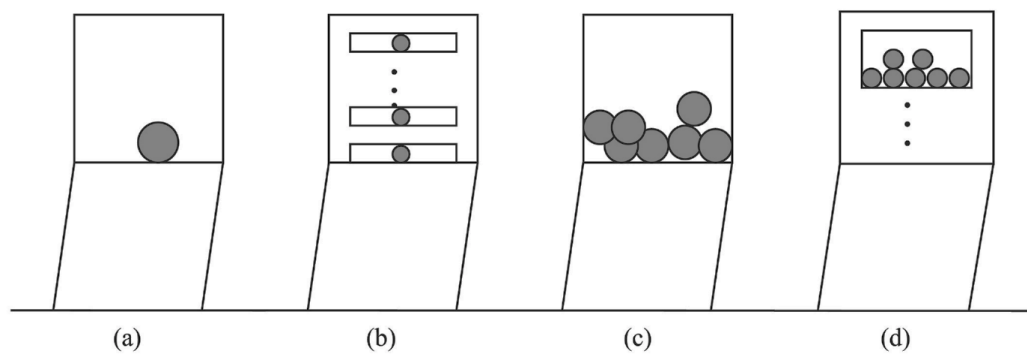
Figure 1-1 Schematic diagrams of (a) single-particle impact damper; (b) multi-unit single-particle impact damper; (c) multi-particle impact damper; (d) multi-unit multi-particle impact damper.

These types of particle impact damper become essential when they are attached to a structure and the aim is to optimize the damping performance. The particle impact damper can be attached to a structure and the structure can be excited to study free or forced vibrations. The damping is measured and the performance of the particle impact damper with different settings can be analysed. This type of analysis is often performed experimentally due to the complexity of the whole system with nonlinearity involved due to various factors (Butt & Akl, 1997; Ekwaro-Osire & Desen, 2001, 2016; IHSAN, 2000; Papalou & Masri, 1998; Wouw et al., 1998; Xu et al., 2004). On the other hand, numerical studies are also possible and can be found in the literature (Du & Wang, 2010; Friend & Kinra, 2000; Wang et al., 2017; Wang et al., 2016; Wouw et al., 1998). Numerical studies are usually coupled with experimental validations due to complex nonlinear phenomena involved in the practical operation of particle impact damper leading to various assumptions in the numerical analysis. The finite element method (FEM) and model order reduction techniques age generally used to model the response of the underlying structure. In contrast, the response of the particle impact damper itself is modelled with DEM models (Sánchez & Pugnaloni, 2011) or simplified single-particle models

(Chehaibi et al., 2019; Duncan et al., 2005; He et al., 2021; Marhadi & Kinra, 2005; Younes, 2017). Theoretically, it becomes even more complicated to study the motion of multiple particles in a container due to increased complex nonlinearities. Therefore, most of the available numerical studies assume the multiple particles as one single mass for simplicity of the investigation. On the other hand, it is nearly impossible to study several combinations of particle impact damper designs experimentally to find out the optimal design.

Unfortunately, numerical and experimental studies on particle impact damper on an underlying structure can be time-consuming. Therefore, the studies are focused on rather simplified models of experimental setups, such as single-degree-of-freedom structures. (Fang & Tang, 2006; Fang et al., 2007) studied the performance of a single-degree-of-freedom system with particle impact damper numerically. They exited the structure with a harmonic force and analysed the response of the structure. They obtained the frequency response function (FRF). Similarly, few other studies (Sánchez et al., 2014; Sánchez & Manuel Carlevaro, 2013; Sánchez & Pugnaloni, 2011; Sánchez et al., 2012) on numerical analysis of an SDOF structure with particle impact damper by applying a harmonic force can be found. For simplicity, beam-like structures are studied as well under free and forced vibration conditions. An early study for vertical free vibrations was presented by (Friend & Kinra, 2000) and (Hollkamp & Gordon, 1998) presented an experimental study for horizontal forced vibrations. Few combined numerical and experimental studies were presented by (Mao et al., 2004; Yang et al., 2005). They studied a particle impact damper only without an underlying structure. (Bannerman et al., 2011) studied the damping performance of a particle impact damper to suppress the free vibrations of a beam-like structure in zero gravity effect. They observed a collect and collide (bouncing) motion of particles where multiple particles move one single particle block and collide with the container walls. (Sack et al., 2013) further provided a detailed analysis of this mode.

Besides simplified single-degree-of-freedom structures, various studies analysed the performance of particle impact dampers in practical applications.(Chen & Georgakis, 2013) studied a tuned rolling ball damper for low-frequency vibrations in wind turbines. The performance of particle impact dampers has also been tested in structural vibration control of high-rise buildings. (Lu et al., 2012) used real earthquake data and applied it to a 6m three-story model with a particle impact damper. They concluded that a reasonable vibration

reduction can be achieved with an intelligently designed particle impact damper with a small mass ratio. They identified that the single-particle impact damper can provide larger damping but produces significantly larger impulse force to the primary structure causing larger noise and damage compared with the multi-particle impact damper. In addition, a single-particle impact damper might be more sensitive to the change in the system's parameters. (Papalou et al., 2015) investigated the performance of a single-particle impact damper to protect vulnerable monuments in seismic excitation. They used a single column in experiments and installed multi-unit single-particle impact dampers at different positions. It was concluded that a particle impact damper can be a good choice for seismic protection of old structures due to its simpler installation procedure and significant vibration suppression performance.

The researchers have identified a few important parameters for designing a particle impact damper(Meyer & Seifried, 2021). As the working principle of particle impact damper is based on momentum transfer and energy dissipation through frictional effects and material deformation during inelastic impacts, it is important to understand the parameters involved in these phenomena for achieving optimal design strategy. (Masri, 1970) investigated the general motion of particle impact damper numerically, and it was observed that the maximum vibration suppression occurs when the particle has two impacts per cycle with the container walls. Later, (Masri, 1973) formulated an analytical solution for the steady-state response of multi-degree structure based on the assumptions that two collisions per cycle and vibrations are steady-state. Afterwards, (Marhadi & Kinra, 2005) showed that two collisions every cycle are possible for certain combinations of design parameters and it might not be the optimal performance. (Li & Darby, 2006) analysed the role of design parameters on the performance of single-particle impact damper. They observed that the mass ratio is incredibly important for momentum transfer, however, a higher mass ratio does not lead to better vibration reduction for frequencies other than the first natural frequency. They also identified that the particle impact damper may worsen the response of structure for certain parameters. Furthermore, they concluded that the clearance length is the most influential parameter in particle impact damper design and it can affect the motion of particles significantly leading to affecting all phenomena providing damping (momentum transfer, energy dissipation, and frictional effects). (Lu et al., 2011) presented a parametric study of particle impact damper under harmonic excitation. It was observed that the particle type and size have a minor effect on the capability of impact damping, mass ratio can increase the damping but up to a certain limit, a higher coefficient of restitution

leads to considerable damping over a wider range of excitation levels, the friction between particle and primary system is generally not recommended. Few other studies on the design parameters of particle impact damper have provided similar conclusions as the clearance magnitude is very important in the designing process of particle impact damper (Lu et al., 2010; Snoun & Trigui, 2018; Wong et al., 2009).

Following the literature review of the design parameters of particle impact damper, it can be concluded that the mass ratio and clearance are particularly important. Besides these two parameters, other important parameters are friction and parameters affecting impact. It is obvious that the impact is the fundamental phenomenon in particle impact damper performance. Therefore, it is necessary to understand the parameters affecting the impact. The impact is an extremely complicated phenomenon with nonlinear characteristics, and it becomes even more challenging to develop numerical models of particle impact damper. In most of the numerical models, the impact is considered with the coefficient of restitution between two colliding bodies. The coefficient of restitution is a ratio of relative velocities before and after between two colliding bodies. It determines the velocity of masses after each impact and physically represents the energy dissipated during an impact in the form of material deformation, sound, and heat (Bapat & Sankar, 1985; Friend & Kinra, 2000). However, such an approach considers that the impact is robust, and the contact time is negligible which might not be true for soft impacts. On the other hand, some researchers used impact force models to determine the collision force on both bodies (Chehaibi et al., 2019; Wang & Dan, 2022). These models accommodate the contact time, material deformations and viscoelastic effects in material deformation.

Friction is another parameter of concern, as it provides damping force during particle motion. There are contradicting opinions found in the literature regarding the presence of friction between particle motion. Each impact transfers momentum between the primary structure and particles, and the particles dissipate some energy from the primary structure due to friction between the particles and the primary structure (Wei-ming et al., 2019). However, the presence of friction leads to reduced velocity of particles before impacts. It has been reported that the vibration suppression with particle impact damper depends on the number of heads-on impacts (face-to-face collision) rather than the total number of impacts (Marhadi & Kinra, 2005). Therefore, maximum momentum transfer occurs when particles and the primary

structure are moving towards each other with maximum velocities, but the presence of friction may reduce the velocity of particles. Hence, higher damping with friction may lead to reduced damping with impact and vice versa. (Huang et al., 2021) studied the effect of rolling friction on the damping performance of particle impact damper. They studied the effect of rolling friction during the non-collision phase of particle motion. They observed that increasing the rolling friction reduces the relative motion of particles to the primary structure, hence, reducing the number of impacts. However, the presence of friction may provide a small amount of damping due to relative motion, but the amount of damping is not significant. They found that there is no damping due to friction once the magnitude of friction is larger than a certain limit where the particle stops moving at all.

Another type of passive vibration absorber is a friction damper. A friction damper is a nonlinear damper which provides damping through sliding of two bodies against each other and dissipating the energy through heat (López et al., 2004). Hence, wear and tear of material and nonlinear motion due to stick-slip conditions are associated with using a friction damper (Feeny, 1992; Leine et al., 1998). The applications of friction damper in structural vibration control are limited due to its ineffectiveness at resonance. However, friction dampers are capable of producing large damping forces with smaller sizes. Furthermore, friction dampers are combined with other damping technologies to make them effective at suppressing resonant vibration amplitude. (Lee et al., 2005) proposed a tuneable friction damper by combining it with a traditional vibration absorber. The aim was to make use of the large damping force provided by friction dampers and traditional vibration absorbers can provide good damping at resonance. It was observed that the combined damper works well over a narrow frequency range, and it was possible to reduce the two peaks seen in traditional vibration absorbers with friction effects. A similar study with a similar conclusion was performed by (Sinha & Trikutam, 2018). (Marino et al., 2019) analysed the displacement transmissibility of friction damper under joint base-wall motion. It was concluded that the friction damper alone is ineffective at resonance frequency when the friction force is within the boundary limit under harmonic excitations. (Sun et al., 2022) combined a friction damper with an electromagnetic shunt damper to effectively reduce the resonance vibration amplitude of a single-degree-of-freedom structure.

It can be concluded from the literature that particle impact damper has a huge potential due to the simple concept and installation process. However, nonlinear behaviour and complex relationships of design parameters lead to a lack of optimal design strategies. In order to successfully use particle impact damper in practical applications, there is room for more investigations and finding answers to the various existing questions. Therefore, this work aims to find a design methodology for a particle impact damper and provide a basis for the engineers to design an effective particle impact damper. Considering the potential of particle impact dampers, they can become an alternative cost-efficient choice for structural vibration control.

1.3. Aim and objectives.

The literature summarises that particle impact dampers have considerable potential in vibration control applications for structures and machinery. Particle impact dampers possess various advantages over other vibration control technologies. Although particle impact damper shows enormous potential in vibration control strategies and provides a highly effective and affordable solution, there are many design processes and analysis challenges due to highly nonlinear phenomena. There are various contradicting opinions found in the literature. In this study, a single-particle impact damper is considered due to various advantages and simplicity explained in the next chapter. This study aims to fill the existing gaps in the literature and enhance the understanding of single-particle impact dampers in vibration control applications. The principal objectives of this work are listed below,

- To establish a fundamental understanding of single-particle impact dampers (SPID) and compare them with multi-particle impact dampers (MPID). The aim is to assess their respective advantages and disadvantages to gain insights into their damping performance.

- To formulate a design methodology for single-particle impact damper design, considering various design parameters comprehensively. This general design method will address both free and forced vibrations, utilizing a numerical approach. The results will be validated through experimental testing on a single-degree-of-freedom structure. The objective is to consider the interrelationships between design parameters, as their effectiveness is interconnected.

- To investigate a novel approach to designing a single-particle impact damper with soft impact in order to mitigate the potential harm caused by large impact forces on the structural integrity. The proposed design involves installing viscoelastic materials to the container walls to achieve soft impact for enhanced energy dissipation during each impact and reduce noise. A numerical model will be developed and validated through experimental analysis.

- To explore the limitations of particle impact damper in achieving similar performance to benchmark passive vibration control systems, such as tuned mass dampers (TMDs), particularly in forced vibrations. To enhance the overall performance of a single-particle impact damper, a hybrid damper combining a single-particle impact damper and a friction damper will be proposed and analysed. A numerical model will be developed, and the results will be validated through experimental investigations.

1.4. Organization of dissertation

This dissertation is composed of six chapters. The chapters are organized as follows,

Chapter 1 provides a basic introduction, literature review, motivations, and objectives of this study.

Chapter 2 presents a brief comparison of single-particle impact dampers and multi-particle impact dampers with small experiments. It provides the advantages and disadvantages of both types and why a single-particle impact damper is chosen for this study.

Chapter 3 presents an optimal design methodology for a single-particle impact damper with a numerical model and experimental validations.

Chapter 4 shows the effects of soft and hard impacts on the performance of single-particle impact dampers with viscoelastic materials. A numerical model with experimental validations is provided.

Chapter 5 presents a hybrid damper combining a friction damper and a single-particle impact damper with a numerical model and experimental validations.

Chapter 6 provides the conclusions from this research and proposes future possible works based on this work.

Chapter 2

Why a single-particle impact damper?

Opinions regarding the efficiency of single and multi-particle impact dampers in vibration control applications have been subject to debate among researchers. While some researchers argue in favour of the simplicity and cost-effectiveness of single-particle impact dampers, others advocate for the enhanced damping capabilities offered by multi-particle impact dampers. Besides the contradicting opinions in the literature, the benefits of single-particle impact damper are summarized as follows,

1. Single-particle impact dampers are simple in terms of the design and manufacture processes, installation and theoretical modelling compared with multi-particle impact dampers. Most of the numerical studies in the literature use the equivalent single-particle model while studying multi-particle impact dampers.

2. The design process for a single-particle impact damper becomes simpler due to only one mass and manufacturing a damper with a specific design parameter (clearance magnitude) is easier compared with a multi-particle impact damper. The clearance length becomes inconsistent in multi-particle impact damper due to the random positioning and motion of multiple particles.

3. The momentum transfer between primary structure and particle is higher for a single-particle impact damper due to one large mass compared with a multi-particle impact damper.

4. The noise during the operation of a single-particle impact damper is less compared with a multi-particle impact damper. The noise in a single-particle impact damper is produced when the particle mass impacts the walls of the container. On the other hand, an MPID produces continuous noise due to particle-particle collisions beside particle-wall collisions.

Further, the mentioned advantages of a single-particle impact damper over a multi-particle impact damper from the literature, and the drawbacks of using a single-particle impact damper over a multi-particle impact damper are summarized as follows,

1. A single-particle impact damper produces a large impact force compared with a multi-particle impact damper when a particle-wall collision occurs. This high-intensity impact induces high stresses to the primary structure, which can be dangerous for some vulnerable structures. Besides the induced stresses, the high-intensity impact generates a higher level of noise as well.

2. A single-particle impact damper may not provide significant damping over a wide range of excitation frequencies due to only one particle mass compared with a multi-particle impact damper. The primary structure is required to reach a certain level of vibration amplitude for a single particle to generate considerable impacts with the wall of the container for damping, while multi-particle impact dampers have numerous particle-particle impacts even at lower vibration amplitudes of primary structure to provide a small amount of damping through friction. Therefore, a multi-particle impact damper may provide damping over a wide range of frequencies.

The aforementioned advantages and disadvantages of single-particle impact damper are extracted from a few studies in the literature (Gagnon et al., 2019; Lu et al., 2018).
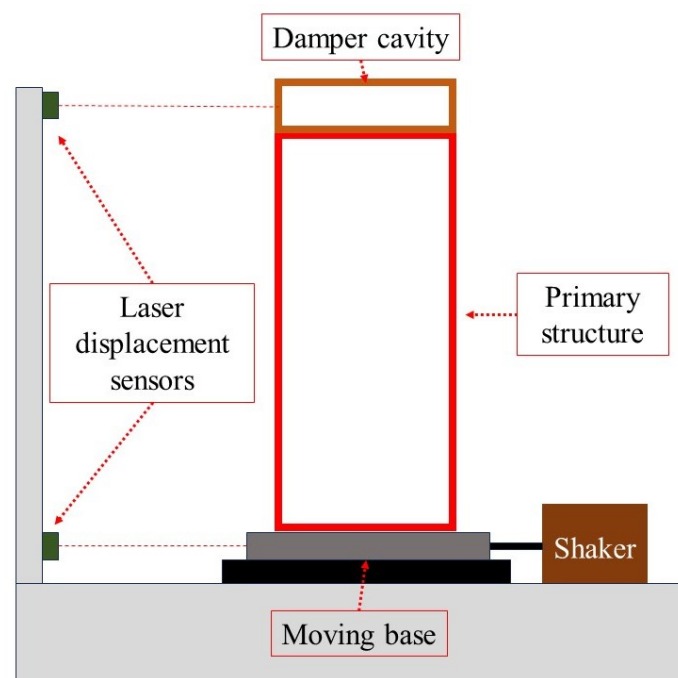
Figure 2-1. Sketch of experimental setup

In order to verify the advantages and disadvantages of single and multi-particle impact dampers, a simple experiment is designed. The experimental setup includes a single-degree-of-freedom structure fixed on a base connected to a shaker. The single-degree-of-freedom structure consists of two steel bars acting as leaf springs and an aluminium mass fixed on the top as shown in Figure 2-1.

Furthermore, there are two laser displacement sensors installed to record the displacement of the base and primary structure, respectively. On the top of the primary structure, a particle impact damper can be installed. There are two different types of particle impact dampers prepared to compare the performance of single-particle impact dampers and multi-particle impact dampers. The mass of the particle in both cases is kept similar for direct comparison. The other design parameters such as clearance magnitude are also kept similar for both types of dampers. The prototype of the single and multi-particle impact damper is presented in Figure 2-2.

(a)   (b)
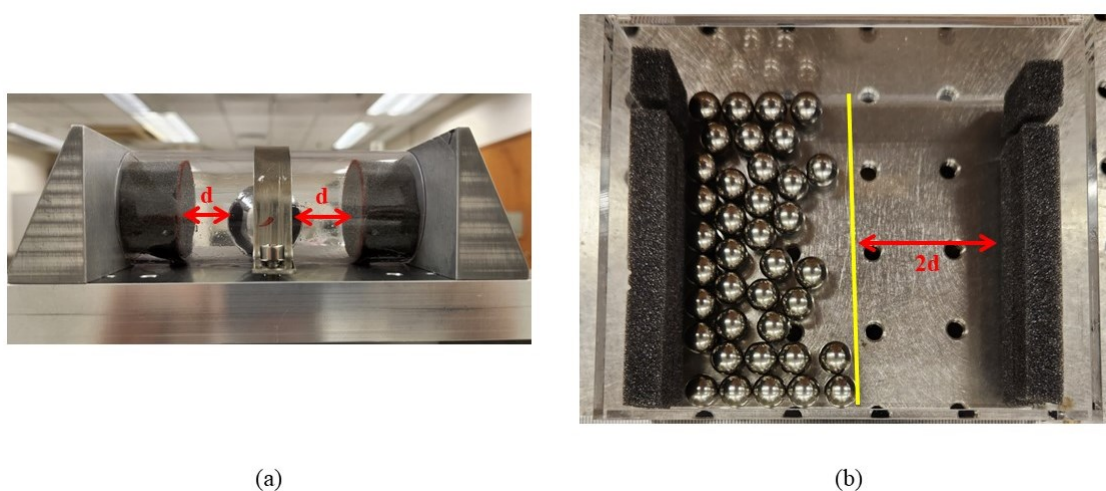
Figure 2-2. Prototypes of particle impact damper in experiments; (a) Single-particle impact damper (SPID); (b) multi-particle impact damper (MPID)

It can be observed that the selecting clearance length becomes simpler in SPID due to only one particle, while it can be challenging for MPID. Additionally, the clearance length might not stay constant during the operation for MPID. Furthermore, noise is a huge problem associated with particle impact dampers and it is claimed that the SPID produced a higher noise level than MPID. Therefore, a simple experiment as described earlier is designed. A sinusoidal ground motion is applied to the structure with a frequency range between 2 Hz to 3.5 Hz. The

magnitude of the wave is controlled by an input voltage; however, the exact input voltage might not replicate the similar base displacement as there are other equipment such as amplifier and control are involved as well. Therefore, a displacement sensor recording the base motion provides the input base motion to the primary structure which reflects a maximum amplitude of around 3 mm. The displacement response is recorded for the top of the primary structure and base. In addition, the entire procedure is recorded with a high-speed camera. The sound from the video is then analysed through MATLAB software to understand the noise level during the operation of SPID and MPID. A single-particle impact damper with hard impact is considered initially to understand the noise levels while the MPID with small steel particles with a diameter of 4mm are used. The mass ratio between the particle and primary structure is kept at 10% for both cases. Understandingly, the mass ratio is one of the important design parameters in this case; however, it is usually limited due to various constraints such as design and limited additional mass requirements. Therefore, a 10 % mass ratio is used throughout in this study to compare the other design parameter only. The mass ratio in MPID case depends on the number of particles.
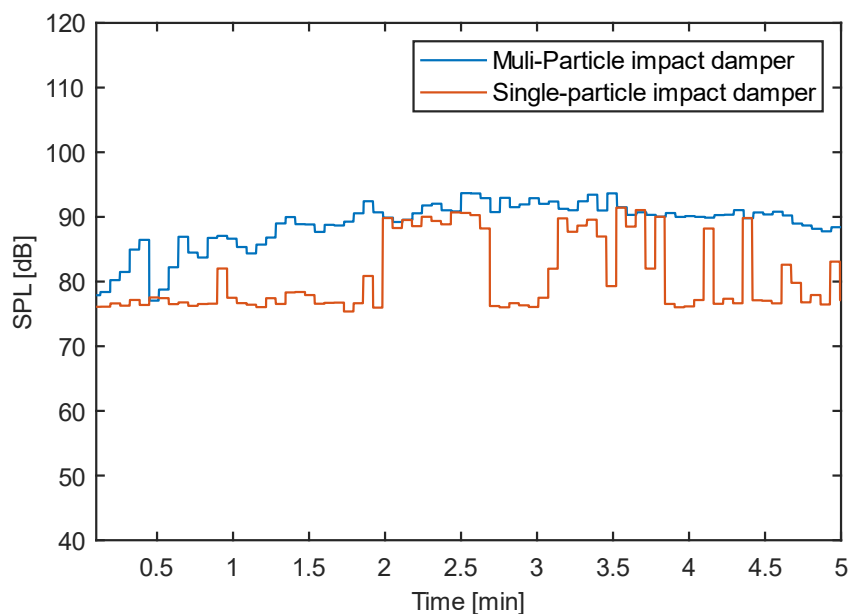
Figure 2-3. Sound pressure level (SPL) comparison of MPID and SPID.

Sound pressure level (SPL) can be calculated directly from the audio data in MATLAB. The SPL for both types of particle impact damper is compared and presented in Figure 2-3. In the case of SPID, the number of impacts increases when the excitation frequency is around

resonance due to the larger motion of the primary structure. Therefore, a higher noise level is expected around the resonance frequency. On the other hand, there are consistent particle-particle collisions with MPID even at a smaller amplitude of the primary structure while vibrating. The comparison shows that the SPID produces a higher noise level when there are a large number of impacts which can be observed from the occurring peaks throughout the SPID curve in Figure 2-3. On the other hand, the MPID curve shows that there is consistent noise due to consistent impacts between particles.
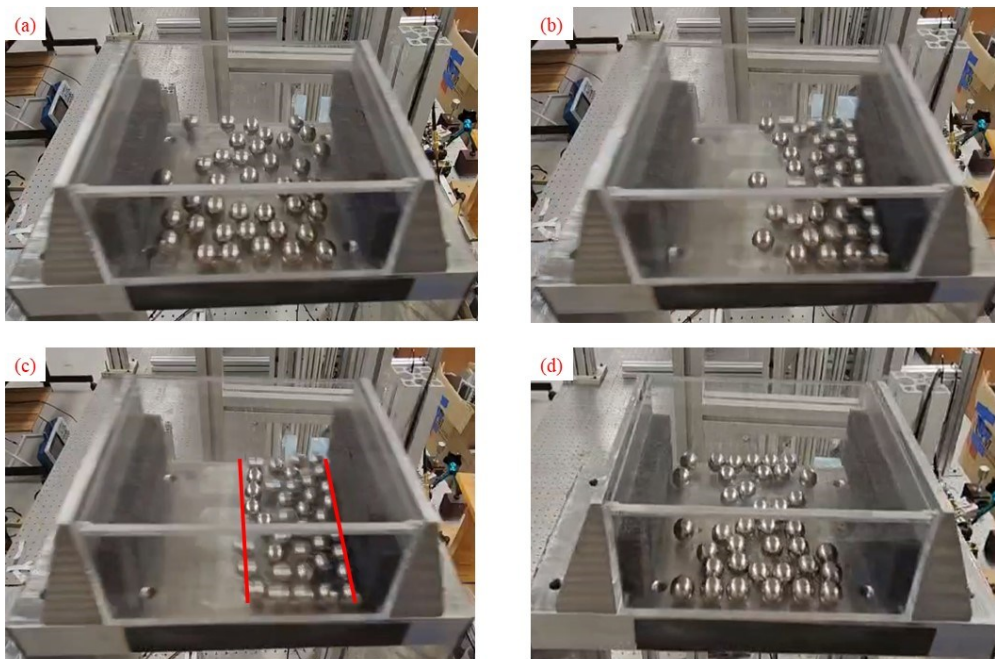
Figure 2-4. Movement of particles at different stages of excitation frequency; (a) before resonance; (b) closer to resonance; (c) resonance; (d) after resonance

Besides the noise extracted from the videos, an interesting phenomenon regarding the operation of the multi-particle impact damper is observed as well. Different motion phases are presented in Figure 2-4. The particles are scattered at the beginning when the excitation frequency is far below the resonance frequency of the primary structure as in Figure 2-4a. The movement of particles is very small at this phase. As the excitation frequency is close to the resonance frequency of the primary structure, the particle moves collectively as shown in Figure 2-4b. This phenomenon is evident when the excitation frequency reaches the resonance frequency of the primary structure, as presented in Figure 2-4c. Here, it can be observed clearly that the multiple particles are moving together and generate impacts with the boundary.

However, a scattered motion of particles can be seen again when the excitation frequency is larger than the resonance frequency of the primary structure (Figure 2-4d). The scattered motion of particles in the phases when the excitation frequency is smaller or larger than the resonance frequency of the primary structure occurs due to the lower amplitude of the primary structure. There is not enough energy for particles. However, this scattered motion results in few particles impacting the walls of the container resulting in a small amount of momentum transfer or with primary structure. This results in a smaller amount of damping to the primary structure over a wide range of excitation frequencies. This outcome depends on various parameters and the conclusion might be different by changing the design parameters in this case such as number of particles, clearance magnitude or different masses. It concludes that a general design methodology for MPID might be extremly challenging to define as there are several phenomena and parameters involved.
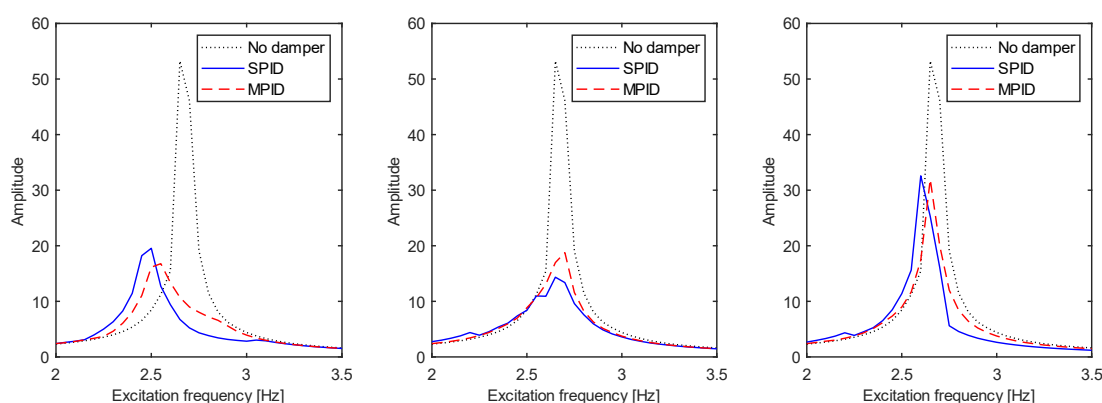
Figure 2-5. Comparison of relative vibration amplitude with SPID and MPID over different cavity lengths; (a) 5 mm; (b) 30 mm; (c) 60 mm

Lastly, the damping performance of both types of particle impact damper is compared. The cavity length has been identified as the most important parameter in PID design. The experimental setup is capable of tuning cavity length by changing the wall distance to any predrilled holes on the top surface. The relative response, which is the ratio of the displacement recorded at the top to the displacement of the base is determined for a few different cavity lengths. The relative amplitude of the primary structure with SPID and MPID is compared in Figure 2-5. The results show that SPID reduces the vibration amplitude of the primary structure by around 24% compared with MPID at a clearance magnitude of 30mm. The benefits of using any of these dampers should solely depend on the nature of the application, available resources,

and ease of specific design. Such direct comparison of SPID and MPID cannot be found in literature.

2.1. Summary

A brief experimental study is conducted for a basic understanding of challenges associated with single-particle impact dampers and multi-particle impact dampers. The results and observations can be summarized as follows,

1. Single-particle impact damper produces a large impact force when colliding with the primary structure and such continuous force can be a question regarding the integrity of the structure using SPID. However, it is possible to find solutions to minimize the transmitted impact force.

2. The presence of various small particles and their random motion during the damping process leads to inconsistent cavity length and it does not remain constant as selected in the designing process. Therefore, the designing process for a multi-particle impact damper can be complicated.

3. Excessive noise is indeed a challenging issue when it comes to particle impact dampers. The noise generated during the impact of a single particle impact damper (SPID) on the wall of the cavity can be mitigated by incorporating noise-absorbing materials at the point of impact. These materials can help absorb and dissipate the energy from the impact, reducing the noise produced. However, when it comes to multi-particle impact damper (MPID), the noise generated from particle-particle collisions poses a significant challenge. Metallic particles are often preferred in MPID because of their larger mass, which helps satisfy the mass ratio requirements for effective damping. The larger the mass ratio, the more efficient the damper tends to be.

4. In contrast, polymer particles have less mass compared to metallic particles. Using the same number of polymer particles may not meet the mass requirements necessary for effective damping. Achieving the desired mass ratio with polymer particles might necessitate a considerably larger number of particles and a correspondingly larger

cavity. This can result in practical challenges such as increased complexity, cost, and space requirements.

5. A phenomenon is observed during the operation of MPID in which the various particles move collectively when the excitation frequency is closer to the resonance frequency of the primary structure. On the other hand, the motion of particles is scattered when the excitation frequency is far from the resonance frequency.

6. Regarding the numerical method for developing an optimum design process for a particle impact damper, it can be incredibly challenging to develop a theoretical model for a multi-particle impact damper considering all nonlinear complexities as random movement, and particle-particle collisions.

7. Finally, the results of brief experiments showed that a single-particle impact damper can reduce vibration amplitude by 24% compared with a multi-particle impact damper.

It can be concluded that the momentum exchange is the fundamental phenomenon in particle impact damper for suppressing vibrations. The momentum exchange is less intense in MPID than in SPID due to the loss of some energy during particle-to-particle interactions. Furthermore, it is very unlikely that all the particles will collide with the walls of the container at each impact leading to smaller momentum transfer due to smaller mass. Hence, a single-particle impact damper produces a higher damping rate due to one significant mass. Therefore, a single-particle impact damper can be easier to formulate design methodology, theoretical approach, and installation. Concluding all these observations, a single-particle impact damper is further studied in this work.

Chapter 3
Design and optimization of a single-particle impact damper

In recent years, the field of structural engineering has witnessed a growing demand for lightweight and high-performance structures. With this demand comes the need for effective vibration control measures to ensure the durability, safety, and comfort of these structures. Among the various vibration control techniques, the use of single-particle impact dampers (SPID) has gained significant attention due to their simplicity, reliability, and cost-effectiveness.

Single-particle impact dampers (SPID) have emerged as a promising solution for mitigating structural vibrations caused by various excitations. These passive vibration control devices operate on the principle of dissipating kinetic energy through momentum transfer and inelastic impacts. However, due to various nonlinear phenomena associated with SPID, designing an optimal damper configuration can be a highly challenging task. The complex relationships between the numerous design parameters further complicate the process. Nonetheless, this study addresses these challenges by presenting a comprehensive optimal design approach specifically for a single-particle impact damper in commonly tested free and forced vibrations.

To develop such a methodology, a mathematical model is developed to simulate and evaluate the damping performance of SPID under different design arrangements. Unlike previous studies that focused on individual parameters, this research considers the relations between the major design parameters to achieve a more accurate representation of the SPID behaviour. By considering these factors together, it might become possible for designers to formulate an optimal range for designing effective SPID. In addition, an important factor considered in the numerical model is internal friction. Internal friction refers to the friction between the primary structure and the particle. Internal friction directly affects the movement of particle mass and is therefore included in the simulations to provide more credible results. The accuracy of the numerical approach is confirmed by comparing the results with experimental findings, ensuring that the model provides reliable predictions.

Additionally, the study establishes a range of design parameters suitable for harmonic excitations to fine-tune the SPID's performance for specific vibration scenarios. Additionally, the primary structure might exhibit a chaotic vibration response if the single-particle impact damper is employed without basic knowledge. Hence, a range of design parameters with a comparatively steady-state response is established by a Poincare map. By following the method proposed in this chapter, highly effective single-particle impact dampers for various vibration applications can be designed. An efficient single-particle impact damper can be constructed by using the approach established in this chapter for free and forced vibration applications.

3.1. Numerical model
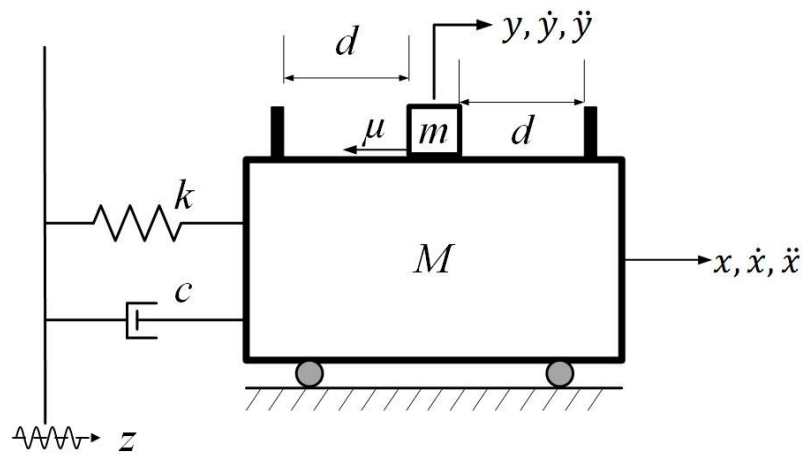
Figure 3-1. Model of a single-particle impact damper.

The mechanical model of the single-degree-of-freedom (SDOF) structure with a single-particle impact damper is illustrated in Figure 3-1. In this model, the primary structure has a mass denoted as M, while the particle itself has a mass m. A particle mass can move within a space of $2d$ and makes interaction with the primary mass when it contacts the boundary.

The equation of motion for the primary structure, considering the friction between the particle and the relative motion of the primary mass, can be expressed as follows,

$$M\ddot{x} + c(\dot{x} - \dot{z}) + k(x - z) + \mu_i N_m \, \text{sgn}(\dot{x} - \dot{y}) = 0 \tag{3.1}$$

The equation of motion for the particle in the context of the single-particle impact damper system can be represented as follows,

$$m\ddot{y} = \mu_i N_m \, \text{sgn}(\dot{x} - \dot{y}) \tag{3.2}$$

where:

- m represents the mass of the particle.

- N_m represents the weight of the particle mass ($N_m = mg$, where g is the acceleration due to gravity).

- sgn is a signum function that determines the friction force direction based on the relative velocity of the particle and primary structure.

- μ is the coefficient of friction between the particle and the primary mass.

- M represents the mass of the primary structure.

The signum function can be defined as,

$$\text{sgn}(\dot{x} - \dot{y}) = \begin{cases} -1, & (\dot{x} - \dot{y}) < 0 \\ 0, & (\dot{x} - \dot{y}) = 0 \\ 1, & (\dot{x} - \dot{y}) > 0 \end{cases} \tag{3.3}$$

In a single-particle impact damper, the particle collides with the primary structure and transfers momentum to dampen the vibrations. This process is crucial in dissipating energy and reducing the response of the structure to external excitations. By applying the law of conservation of momentum, the numerical model ensures that the total momentum of the system is conserved before and after each collision between the particle and the primary structure. The mathematical expression of conservation of momentum for two impacting masses can be written as

$$M\dot{x}_n^- + m\dot{y}_n^- = M\dot{x}_n^+ + m\dot{y}_n^+ \tag{3.4}$$

Here

- $(\dot{x}_n^+, \dot{x}_n^-)$ represents the velocity of the primary mass before and after the nth impact.

  - $\dot{x}_n^+$ denotes the velocity of the primary structure after the impact.

  - $\dot{x}_n^-$ denotes the velocity of the primary structure before the impact.

- $(\dot{y}_n^+, \dot{y}_n^-)$ denotes the velocities of the particle before and after the n-th impact.

  - $\dot{y}_n^+$ denotes the velocity of the particle after the impact.

  - $\dot{y}_n^-$ denotes the velocity of the particle before the impact.

These velocity terms play a crucial role in capturing the dynamics of the collision events between the particle and the primary structure. By tracking and analysing the velocities before and after each impact, the numerical model can accurately simulate the transfer of momentum during the collision process.

Furthermore, the coefficient of restitution is a fundamental parameter in the theory of single-particle impact dampers. The coefficient of restitution calculates the elasticity of the collision between the particle and the primary structure. It represents the ratio of the relative velocities of the bodies after the collision to the relative velocities before the collision. It influences the transfer of momentum and energy between the particle and the primary structure, thereby affecting the damping performance. There is some energy dissipated based on the coefficient of restitution magnitude at each impact. Therefore, it is necessary to determine the velocity of both colliding bodies after each impact by combining the conservation of momentum and coefficient of restitution.

The coefficient of restitution (e) is defined as,

$$e = -\frac{\dot{x}_n^+ - \dot{y}_n^+}{\dot{x}_n^- - \dot{y}_n^-} \tag{3.5}$$

The velocity of the particle and the primary structure after each impact changes and is influenced by both energy dissipation and momentum exchange, with the coefficient of restitution used to determine the level of energy dissipation. Energy dissipation during impacts is due to factors such as surface deformation, sound, and heat, and the coefficient of restitution determines this. There is no energy dissipation theoretically when the coefficient of restitution (e) is equal to 1. In such cases, a maximum momentum exchange occurs between the bodies, subject to the mass ratio and direction. On the other hand, when $e = 0$, resulting in minimal momentum exchange with maximum energy absorption occurs between the bodies.

By merging equations (3.4) and (3.5), the velocities of the particle and primary structure after each impact can be obtained as,

$$\dot{x}_n^+ = \frac{[\{(1 - \beta e)\dot{x}_n^-\} + \{\beta(1 + e)\dot{y}_n^-\}]}{(1 + \beta)} \tag{3.6}$$

$$\dot{y}_n^+ = \frac{[\{(1 + e)\dot{x}_n^-\} + \{(\beta - e)\dot{y}_n^-\}]}{(1 + \beta)} \tag{3.7}$$

The parameter β represents the mass ratio and it can be determined as $\beta = m/M$, where m is the mass of the particle and M is the mass of the primary structure. These equations, (3.6) and (3.7), are utilized to calculate the velocities of the particle and primary structure after each impact. The condition for identifying a collision is specified in Equation (3.8). By considering the absolute difference between the position of the primary structure (x) and particle (y), it is possible to determine whether an impact occurs on either end of the cavity.

$$|x(t) - y(t)| \geq d \tag{3.8}$$
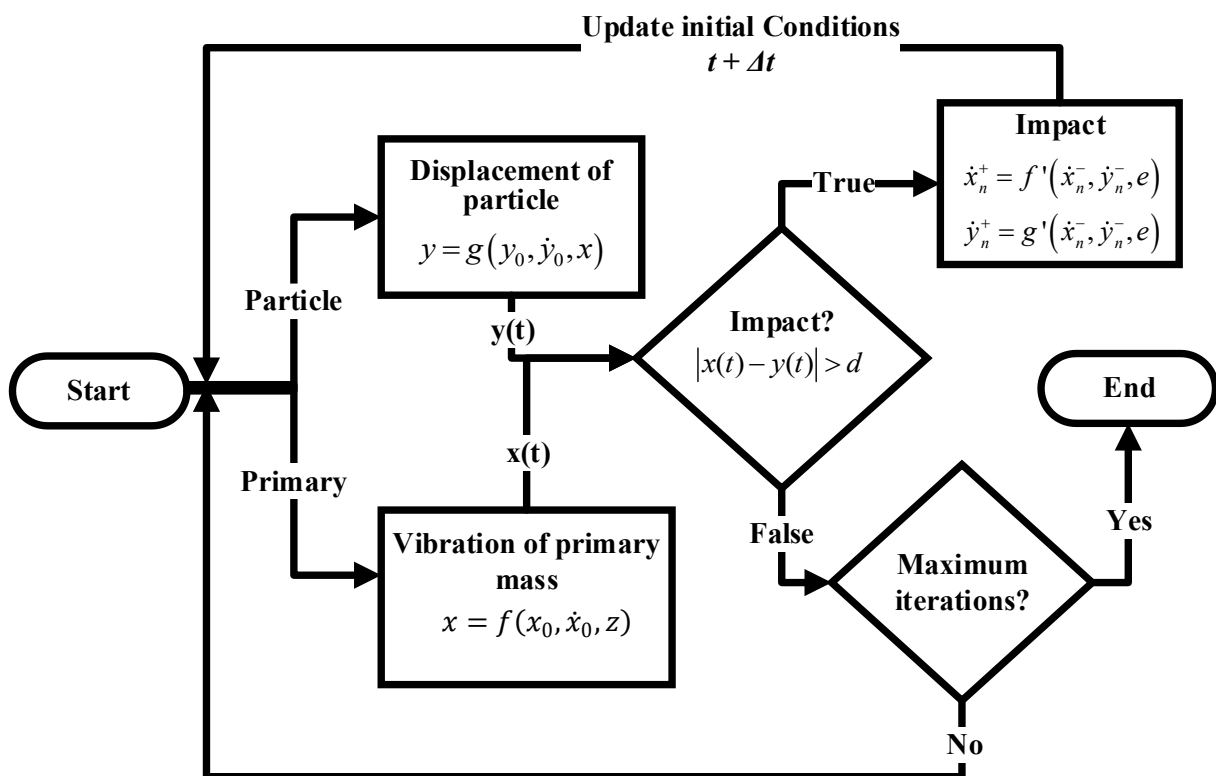
Figure 3-2. Process flow chart of the numerical model.

The flowchart presented in Figure 3-2 illustrates the computational principle for the motions of the model represented in Figure 3-1. The computation method commences with vibrations of the primary structure, which can result from either an initial condition $(x_0, \dot{x}_0)$ or base motion, $z(t)$. The next step involves identifying the occurrence of an impact by evaluating the condition $|x(t) - y(t)| > d$, where $x(t)$ and $y(t)$ represent the positions of the masses and d denotes a threshold value.

Upon detecting an impact, the velocities of both colliding masses M and m after the collision are determined using Equations (3.6) and (3.7) respectively. Subsequently, the computation restarts, using the newly computed parameters of the primary and secondary mass after the collision as the updated conditions. However, if the relative positions do not satisfy the condition for the collision, the computation proceeds to the next time step. It is worth noting that employing the smallest time-step is suggested to accurately determine the impact time, despite the potential growth in computational power.

The design of a single-particle impact damper relies on key design parameters, namely the clearance (d), coefficient of restitution (e), and mass ratio (β). While these major parameters are well-established, the development of optimum design methodologies has been limited because of non-linear relationships among the design parameters. Besides these parameters, friction is also considered in the motion of particles in this chapter. Friction is a universal phenomenon in most mechanical systems and incorporating it into the analysis allows for more practical and realistic conclusions.

A crucial aspect of single-particle impact dampers is their working principle, which depends on the collision of the primary mass and the particle. Another critical parameter that plays an important role in understanding the dynamics of primary mass is the velocity of the particle. Therefore, understanding the behaviour of the particle velocity is crucial for comprehending the overall response of the system. This knowledge can guide the design and optimization of single-particle impact dampers to effectively control vibrations.

3.1.1. Tuned Mass Damper (TMD)

Tuned Mass Dampers (TMDs) have emerged as effective vibration control devices widely used in various engineering applications. Their purpose is to mitigate unwanted vibrations and enhance the performance and stability of structures subjected to dynamic loads. TMDs consist of a mass-spring-damping system that is carefully tuned to counteract the resonant vibrations of the primary structure.

The concept behind TMDs is to introduce an additional mass, typically connected to the primary structure through springs and dampers. TMDs find applications in a broad range of structures, such as buildings, bridges, cranes, wind turbines, and even in lightweight structures like aerospace systems. They are particularly effective in attenuating vibrations caused by

external forces, such as wind or seismic events, as well as internal excitations, like machinery or human-induced vibrations.

The design and optimization of TMDs involves careful consideration of various parameters, including the mass ratio, natural frequency, damping ratio, and stiffness of the TMD system. These parameters are adjusted to match the characteristics of the primary structure, ensuring effective vibration control. A standard tuned mass damper (TMD) is shown in Figure 3-3.
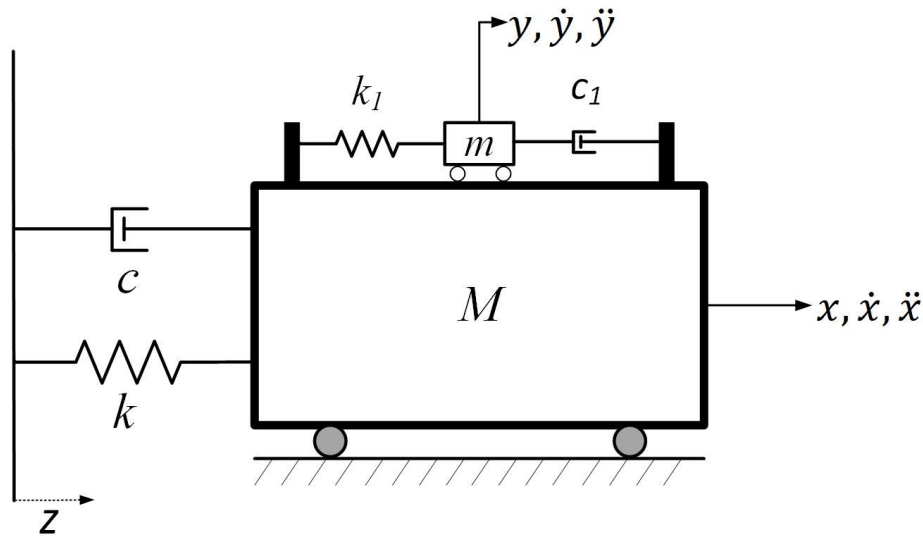
Figure 3-3. Model of tuned mass damper (TMD)

The equation of motion of the primary mass and secondary mass could be determined as,

$$M\ddot{x} + k(x - z) + k_1(x - y) + c(\dot{x} - \dot{z}) + c_1(\dot{x} - \dot{y}) = 0 \tag{3.9}$$

$$m\ddot{y} + k_1(y - x) + c_1(\dot{y} - \dot{x}) \tag{3.10}$$

Here,

- M: Mass of the primary structure

- $x, \dot{x}, \ddot{x}$: Displacement, velocity, and acceleration of the primary mass

- c: Damping coefficient associated with the primary mass.

- k: Stiffness coefficient associated with the primary mass.

- $y, \dot{y}, \ddot{y}$: Displacement, velocity, and acceleration of the secondary mass (tuned mass).

26

- Z: Amplitude of base excitation.

- m: Mass of the secondary mass (tuned mass).

- c_1: Damping coefficient associated with the secondary mass.

- k_1: Stiffness coefficient associated with the connection between the primary and secondary mass.

The optimal frequency and damping ratios of a tuned mass damper (TMD) can be derived and written as follows (Den Hartog, 1934):

The optimum frequency of the TMD is typically set to match the resonant frequency of the primary mass (M) or the dominant vibration mode of the structure. The optimum frequency ratio can be calculated as,

$$\gamma_{opt} = \frac{1}{1 + \mu_1} \tag{3.11}$$

The optimum damping ratio of the TMD denoted as ζ_{opt}, can be determined based on the desired level of vibration suppression. The optimum damping ratio is given by:

$$\zeta_{opt} = \sqrt{\frac{3\mu_1}{8(1 + \mu_1)}} \tag{3.12}$$

Here

- $\mu_1 = m/M$: Mass ratio between the primary and secondary mass

- $\omega_n = \sqrt{k/M}$: Natural frequency of primary structure

- $\omega_a = \sqrt{(k_1/m)}$: Natural frequency of tuned mass

- $\gamma = \omega_a/\omega_n$: Frequency ratio between primary structure and tuned mass

- $\zeta = c/(2\sqrt{mk_1})$: Damping ratio of tuned mass

3.2. Experiment Setup

In order to validate the numerical results, a prototype of a single-particle impact damper (SPID) shown in Figure 3-4a is manufactured. The manufactured SPID damper is then installed on the SDOF structure for further investigation of the damping performance.

(a)

(b)

(c)
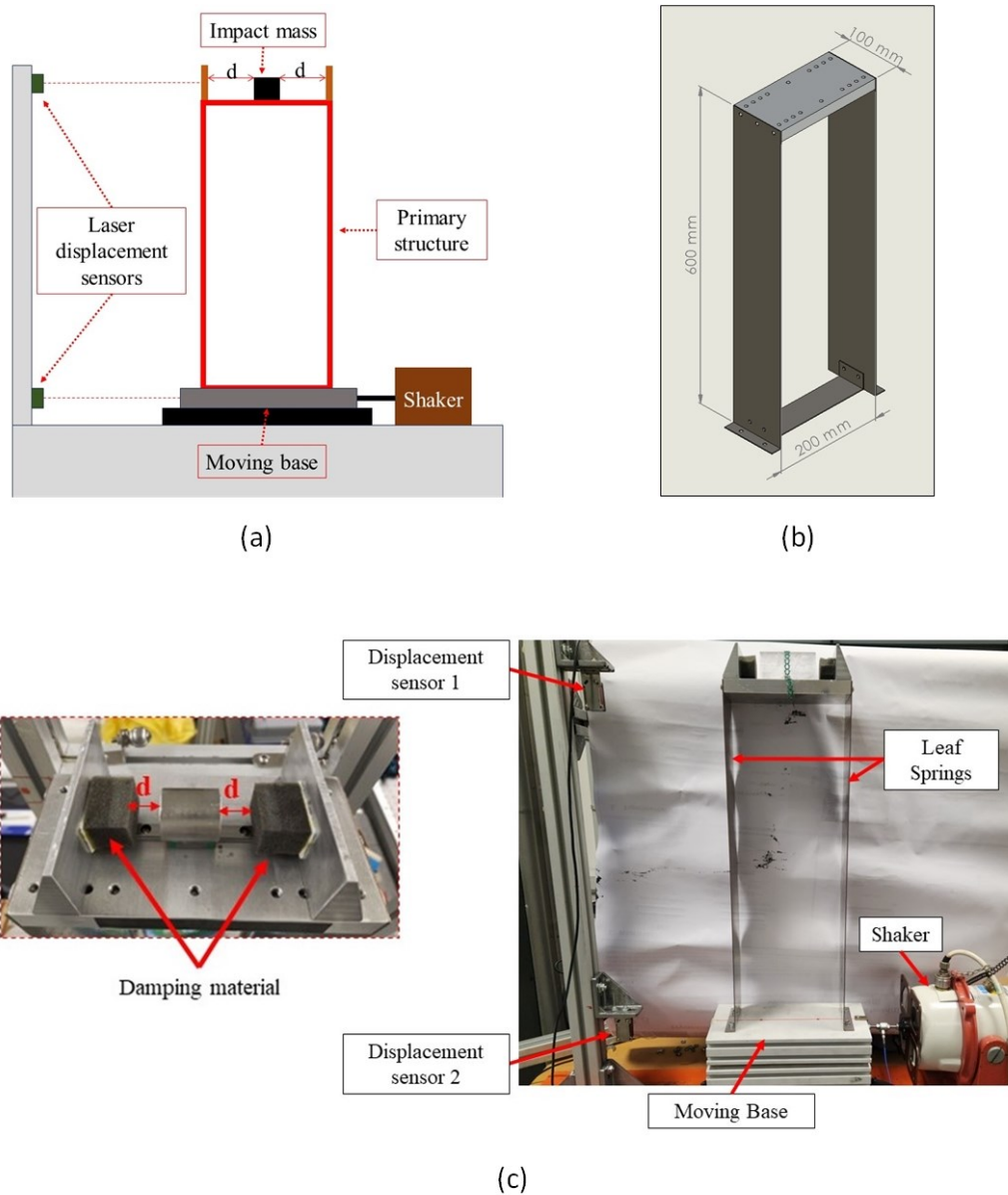
Figure 3-4. (a) Sketch of experiments; (b) Primary system dimensions (c) Prototype

The experimental setup is illustrated in Figure 3-4, where the primary system is composed of a frame structure with two steel beams that serve as springs with a thickness of 1.5mm. The dimensions of the primary structure are presented in Figure 3-4b. On top of these

springs, an aluminium plate is fixed, which forms the primary mass of the system. The experimental setup contains two contactless displacement sensors (Panasonic HG-C1200). These sensors are used to measure the displacement of the primary mass and the displacement of the base during the experiments. They provide accurate measurements without physically contacting the primary mass, ensuring non-intrusive data acquisition. In addition, a shaker (B&K LDS-V406) is used to induce vibrations in the SDOF structure. The shaker is connected to a moving base and the primary structure is fixed on the top of this base. The shaker can produce sinusoidal excitation to the base of the primary structure. Furthermore, a data acquisition system is linked to a computer to record the measurements from the contactless displacement sensors. It enables real-time data acquisition, analysis, and visualization of the experimental results.

The single-particle impact damper (SPID) as shown in Figure 3-4c, is composed of a cylinder-shaped particle. The particle mass is fixed on a slider with a rail-train mechanism. The linear slider reduces the friction between particle and primary mass and ensures the motion of particle in straight line. Furthermore, the linear guide can be removed to allow particle skid on top of the primary mass inside an acrylic tube to assess different internal friction mechanism. Further details about the surface are provided in next sections. The design allows for flexibility in altering the impact surface of the damper by adjusting the damping material. This enables testing of the effect of the coefficient of restitution (e) on the damping performance of the single-particle impact damper. Figure 3-4c illustrates the experiment rig that was manufactured for conducting the tests. This rig incorporates the necessary components and configurations for the experimental setup. To provide a clearer understanding of the experimental setup, Figure 3-4a presents a sketch that outlines the different elements and their arrangement.

3.2.1. Parameter's identification

It is assumed that the structure under investigation does not possess any additional damping sources apart from the single-particle impact damper. However, it is important to consider that various factors contribute to damping in the vibrating structure. Therefore, in order to assess the structural damping, free-vibration assessments of the primary mass are conducted with no other additional damping. During these tests, the primary structure is provided with an initial displacement of $x_0 = 35$ mm to start the free vibrations. The response of the structure's free vibrations is recorded, and the logarithmic decrement method is employed

to determine the magnitude of the structural damping present within the structure. Additionally, a Fast Fourier Transform (FFT) is performed on the displacement response data to extract the frequency spectrum of the primary structure. Measured parameters of the primary structure from the free vibration test are presented in Table 3-1.

Table 3-1. The parameters of the structure

Parameter	Magnitude
Damping ratio (ζ)	0.0038
Natural frequency (f_n)	2.50 Hz
Primary mass (M)	1.6 kg

3.2.2. Single-particle impact damper

In the numerical simulation model of the single-particle impact damper (SPID), the primary mechanism for vibration suppression is attributed to the dissipation of energy and momentum exchange with collisions. The simulations assume that the impact time is extremely small and can be neglected. Another assumption made in this simulation is that the coefficient of restitution (COR) is constant throughout the functioning of SPID. Although a negligible contact time can be justified for hard collisions due to their robust nature and extremely short contact time, this chapter considers a wide range of parameters, including the COR, to establish a procedure for the optimum design of the SPID.

To investigate the influence of the COR on the damping performance of the SPID, a smaller coefficient of restitution is used to represent soft impacts. This is achieved by utilizing a soft surface, e.g., cushion foam. Consequently, a comparatively longer contact time can be presumed in cases involving soft impacts. To address this limitation and enhance the accuracy of the numerical model, the design of the SPID incorporates a cushioning material, specifically Polyurethane Foam. This addition serves to validate the mid-range coefficient of restitution and ensure that the numerical model aligns with experimental observations. To refine the numerical model and determine the contact time and coefficient of restitution, a series of experiments are conducted. These experiments involve both "hard" impacts, such as steel-to-aluminium collisions, and "soft" impacts, such as steel-to-foam collisions. The experimental setup is shown in Figure 3-5.
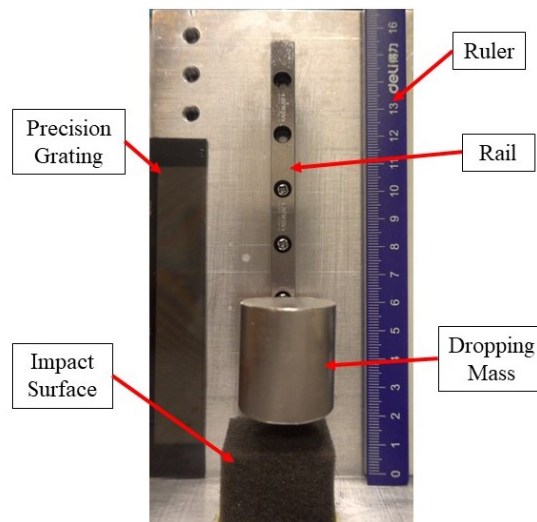
Figure 3-5. Experiment to determine the COR and contact time.

In the experiment, a steel particle is fixed onto a train using a rail-train mechanism. The particle is then dropped from various heights. To capture the dynamics of the experiment, a high-speed camera, specifically the Sony RX100-M7 is employed. The camera records the experiment in 20x slow-motion video at a rate of 1000 frames per second. These recorded frames are subsequently extracted and analysed to determine the exact moment of contact between the particle and the primary structure, as well as the duration of separation during rebound, which allows for the calculation of the contact time. To ensure accurate measurements and provide a reference for any potential image distortion caused by the camera lens and resolution, a ruler and a precision grating from Sine Patterns LLC are utilized in the experiment. The combination of these tools assists in establishing a spatial reference for analysing any image distortions that may occur. Additionally, the recorded videos are processed, and frames with the release of the particle and its final rebound height are selected for further analysis in a computer-aided design (CAD) software program. This software enables the calculation of the coefficient of restitution (COR). Each frame extracted from the recorded videos has a resolution of 3456 x 2304 pixels, providing detailed visual information for accurate calculations.

The impact velocity of the particle is determined based on the dropping height and the acceleration due to gravity. Using this information, the coefficient of restitution (COR) is defined as $e = v_f / v_i$, where v_f represents the final velocity after the rebound, and v_i denotes the initial velocity before impact. The kinetic and potential energy is defined as,

$$\frac{1}{2}mv^2 = mgh$$

$$v = \sqrt{2gh}$$

Hence, replacing this in the coefficient of restitution equation gives,

$$e = \frac{v_f}{v_i} = \frac{\sqrt{2gh_f}}{\sqrt{2gh_i}} = \sqrt{\frac{h_f}{h_i}} \qquad (3.13)$$

The free-fall experiment is conducted by repeating the procedure three times to ensure reliable results. From the recorded data and frame analysis, the magnitude of the coefficient of restitution (COR) is determined using Equation (3.13) for each trial. Based on the calculations, the average magnitude of the COR is determined separately for soft and hard impacts. For soft impact scenarios, the average magnitude of the COR is measured as 0.47. On the other hand, for hard-impact situations, the average magnitude of the COR is found to be 0.82.
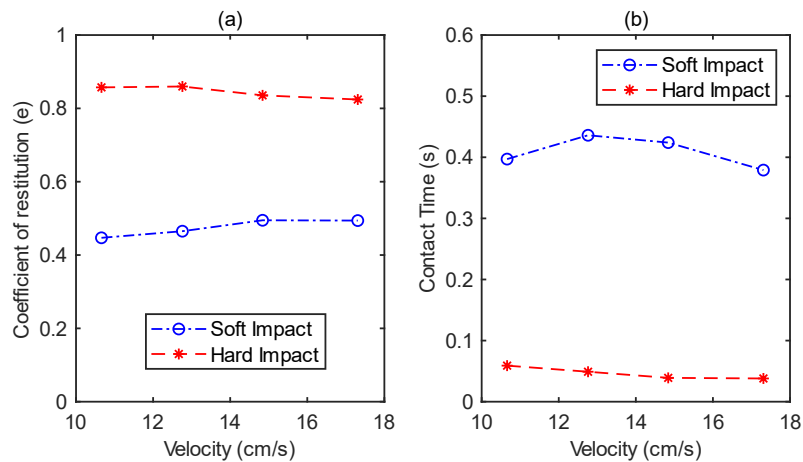
Figure 3-6. (a) The coefficient of restitution of hard and soft impact; (b) Contact time.

To validate the assumption that the coefficient of restitution (COR) remains constant during each impact, different impact velocities are considered, and their corresponding COR values are determined. This analysis is depicted in Figure 3-6a, where the impact velocities are varied, and the resulting COR values are plotted. The data shows that the COR remains consistent across different impact velocities, supporting the assumption of a constant COR within each impact scenario. Furthermore, the contact time between the particle and the

primary mass during impact is measured and presented in Figure 3-6b. The plot illustrates the contact times for different impact velocities. The average contact time obtained from these measurements represents the duration of contact between the particle and primary mass in scenarios involving a hard-impact surface and the presence of a cushioning material. The resulting measurements for contact time and coefficient of restitution are then organized and shown in Table 3-2.

Table 3-2. Contact-time and average coefficient of restitution between different impact types.

Impact type	Contact Time (s)	Coefficient of restitution
Soft	0.046	0.47
Hard	0.411	0.82

The experimental results indicate that the duration of a soft impact is around 9 times longer compared to a hard collision. This difference in duration is measured by introducing a cushioning foam, specifically polyurethane foam, at the impact surface to generate the soft impact. Conversely, the hard impact is produced by utilizing a metallic impact surface within the single-particle impact damper (SPID). The use of polyurethane foam effectively extends the contact time during the impact, resulting in a significantly longer duration compared to the impact with the rigid surface. The longer contact time in soft materials is related to the higher energy dissipation.

3.3. Results and discussions (Free vibrations)

This section focuses on the evaluation of the single-particle impact damper's (SPID) performance in free vibration damping. Free vibrations occur when a dynamic system experiences an impulse or a sudden seismic disturbance, resulting in an initial displacement, velocity, or acceleration of the system. The analysis in this section specifically examines the free vibration response of a single-degree-of-freedom (SDOF) structure associated with a single-particle impact damper. The equation of motion for the primary mass can be derived from Equation (3.1) by assuming that the base motion is equal to zero.

3.3.1. Numerical simulations

The simulations of the free vibration response of mass M involve applying an initial displacement of 35 mm to the primary structure. The equations of motion, specifically

equations (3.1) and (3.2), are computed by constructing a code in MATLAB software. Runge-Kutta 4th order method is used to write the MATLAB script for numerical simulations. The resulting amplitudes of the primary mass M are plotted in Figure 3-7 by varying the clearance (d/x_0) and the coefficient of restitution e different simulations are conducted.
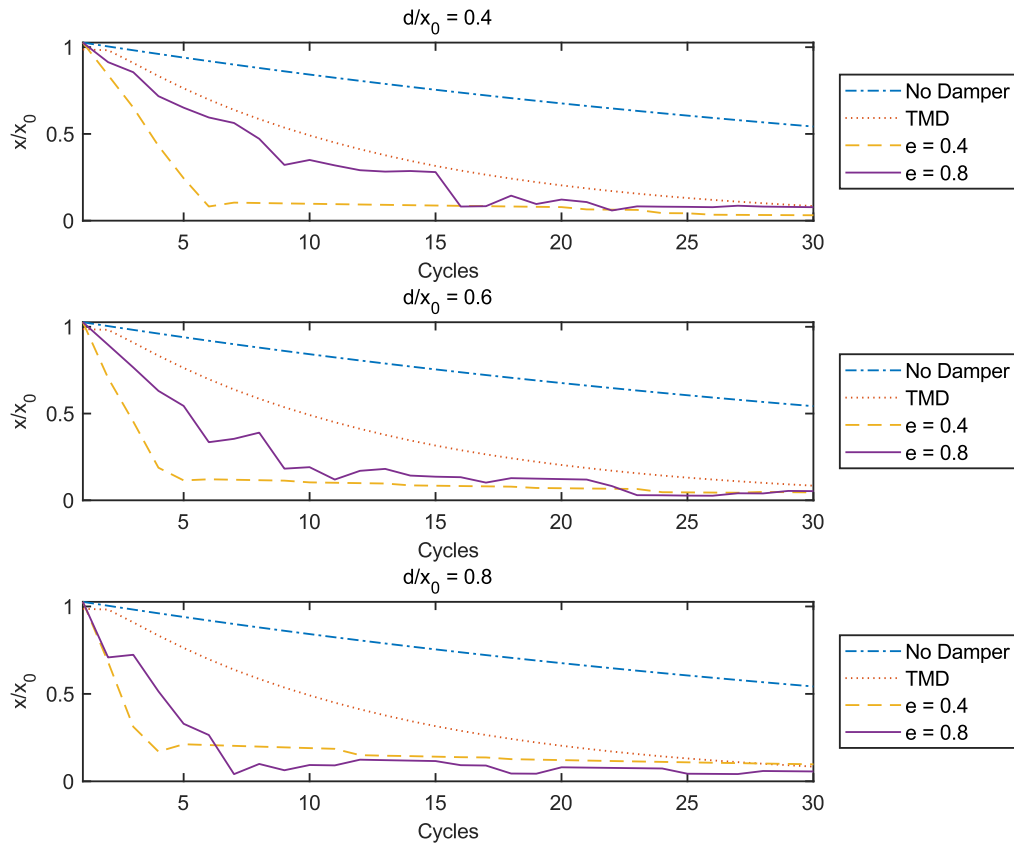
Figure 3-7. Response of the primary mass with SPID; $\mu_i = 0$

The graph shows the maximum amplitude of the primary cycle in time domain; however, the x-axis in the plot is modified as cycles $\left(\frac{t}{T}\right)$, where T is the period of the vibrations. The response in cycles is used to observe the damping in each cycle for simplicity. For the sake of general analysis, a relative clearance magnitude, denoted as d/x_0, is introduced in this study. This relative clearance magnitude provides a standardized measure by which the actual length of the cavity is compared to the initial displacement of the system. By defining the relative clearance magnitude as the ratio of the actual cavity length to the initial displacement, the results obtained from the analysis can be considered in a more general context. This approach

allows for a consistent comparison and interpretation of the findings across different scenarios and systems, enabling a broader understanding of the impact and effectiveness of the studied parameters. Furthermore, to provide a basis for comparison, the free vibration amplitudes of the structure with an optimally tuned mass damper (TMD) with a spring constant of ($k_1 = 32.83$ N/m) and a same mass ratio as the SPID (mass ratio = 0.1) are also numerically solved and shown in Figure 3-7. The spring constant is measured through the optimal tuned mass damper equations presented in Section 3.1.1.

As illustrated in Figure 3-7, it is evident that without any form of damping provided by either the TMD or SPID, the vibration amplitude of mass M decreases very slowly. However, the SPID demonstrates more effective damping capabilities compared to the TMD. While the TMD gradually reduces the vibration amplitude of mass M, the damping provided by the SPID exhibits uneven behaviour across different vibration cycles. Furthermore, the SPID with a soft surface outperforms the SPID with a hard surface in dampening the vibration amplitude of mass M. Additionally, a larger clearance within the SPID leads to faster damping of the vibration of mass M. This can be attributed to the higher velocity gained by the particle within the SPID before impact, resulting in more efficient energy dissipation between the two masses during the collision.

The velocity of the particle within the single-particle impact damper (SPID) plays a crucial role in its functioning. This velocity is influenced by the friction that exists between the particle and the primary structure. Therefore, analysing the behaviour of the SPID requires consideration of this internal friction. In most mechanical systems, friction cannot be disregarded, emphasizing the need for a comprehensive analysis of the primary mass response while studying the internal friction of the SPID.

By computing the vibration response of the primary structure with varying magnitudes of the coefficient of friction within the single-particle impact damper, it becomes evident that the damping performance of the SPID is directly affected. This can be observed in Figure 3-8, where different cases of internal friction are analysed. It is noteworthy that the cases with zero or exceptionally low internal friction (e.g., $\mu_i = 0.05$) exhibit the most effective damping performance in reducing the free vibration amplitudes of the primary structure. Based on these

observations, it is advisable to maintain a low internal friction value within the SPID to optimize its practical damping performance.
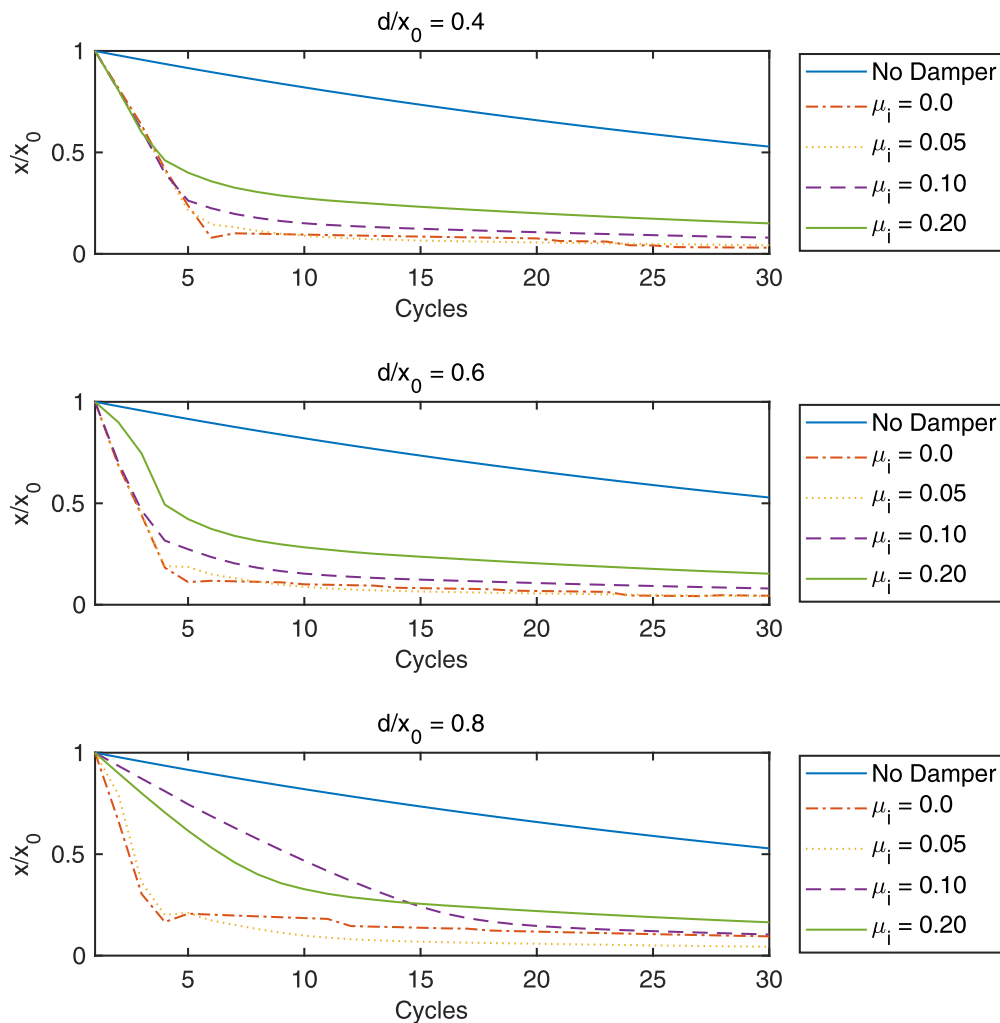
Figure 3-8. Computed free vibration amplitude of the primary mass with various internal friction (μ_i); $e = 0.4$

3.3.2. Optimal design valuation

In this section, the impact of internal friction on the different combinations of the parameters of the single-particle impact damper (SPID) design is analysed. Building upon the previous section's discussion on the non-uniform damping performance of the SPID, the root-mean-square (RMS) displacement magnitude of thirty cycles of vibrations in the primary structure is calculated. This RMS value is then plotted in Figure 3-9 to evaluate the overall damping performance of the SPID. The utilization of RMS displacement provides a means to assess the overall energy dissipation within the system. This approach proves advantageous,

particularly for systems characterized by non-uniform damping behaviour. By calculating the RMS displacement magnitude, a more comprehensive understanding of the damping performance of the SPID across multiple cycles of vibration can be obtained.
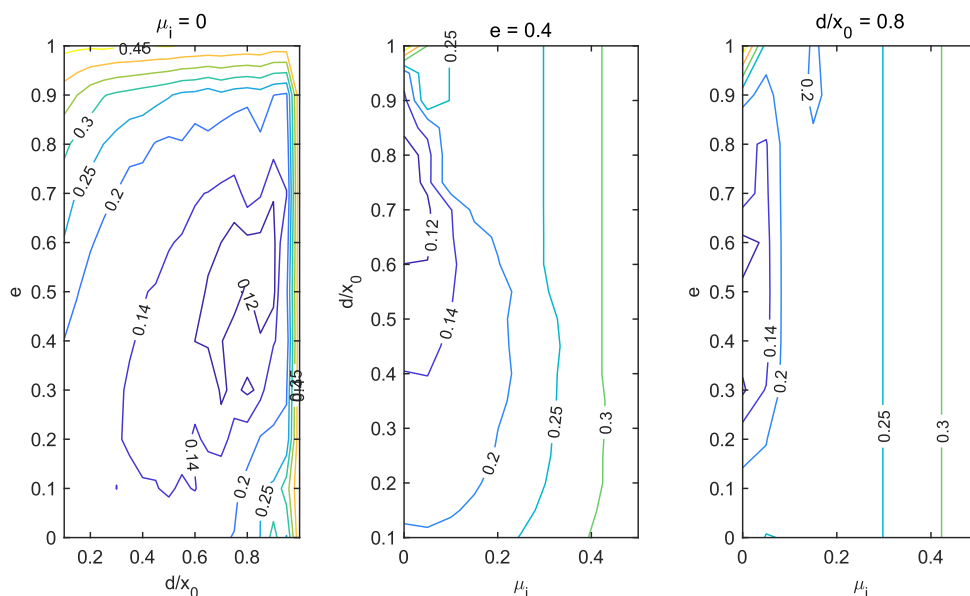
Figure 3-9. Displacement (RMS) of the primary structure with different combinations of design parameters of the SPID. $\beta = 0.1$; (a) $\mu_i = 0$; (b) $e = 0.4$; (c) $d/x_0 = 0.8$.

As represented in Figure 3-9a, the root mean square (RMS) displacement of mass M exhibits insensitivity to the relative clearance magnitudes (d/x_0), when the coefficient of restitution (e) approaches 1. This insensitivity arises because of minimal energy dissipation caused by the impacts in such cases. Interestingly, a smaller magnitude of the coefficient of restitution (e), which corresponds to better energy dissipation, does not automatically result in better damping. This emphasizes that momentum exchange through impacts is equally crucial for effective damping in the context of the single-particle impact damper. Figure 3-9a further illustrates that the minimum RMS displacement of mass M occurs at approximately $e \approx 0.55$ and $d/x_0 \approx 0.85$. This highlights the significance of establishing the optimum values for the design parameters of the SPID to achieve optimum energy dissipation and momentum exchange. Finding these optimal values becomes vital to maximize damping performance and achieve the desired level of vibration reduction in practical applications. In Figure 3-9b, the contours represent the changes in the RMS displacement magnitude with the relative clearance, considering the influence of internal friction. This graph demonstrates how internal friction affects the damping performance of the SPID in combination with changes in the clearance

magnitude. It indicates that internal friction harms the overall performance of the SPID. Similarly, in Figure 3-9c, the contours illustrate the impact of internal friction with the coefficient of restitution on the RMS displacement magnitude. This graph provides insights into how internal friction, in combination with variations in the coefficient of restitution, affects the damping performance of the SPID. It reveals that internal friction plays a significant role in influencing damping performance and highlights its adverse effect in this context as well.

3.3.3. Experimental Validations

In this section, the experimental assessment of the free vibration of the structure with different dampers is presented. The experimental prototype, represented in Figure 3-4, allows for testing various sets of design parameters for the single-particle impact damper (SPID). These parameters include the clearance magnitude, internal friction, and coefficient of restitution of the SPID.
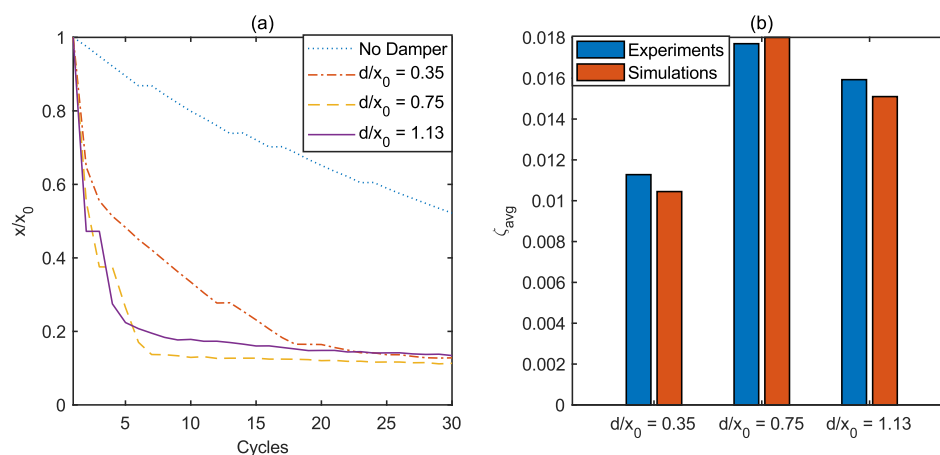
Figure 3-10. (a) Normalized displacement of the primary structure with various relative clearance of SPID; (b) Average damping ratio with different relative clearance magnitudes

During the optimum design consideration from numerical analysis, it was determined that the coefficient of restitution should fall within the range of 0.4 to 0.6. To achieve this, a polyurethane (PU) foam is installed on the walls of the SPID, resulting in a coefficient of restitution of 0.47. The clearance magnitude can be adjusted to assess different design combinations of SPID. Moreover, a slider with linear bearings is implemented on the top of the primary structure, as shown in Figure 3-4. This mechanism is designed to minimize friction during the particle's motion, ensuring that the sliding movement of the particle aligns with the mathematical model.

In the experimental analysis, the relative clearance (d/x_0) is varied to assess various design combinations of the single-particle impact damper. The vibration response of the primary structure is recorded by applying an initial displacement $(x_0 = 35 \text{ mm})$. The initial displacement is provided by displacing the top mass and released. An aluminium column is fixed on the optical table (where experiments are performed) 35 mm away from the primary mass. The column is high enough that the top of the primary mass can touch it when displaced from its initial position. In order to make consistent measurements, the top mass is displaced until it touches the column and then it is released to record free vibration response. The normalized displacement response of the primary structure, corresponding to various relative clearance magnitudes, is presented in Figure 3-10. The results indicate that a smaller relative clearance magnitude can provide damping for an extended duration. However, the magnitude of damping accomplished is relatively smaller due to the reduced energy of the particle resulting from the smaller clearance. Conversely, a bigger clearance magnitude initially yields greater damping in the first few cycles, but the damping declines quickly, leading to significantly lesser damping after a few cycles.

Based on these findings, it is determined that a relative clearance magnitude (d/x_0) of 0.75 achieves robust and longer-duration damping. This conclusion aligns with the suggestions made in the numerical analysis. Figure 3-10b demonstrates a reasonable agreement between the experimental and simulated results, highlighting the influence of the clearance magnitude on the damping performance of the single-particle impact damper. It further emphasizes that the relationship between these parameters is nonlinear, indicating the need for careful consideration and optimization of the clearance magnitude to achieve the desired damping performance.

In order to examine the influence of internal friction on the damping of the single-particle impact damper (SPID), three different methods are constructed to provide different levels of internal friction. The coefficients of friction between the internal surfaces are experimentally determined and listed in Table 3-3. The first mechanism, referred to as the "slider," utilizes a rail-train setup where a rail is installed on the top surface, and the particle is fixed on the corresponding train, as shown in Figure 3-4a. This configuration offers the lowest internal friction among the three mechanisms. The second mechanism involves installing an acrylic cylinder on the primary mass. In this setup, the particle can slide on the surface of the acrylic

tube without any additional sliding assistance The friction between the acrylic surface and the steel particle is larger than that in the rail-train mechanism, resulting in increased internal friction. To further increase the internal friction, sandpaper with a grit size of 280cw is fixed inside the acrylic tube. This creates a rough surface for the particle to slide on, enhancing the friction between the sandpaper and the steel particle as presented in Figure 3-11.

| (a) | (b) |
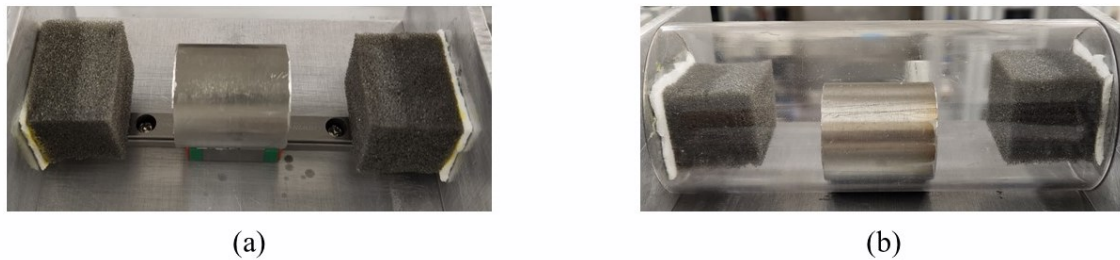
Figure 3-11. Different internal friction mechanism; (a) With slider; (b) Without slider

In the experimental setup, the tested surfaces are fixed on an inclined plane with an inclination angle (θ). This arrangement enables the particle to slide down the surface while being evaluated. The sliding motion of the particle is recorded using a high-speed camera. To determine the coefficient of friction for each tested surface, the time taken for the particle to reach the lowest end of the plate is recorded. This time measurement allows for the calculation of the particle's acceleration on each surface.

$$\mu_i = \frac{g\sin(\theta) - a}{g\sin(\theta)} \tag{3.14}$$

Table 3-3. Measured internal friction coefficient by changing surface in the SPID.

Internal Surface	Coefficient of friction (μ_i)
Slider only	0.08
Without slider	0.18
Sandpaper (280cw)	0.25

The coefficient of friction for each case is determined using Equation 3.14, which relates the coefficient of friction (μ_i) to the acceleration of the particle (a) and the gravitational acceleration (g). By measuring the acceleration of the particle on each tested surface and dividing it by gravitational acceleration, the coefficient of friction for that surface can be obtained. This approach is also applied to determine the coefficient of friction for the slider

mechanism. The time taken for the particle to slide down the rail is recorded, and the coefficient of friction is calculated using Equation 3.14 with the acceleration of the particle and the gravitational acceleration.
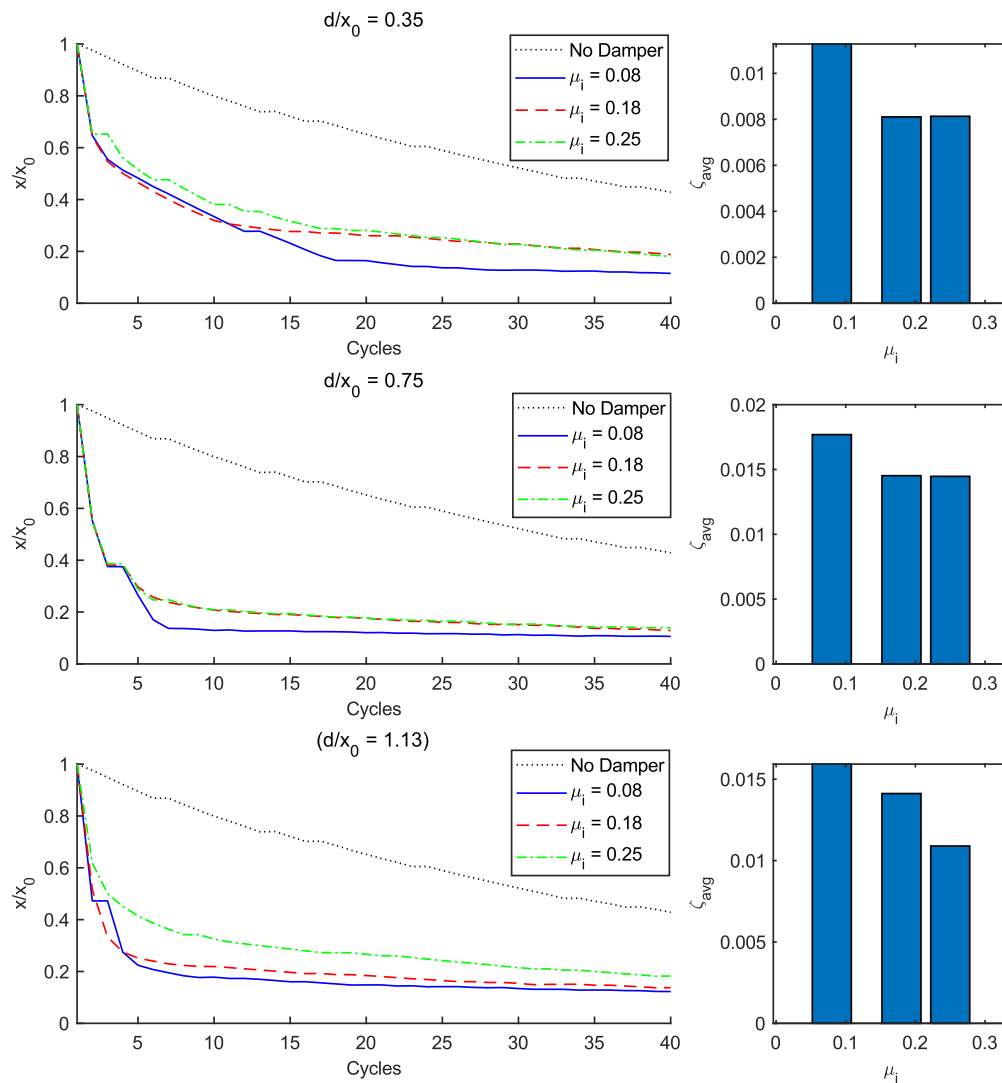
Figure 3-12. Normalized displacement of the primary structure with different internal friction levels (Experiments).

In Figure 3-12a, the normalized response of the primary structure, considering different magnitudes of internal friction coefficients is presented. The results demonstrate that reducing internal friction enhances vibration suppression for all tested combinations. These findings confirm the results obtained from the numerical analysis, further validating the influence of internal friction on the damping performance of the single-particle impact damper (SPID). The

experimental data supports the conclusion that lower levels of internal friction contribute to improved vibration suppression.

3.4. Results and discussion (Forced vibrations)

In this section, numerical and experimental analyses are conducted to investigate the behaviour of a single-particle impact damper (SPID) when the structure is subjected to harmonic excitations. The objective is to evaluate the damping performance of the SPID under such conditions.

The numerical analysis involves using appropriate mathematical models and simulation techniques to predict the response of the structure with the SPID. Various parameters, such as the excitation frequency, amplitude, and damping characteristics of the SPID, are considered in the numerical simulations. Simultaneously, experimental tests are conducted using a physical model of the structure equipped with the SPID. The structure is subjected to harmonic excitations with specified frequencies and amplitudes, while the response of the structure is measured and recorded. The experimental setup allows for the evaluation of the damping effectiveness of the SPID in a real-world scenario.

3.4.1. Numerical Evaluation

In numerical modelling, the equations of motion for the primary structure and particle, as described in Section 3.2, are solved using the fourth order Runge-Kutta method. The base excitation is represented by the equation $z(t) = Z\sin(\omega t)$, where Z is the amplitude and ω is the frequency of the base motion. The simulation results in Figure 3-13 provide insights into the damping performance of the single-particle impact damper (SPID) on the resonant vibration of the primary structure. By examining the vibration amplitude of mass M in the frequency domain, the influence of the clearance to base motion amplitude ratio (d/Z) on the vibration amplitude of the single-degree-of-freedom (SDOF) primary structure can be observed. Like the free vibration analysis (Section 3.3), a relative clearance magnitude d/Z is introduced for forced vibration as well. Here the relative clearance magnitude is the ratio of the clearance length (d) and base excitation magnitude (Z).
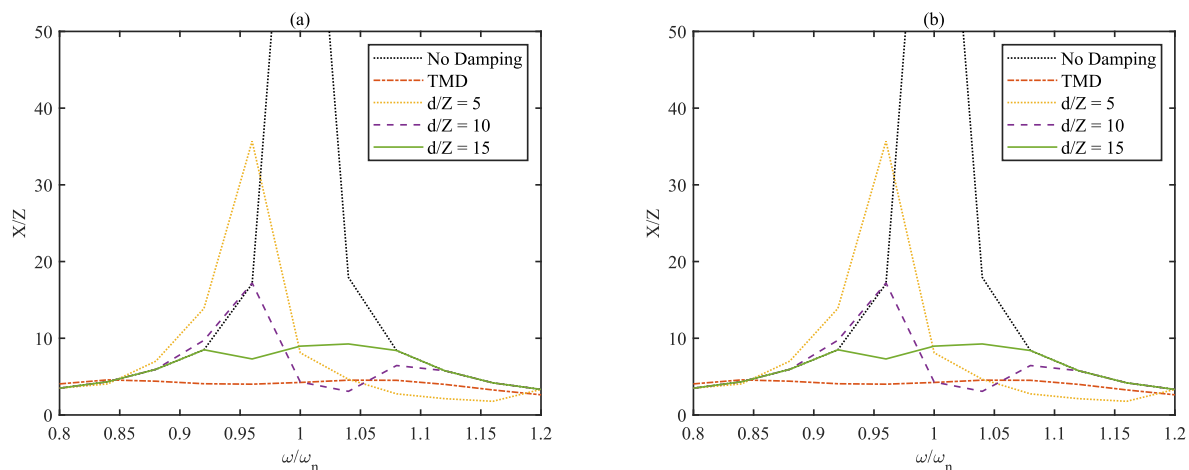
Figure 3-13. The response of the structure with different relative clearance magnitudes. $e = 0.5$; (a) $Z = 3$mm; (b) $Z = 30$mm.

In addition to examining the effect of relative clearance on the amplitudes of the primary structure, the response amplitudes of the primary mass M are determined for different amplitudes of base excitation. Specifically, Figure 3-13a displays the vibration response of the structure for a base excitation magnitude of $Z = 3$ mm, while Figure 3-13b shows the vibration response for $Z = 30$ mm. The results reveal an important observation: the relative clearance magnitude can be determined for any excitation amplitude if the ratio of d/Z remains constant. This finding suggests that by maintaining a consistent ratio between the clearance magnitude (d) and the base excitation amplitude (Z), the damping performance of the single-particle impact damper can be effectively maintained across different excitation levels.

As observed in Figure 3-13, the clearance magnitude of the single-particle impact damper (SPID) plays a crucial part, similar to the findings in free vibration analysis. A smaller relative clearance in the SPID leads to more impacts with smaller relative velocity, leading to reduced energy dissipation from the damper. Essentially, the particle mass in the SPID appears as an attached mass to the primary structure, which causes a decrease in the resonant frequency of the system. The frequency response of the primary structure with a tuned mass damper (TMD) is also computed as shown in Figure 3-13. The results demonstrate that the single-particle impact damper is not as effective as an optimized TMD in reducing the resonant vibration amplitude of the primary mass. The optimized TMD requires precise tuning of both the frequency ratio and damping ratio for optimal operation. Achieving this optimization in practice can be challenging.

In contrast, the single-particle impact damper is simple to design and install. It can be applied to structures with any natural frequency without requiring specific tuning. Additionally, a single-particle impact damper can work effectively across a range of frequencies, whereas a TMD is typically tuned for a specific frequency and may only be effective at that frequency. Furthermore, the cost-effectiveness of the single-particle impact damper makes it an attractive solution for various vibration control problems. Its simplicity and versatility in application contribute to its potential as a cost-effective solution. Therefore, when a cost-effective solution is required for vibration control, a single-particle impact damper can be a suitable choice.
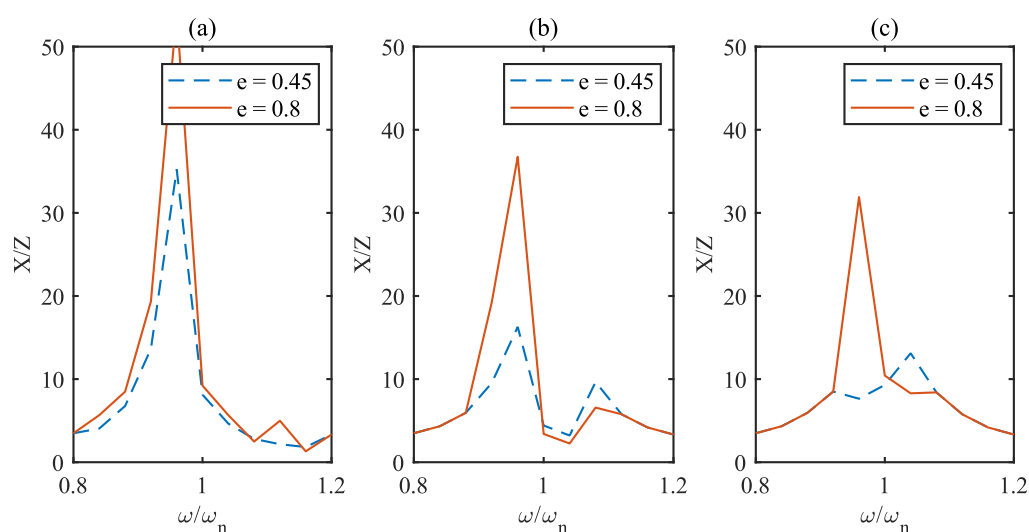
Figure 3-14. The response of the primary structure with SPID with different COR; (a) $d/Z = 5$; (b) $d/Z = 10$; (c) $d/Z = 15$

In Figure 3-14, the effect of the coefficient of restitution on the vibration amplitude of the primary mass M, considering different clearance magnitudes is presented. The graphs in Figure 3-14 reveal that a higher coefficient of restitution does not enhance the performance of the single-particle impact damper. The analysis indicates that when an additional mass (in this case, the particle) is introduced, proper selection of design parameters such as clearance and coefficient of restitution is crucial to achieve controlled movement and desirable damping. If these design parameters are not appropriately chosen, the added mass can lead to uncontrolled movement, chaos, and other nonlinear phenomena, negatively impacting the damping performance.

Figure 3-14a demonstrates that the coefficient of restitution has minimal impact on damping performance when the clearance magnitude is small. In this case, the particle has restricted movement due to the smaller clearance, resulting in numerous impacts with small relative velocity. Consequently, energy dissipation and conservation of momentum are not significantly affected by the coefficient of restitution. However, as shown in Figure 3-14b and Figure 3-14c, the coefficient of restitution starts to influence the damping performance as the relative clearance magnitude increases. With larger clearances, the particle has more freedom of movement, and the coefficient of restitution becomes more relevant. The interaction between the particle and the primary structure, including energy dissipation and momentum transfer, is influenced by the coefficient of restitution. Therefore, understanding the part of the coefficient of restitution in the design of a single-particle impact damper is necessary. Proper selection of the coefficient of restitution, in combination with the appropriate clearance magnitude, is essential to achieve the desired damping performance.

The chaotic response of the primary structure is another important aspect to analyse when considering a single-particle impact damper. The behaviour of the system can vary significantly depending on different design combinations of the damper. To gain insights into the nature of the displacement of the structure associated with the impact damper, a Poincare map can be utilized. A Poincare map is a recurrence plot that captures the state of the dynamic system at each cycle of vibration (Hirsch et al., 2013). It provides a visual representation of the system's behaviour and can reveal patterns, periodicities, or chaotic dynamics.

A Poincare map is computed over various relative clearance magnitudes and coefficient of restitution as illustrated in Figure 3-15, providing insights into the nature of the vibration response and the impact damper's effectiveness. Figure 3-15a demonstrates that different clearance magnitudes result in different responses of the system. The clearance magnitude directly influences the velocity of the particle before each impact. Smaller clearance magnitudes correspond to lower velocities before impact, resulting in extremely low damping. On the other hand, bigger clearance magnitudes allow for higher particle velocities, which can benefit damping through impacts up to a certain extent. However, when the clearance magnitude becomes excessively large, the impact velocity increases significantly, potentially leading to chaotic responses of the primary mass during vibrations.

45
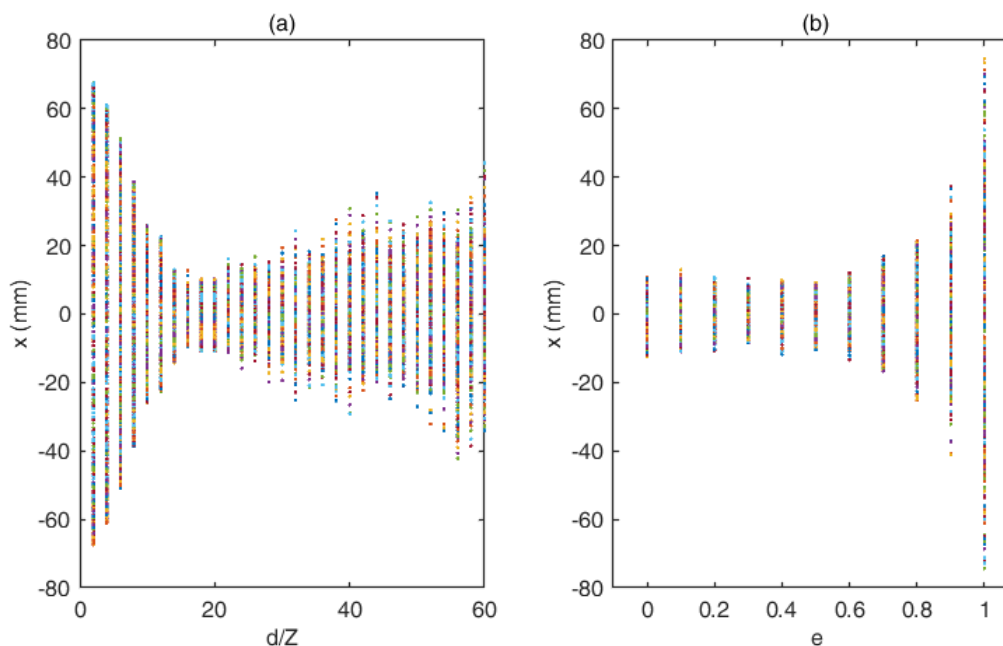
Figure 3-15. Poincare map simulated for the primary mass displacement at resonance;

(a) $e = 0.5$; (b) $d/Z = 14$

In Figure 3-15b, it can be observed that the magnitude of the coefficient of restitution lower than 0.7 exhibits a relatively steady response at resonance. A larger coefficient of restitution indicates lower energy dissipation during collisions but higher momentum exchange between the particle and the primary mass. Consequently, a larger COR provides less damping as the particle and primary mass exchange momentum at each impact. Based on these findings, it becomes evident that the clearance magnitude is of utmost importance in the design of a single-particle impact damper. The selection of the coefficient of restitution can be made below 0.7, depending on the availability of materials. Once the coefficient of restitution is determined, a suitable clearance magnitude can be chosen to achieve the desired damping performance.

3.4.2. Optimal design valuation

The numerical analysis reveals that there are numerous combinations of single-particle impact damper designs, making it challenging to represent the results for all combinations. In such cases, contour plots are commonly used to observe the changes in response across different combinations of design parameters. To determine the optimal design combination, a contour plot is constructed for the internal friction combined with the coefficient of restitution (e) and the relative clearance magnitude (d/Z). Figure 3-16a represents the contour plot

between internal friction and coefficient of restitution, Figure 3-16b shows the contour plot between internal friction and relative clearance magnitude, and Figure 3-16c displays the contour plot between relative clearance magnitude and coefficient of restitution. In these contour maps, the maximum amplitude of the primary structure is shown, allowing for the identification of regions that exhibit minimum vibration amplitudes. These regions can be considered as the optimal design combinations for the single-particle impact damper.
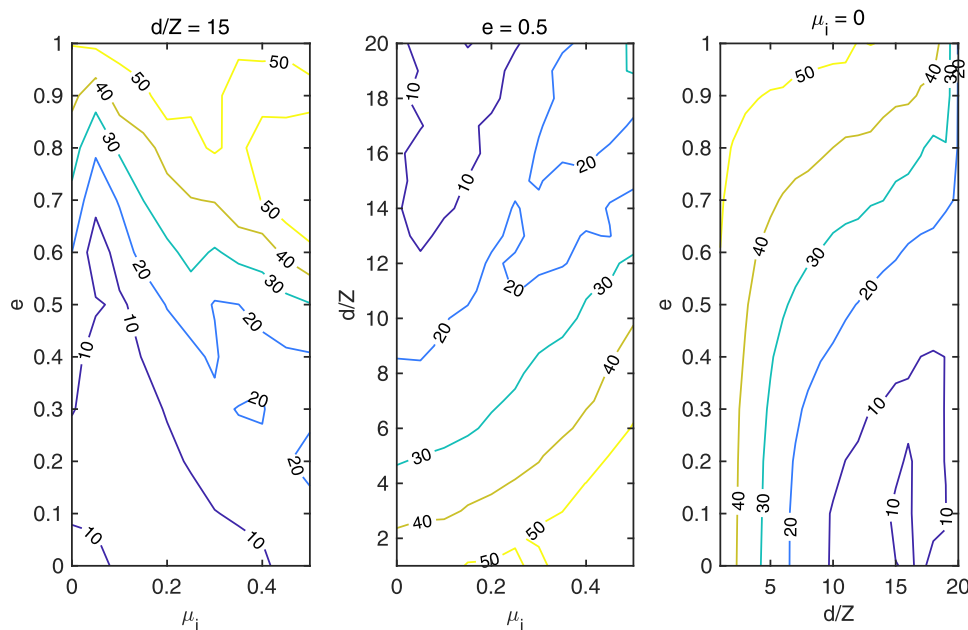
Figure 3-16. Steady-state vibration amplitude contours of the SDOF structure at resonance;
(a) $d/Z = 15$; (b) $e = 0.5$; (c) $\mu_i = 0$.

The contour map in Figure 3-16a demonstrates that as the internal friction level increases, the steady-state amplitude of the primary structure also increases. Therefore, it is recommended to have minimum internal friction for achieving optimal damping performance. Figure 3-16b shows the contour map for the relative clearance magnitude. It indicates that the optimal design combination lies within a relative clearance magnitude range of 14 to 17. Within this range, the vibration amplitudes of the primary structure are minimized. In this case, the contour plots indicate that the optimal design combination involves a minimum internal friction level, a relative clearance magnitude between 14 and 17, and a coefficient of restitution between 0 and 0.5.

It is implied that internal friction must be reduced for the optimum damping performance of a single-particle impact damper. Thus, the best design combination can be concluded by a

contour involving relative clearance magnitude and coefficient of restitution as illustrated in Figure 3-16c. The contour plot indicates that exceedingly small clearance and a larger coefficient of restitution have minimum effects on the energy dissipation of the primary structure. Furthermore, a zone where the relative clearance magnitude is between 10 to 16 and the coefficient of restitution is between 0 to 0.5 improves the damping. The design parameters selected within this region can increase energy dissipation leading to a better damping performance.

3.4.3. Experimental Validations

In this section, the optimum design combinations obtained from the numerical evaluation are experimentally validated. The experimental setup (Section 3.2) is utilized to measure the vibration amplitudes of the structure with various parametric combinations of the single-particle impact damper. The primary structure is mounted on a base, which is excited using a shaker. Two laser displacement sensors are positioned in the experimental rig. One sensor tracks the displacement of the primary mass, while the second sensor simultaneously measures the movement of the base. The recorded data from the displacement sensors provides evidence to validate the effectiveness of the optimum design combinations identified through numerical investigation.
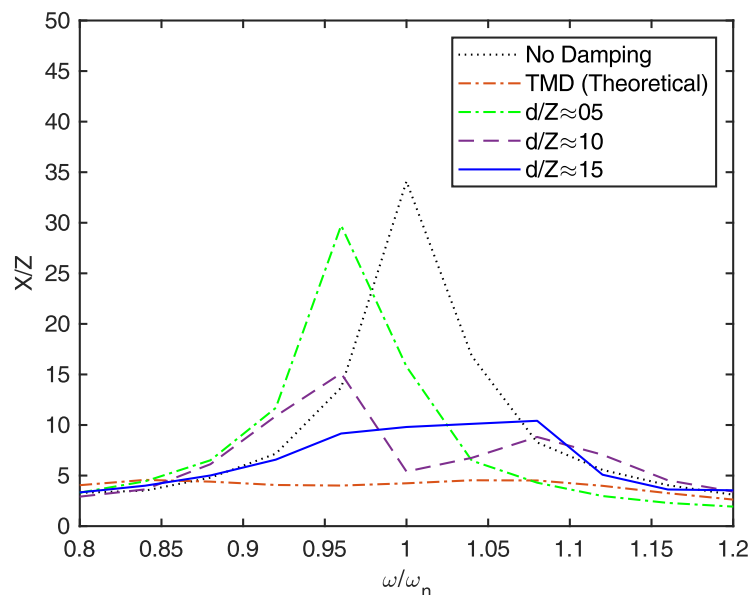
Figure 3-17. Comparison of the performance of SPID with TMD recorded experimentally.

In the case of a single-particle impact damper (SPID), generally used sweep sine test may lead to misleading data due to non-uniform damping characteristics. The available equipment

is capable of performing a classic sweep sine test; however, the time at each frequency is not enough to justify the performance of SPID. Instead, a modified sweep sine test is employed to evaluate the performance of the SPID. This modified test involves exciting the structure over a range of frequencies (2-3 Hz). A single set of experiment is performed at each frequency with 32 sec time history data. The frequency step is used as 0.05 to ensure that any important information is not lost. All set of data is then complied to determine the average maximum displacement at each excitation frequency to form a whole frequency sweep result. The shaker settings are kept constant in all cases and the base amplitude is recorded approximately at 3 mm for consistency. It is worth noting that the recorded base amplitude may not be constant over different excitation frequencies due to the influence of the primary mass motion. To validate the numerical results, experiments are conducted using an experimental model for different values of relative clearance. However, due to the constraints of the experimental setup, the experiments are performed for three clearance magnitudes while keeping the coefficient of restitution approximately at 0.45 and 0.8.

The measured frequency response of the primary structure is plotted in Figure 3-17, and they exhibit a similar tendency to the numerical predictions from Section 3.4.1. This alignment between the experimental and numerical results strengthens the validity of the numerical model and the accuracy of the design parameter recommendations. The plotted frequency response curves demonstrate the significant influence of the clearance magnitude on the damping performance of the SPID. A smaller clearance magnitude ($d/Z \approx 5$) results in extremely low damping since there is insufficient space for the particle to generate impacts with significant velocity. On the other hand, the damping from a single-particle impact damper becomes effective as the clearance magnitude is increased further. However, the clearance magnitude is required to be selected appropriately because an extremely larger clearance magnitude might result in no impacts at all. Hence, the optimal design combinations can be predicted from the numerical approach presented in this work.

Table 3-4. The peak of the displacement ratio from experiments and numerical results by altering relative clearance

	$d/Z \approx 5$	$d/Z \approx 10$	$d/Z \approx 15$
Numerical	35.6	17.2	9.3
Experimental	29.7	15.1	10.4

To assess the validity of the numerical simulations, the maximum amplitude ratios for different clearance magnitudes are compared in Table 3-4. It is recognized that the phenomenon of impact damping involves complex nonlinear behaviour, making it challenging to capture every aspect of the numerical model. However, despite these challenges, the comparison between numerical and experimental data demonstrates a good agreement.
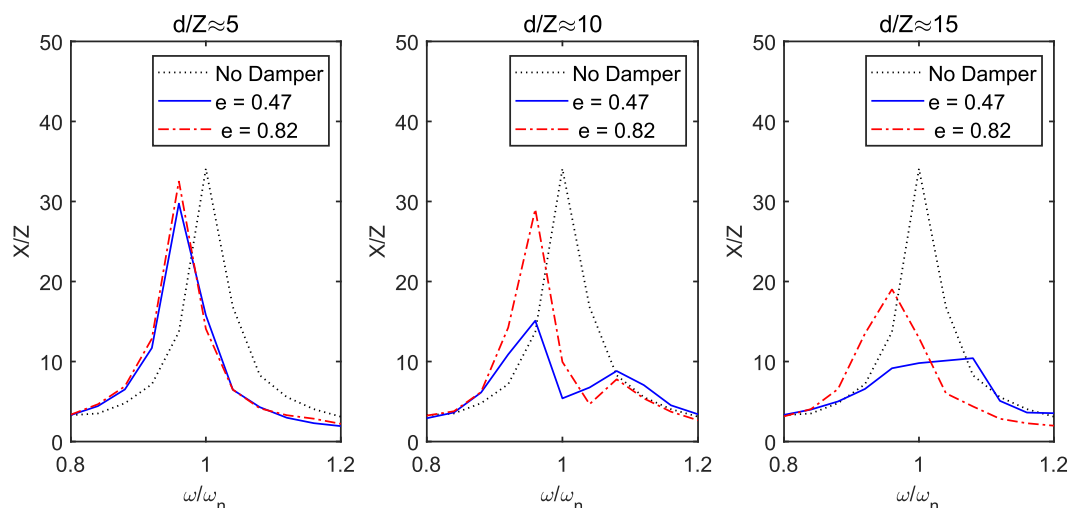
Figure 3-18. Frequency response of the primary mass with various coefficients of restitution (experiments).

The displacement ratio of the primary structure with different levels of the coefficient of restitution is measured and plotted as shown in Figure 3-18. The results demonstrate the impact of the coefficient of restitution on the damping effectiveness, particularly as the clearance magnitude is varied. In Figure 3-18a, it is observed that the coefficient of restitution has minimal influence on the displacement of the primary structure when the clearance magnitude is relatively small. However, as shown in Figure 3-18b and Figure 3-18c, the influence of the coefficient of restitution becomes evident as the clearance magnitude increases. The graphs in Figure 3-18 collectively indicate that the single-particle impact damper with a larger clearance magnitude and a lower coefficient of restitution ($e = 0.5$) exhibits the best damping performance. This finding suggests that a design combination involving a larger clearance magnitude and a smaller coefficient of restitution is particularly effective in enhancing the damping capabilities of the single-particle impact damper.
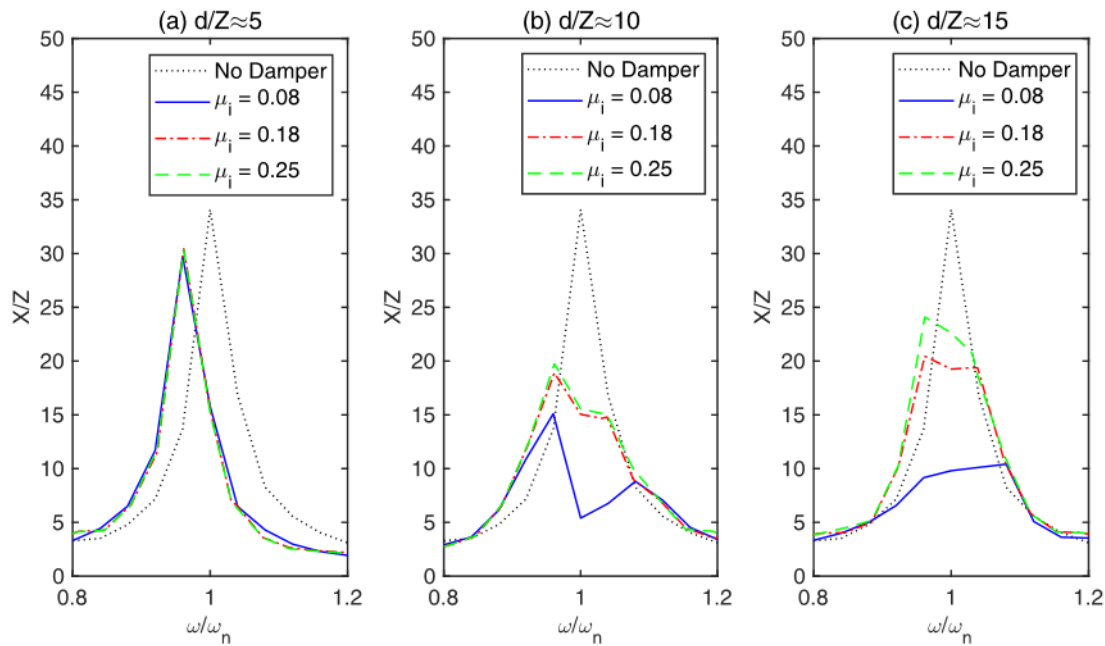
Figure 3-19. Response of the primary structure with internal friction (experiments).

In Figure 3-19, the vibration amplitude is compared for different levels of internal friction in the single-particle impact damper (SPID). The results demonstrate the effect of internal friction on the vibration amplitude, particularly in relation to the clearance magnitude. In Figure 3-19a, it can be observed that when the clearance magnitude is smaller, the influence of internal friction on the vibration amplitude is minimal. Conversely, the effect of internal friction becomes more significant as the clearance magnitude increases evident in Figure 3-19b and Figure 3-19c. The overall trend revealed in the results is that increased internal friction reduces the damping provided by the SPID and leads to higher vibration amplitudes in the primary single-degree-of-freedom (SDOF) structure. This finding highlights the importance of minimizing internal friction to optimize the damping performance of the SPID. The results validate the conclusions drawn from the numerical analysis.

3.5. Conclusion

This study presents a comprehensive approach to designing and optimizing the performance of a single-particle impact damper (SPID). The methodology combines numerical analysis, experimental validation, and practical considerations of potential effective parameters to reach design recommendations for optimal SPID performance. The conclusions drawn from the study are as follows,

- The presence of friction in the SPID lowers the kinetic energy of particles, leading to less meaningful collisions. Both the numerical and experimental results consistently exhibit that greater friction results in lesser damping in free and forced vibrations. Hence, reducing internal friction is suggested to achieve optimum performance.

- Through the analysis of a large dataset involving a large range of design combinations, it is determined that an optimum design for the SPID exists for any particular excitation. The recommended design parameters include a relative clearance (d/Z) from 14 to 18, Z is the amplitude of base motion and a coefficient of restitution (e) from 0 to 0.5. In free vibrations, the relative clearance magnitude (d/x_0) must be between 0.7 to 0.9, and the coefficient of restitution should be between 0.4 to 0.6 for optimal damping. The experimental results confirm the conclusions derived from the numerical analysis.

- The study employs the Poincare map to identify regions where relatively steady responses are observed. This analysis indicates that selecting the design parameters correctly leads to a stable response, while an improper design may result in chaotic vibration patterns. This understanding emphasizes the importance of designing the SPID with a proper understanding of its behaviour.

- The optimized SPID is compared to an optimized TMD in terms of its effectiveness in reducing free and resonant forced vibrations of a single-degree-of-freedom (SDOF) primary system. The results show that the SPID can reduce free vibrations faster than the optimized TMD, but it is less effective in suppressing resonant forced vibration amplitudes. However, the SPID offers advantages in its ability to work over a broad range of excitation frequencies compared to the tuned mass damper, which is typically tuned for a specific frequency. Considering the simple design and easy installation of the SPID, it can be a favourable choice for certain vibration control applications.

Overall, this chapter contributes to the understanding of single-particle impact dampers (SPID) and demonstrates their potential as a simple yet effective solution for structural vibration control. While the understanding of SPID is still in its early stages, this research provides valuable insights and lays the foundation for further exploration and practical applications of SPID technology.

3.6.   Summary

This chapter introduces a numerical approach to establish an optimum design methodology for a single-particle impact damper (SPID), which is a passive energy dissipation device known for its robust performance. The nonlinear characteristics of SPID and the lack of analytical models have posed challenges in designing SPID with optimal combinations. The chapter addresses these challenges and explores the performance of SPID in controlling vibrations. Through numerical simulations and experimental validation, the study identifies a range of design parameters for SPID that ensure non-chaotic responses and improve vibration damping. The results demonstrate that SPID designed with optimal combinations exhibit steady responses and superior vibration-damping capabilities. A comparison is also made with an optimized tuned mass damper (TMD), revealing that while SPID may not suppress forced vibration amplitudes as effectively as TMDs at resonance, they offer advantages such as simpler design and lower cost.

The results emphasize the significance of minimizing internal friction in SPID for optimal performance. Additionally, the research introduces the Poincare map as a tool to identify design parameter ranges that yield relatively steady responses, aiding in the selection of appropriate design parameters. Concluding on the practical implications, the study highlights that SPID, despite being in the preliminary stages of understanding, presents a promising alternative to other passive vibration control technologies. With their simple design and ease of installation, SPID offers an effective solution that can contribute to structural vibration control. Overall, this chapter establishes a solid foundation for the optimal design of SPID, addresses issues related to design methodology and chaotic vibration responses, and highlights their potential as viable options in the field of vibration control.

Chapter 4

Single-Particle Impact Damper with soft impact design

One of the common issues regarding a single-particle impact damper is the high-intensity force and noise during impact. In Chapter 3, it was concluded that the smaller coefficient of restitution can provide better damping and it was achieved by installing a soft material (PU foam) at the walls of the container. Therefore, it is considered that a soft impact might be a solution to the long-lasting drawbacks related to a single-particle impact damper such as large force and higher noise levels. Therefore, this chapter aims to investigate the damping effects of two types of impacts in a single-particle impact damper: soft impact and hard impact. Soft impact involves the use of viscoelastic materials that deform and dissipate energy upon impact, while hard impact refers to materials that exhibit minimal deformation. By studying the behaviour and performance of these impact types, valuable insights can be gained regarding the selection and optimization of impact materials for enhanced damping and noise control.

To achieve this objective, a numerical model considering the viscoelastic behaviour of the impact materials is constructed. It is deemed that using the coefficient of restitution only to model the behaviour of soft impact is insufficient as it cannot accommodate the viscous and elastic behaviours of soft materials. Additionally, an experimental rig is designed and constructed to validate the findings from the numerical model. Various damping materials, such as rubber, acrylic foam, Ethylene vinyl acetate (EVA) plastic, and Polyurethane (PU) foam, are used in the experiments to study the damping performance of single-particle impact damper. Dynamic compression tests are performed using a Dynamic Mechanical Analyzer (DMA) machine to determine the dynamic mechanical properties of these materials.

By systematically investigating the effects of different impact materials and analysing their damping performance, this research aims to identify optimal material properties that maximize damping efficiency and overall system performance.

4.1. Methodology

In this section, the methodology for the numerical and experimental methods is described. First, a numerical model for a single-particle impact damper with viscoelastic

material is developed. A numerical analysis is conducted through simulations and the performance is analysed. Later, an experimental setup is designed, and the conclusions drawn from numerical models are validated.

4.1.1. Theory
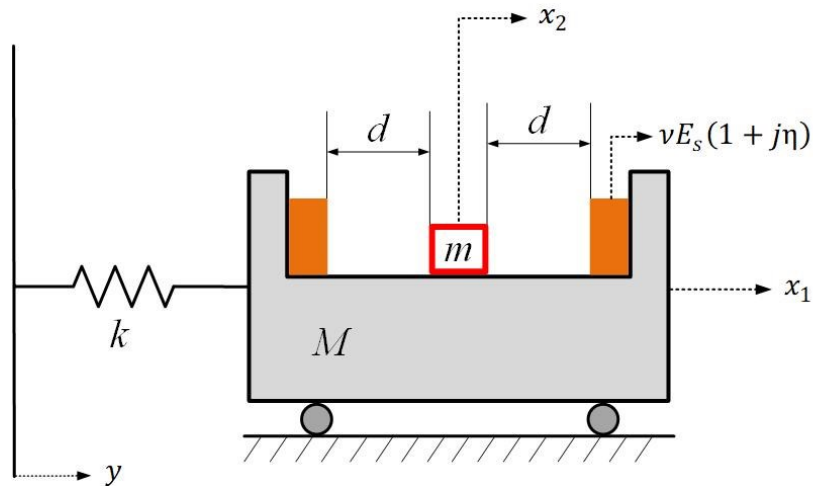
Figure 4-1. Mechanical model of a single-particle impact damper with viscoelastic material attached to a single-degree-of-freedom structure.

The mechanical model of a single-particle impact damper with viscoelastic material attached to a single-degree-of-freedom (SDOF) structure, as shown in Figure 4-1, includes several key parameters:

- M represents the mass of the primary structure.

- k denotes the stiffness of the primary structure.

- x_1 represents the displacement of the primary structure.

- m corresponds to the mass of the particle.

- x_2 signifies the displacement of the particle.

- d indicates the clearance magnitude between the particle and primary mass. The collision occurs when the difference between x_1 and x_2 is equal to d.

- y represents the base motion or excitation applied to the primary structure.

In this model, the stiffness of the viscoelastic material is represented by a complex stiffness term, which accounts for both the elastic and damping behaviour of the material. The complex stiffness can be expressed as a complex number in the form:

$$k_s(\omega) = \nu E_c(\omega) = \nu\big(E_s(\omega) + jE_l(\omega)\big) = \nu E_s(\omega)\big(1 + j\eta(\omega)\big) \qquad (4.1)$$

In this equation:

- ω represents the angular frequency.

- ν is the shape factor related to the geometry of the viscoelastic material.

- $E_c(\omega)$ is the complex modulus of elasticity of the viscoelastic material.

- $E_s(\omega)$ represents the storage modulus of the viscoelastic material.

- $E_l(\omega)$ represents the loss modulus of the viscoelastic material.

- $\eta(\omega)$ is the loss factor, also known as the damping factor, defined as the ratio of the loss modulus to the storage modulus:

$$\eta(\omega) = \frac{E_l(\omega)}{E_s(\omega)} \qquad (4.2)$$

The mechanical behaviour of viscoelastic materials is known to be nonlinear, meaning that their response does not follow a simple linear relationship. One crucial factor affecting their behaviour is the complex shear modulus, which characterizes the material's ability to store and dissipate energy. This complex shear modulus is influenced by two main factors: the vibration frequency and the temperature of the material. In the context of this study, the effect of temperature on the viscoelastic behaviour is considered constant. Consequently, the moduli of the viscoelastic material, which represent its stiffness and damping properties, are exclusively presented as functions of the vibration frequency.

The entire system can be divided into two distinct phases of motion. During the first phase, the particle and primary structure exhibit independent movements, connected only by a frictional connection. However, in the second phase, a direct connection is established between the particle mass and the primary structure through the viscoelastic material. Although this second phase is relatively brief compared to the initial phase, it transforms the entire system

into a two-degree-of-freedom system, with a second mass linked to the primary mass via the viscoelastic material. It is important to note that the second mass often possesses an initial condition, such as an initial velocity, indicating its pre-existing motion before being connected to the primary mass.

The equation of motion of the primary mass and particle shown in Figure 4-1, when the particle is not in contact with the viscoelastic material can be written as,

$$M\ddot{x}_1 + k(x_1 - y) = 0 \qquad (4.3)$$

$$m\ddot{x}_2 = 0 \qquad (4.4)$$

When the particle is in contact with the viscoelastic material, the equations of motion of the primary structure and particle can be written as,

$$M\ddot{x}_1 + k(x_1 - y) + F_c = 0 \qquad (4.5)$$

$$m\ddot{x}_2 - F_c = 0 \qquad (4.6)$$

F_c in equation 4.5 & 4.6 is a nonlinear contact force. Generally, impact force depends on the properties of the impact surface, relative position, and velocity between colliding bodies. The hysteretic damping model with complex stiffness is acausal, although it describes the material appropriately in the frequency domain but cannot be used for time domain simulations, hence an approximate model is required for time domain simulations.

The behavior of viscoelastic material can be highly complicated and its dependence on vibration frequency makes it difficult to model accurately. Therefore, an approximation is needed for numerical analysis. In this study, Voigt model is used to approximate the stiffness and damping component of the viscoelastic material from the complex modulus. Voigt model is commonly used due to its simplicity and direct approach in modelling viscous and elastic behaviors of any viscoelastic material. It consists of a spring element and a dashpot element connected in parallel as shown in Figure 4-2. The spring element represents the material's elastic response, generating a force proportional to the displacement. The dashpot element represents the material's viscous response, generating a force proportional to the velocity. The Voigt model provides a simplified representation of viscoelastic behavior and is commonly

utilized in engineering and materials science to analyze and predict the response of viscoelastic materials under different loading conditions.
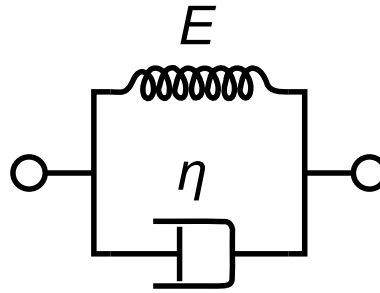
Figure 4-2. Graphical representation of Voigt model

The viscoelastic force from the Voigt model (Zhou et al., 2016) can be determined as,

$$F_c = k_1 H(x_1, x_2) + c_1 G(\dot{x}_1, \dot{x}_2) \qquad (4.7)$$

Here k_1 represents the elastic behaviour or the stiffness of the viscoelastic material. It can be related to the storage modulus of the viscoelastic material as $k_1 = v E_s(\omega)$, which is the real part of the complex modulus. On the other hand, c_1 represents the viscous behavior of the viscoelastic material or the damping and can be related to the loss factor and vibration frequency (f) as $c_1 = v E_s(\omega) \eta / f = k_1 \eta / f$, which is the imaginary part of the complex modulus (Kaul, 2021; Li, 2020; Momani et al., 2021). Utilizing the approximate model to represent the viscoelasticity of impact material, it is possible to analyze the system numerically. $H(x_1, x_2)$ and $G(\dot{x}_1, \dot{x}_2)$ are functions representing the relative positions and velocity between primary structure and particle (Chatterjee et al., 1995; Masri & Caughey, 1966). These functions are defined as,

$$H(x_1, x_2) = (x_1 - x_2 - d)\, U(x_1 - x_2 - d) + (x_1 - x_2 + d)\, U(-x_1 + x_2 - d) \qquad (4.8)$$

$$G(\dot{x}_1, \dot{x}_2) = (\dot{x}_1 - \dot{x}_2) U(x_1 - x_2 - d) + (\dot{x}_1 - \dot{x}_2) U(-x_1 + x_2 - d) \qquad (4.9)$$

$U(x)$ is a commonly used unit-step function known as the "Heaviside". The output of this function is 0 or 1. The step function detects the impact on either side of the boundary during numerical simulations. Furthermore, the natural frequency of the primary structure is defined as,

$$\omega_1 = \sqrt{\frac{k}{M}} \qquad\qquad (4.10)$$
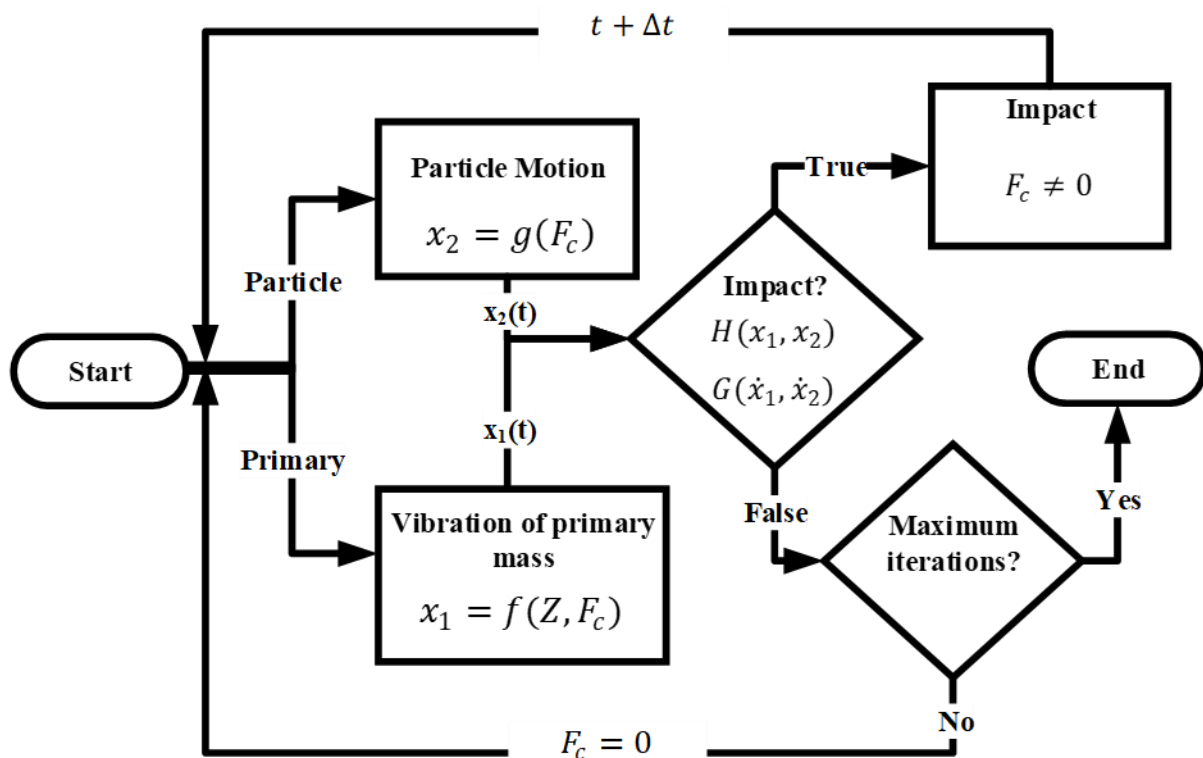
Figure 4-3. Computation process flow chart.

A MATLAB program is written to simulate the system using the equations mentioned before. The flowchart of the computation process is presented in Figure 4-3. First of all, the primary structure vibrates under the influence of ground motion. The motion of particle starts with the impact. The computation algorithm keeps track of the positions of the primary structure and particle, an impact is detected whenever the positions of the primary structure x_1 and particle x_2 satisfy the impact conditions presented in equations 4.8 and 4.9. When the impact is detected on either side of the cavity boundary, the impact force F_c is calculated based on the $H(x_1, x_2)$ and $G(\dot{x}_1, \dot{x}_2)$ and properties of the viscoelastic material ($k_1 - c_1$). Now, the impact force is updated, and the equations of motion are computed again for the next time step under the influence of impact force. A very small-time step is recommended to capture the dynamics precisely; however, higher computational power is required.

4.1.2. Experiment setup

The experiment rig described in Chapter 3 is used here as well. However, a few modifications are made for additional measurements. Two force sensors (B&K 8200) are installed to the either side of the SPID as shown in Figure 4-4. The force sensors are fixed on one end and the other end is towards the particle mass. A compression force is exerted by the particle mass at each collision during the operation of SPID, and the force data is recorded simultaneously with other parameters for further processing. Additionally, the system parameters are same as described in Chapter 3, Table 3-1.
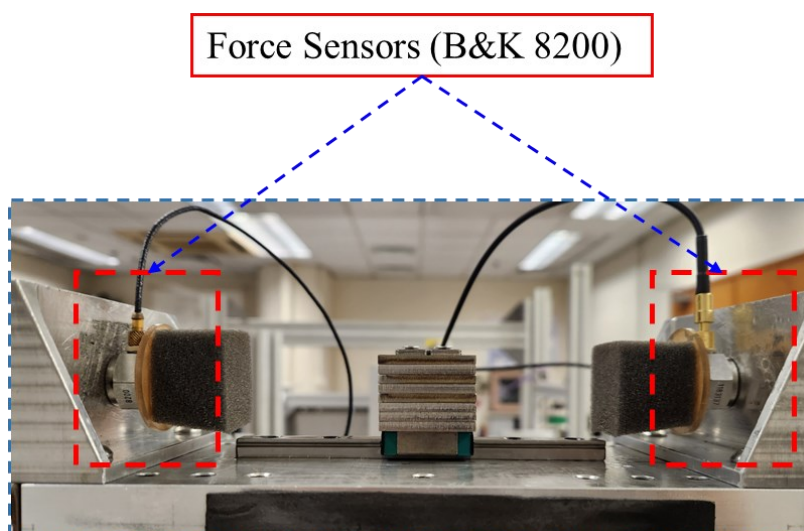
Figure 4-4. Force sensors placement in the experiment rig.

4.1.3. Materials

In this section, the materials assessed in this study are discussed. In order to see the effect of viscoelastic materials on the damping performance of the SPID, a few soft materials exhibiting viscoelastic properties are used and compared with the hard impact where no material deformation is evident. Viscoelastic materials are generally commercially available and have various applications in vibration control (Oyadiji, 1996; Wong et al., 2018). The advantage of using viscoelastic materials is that they are easily available. However, their mechanical properties such as elastic and viscous behaviour are not independent and cannot be selected separately. Their properties are usually dependent on the shape, material, and internal design. They exhibit nonlinear elastic and viscous behaviour generally dependent on the temperature and vibration frequency.

Rubber   Anti-vibration pad   Acrylic Foam   Polyurethane (PU) foam
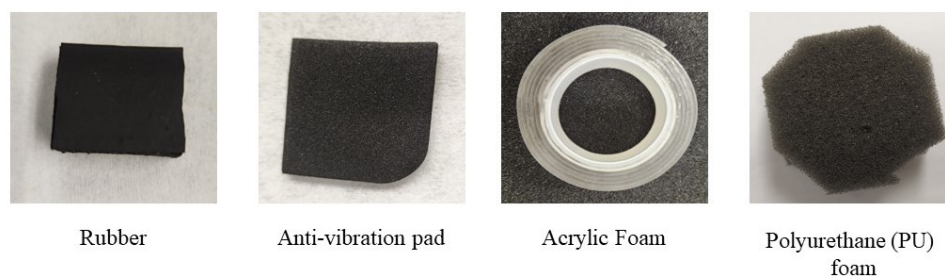
Figure 4-5. Pictures of the viscoelastic materials used in this study.

The materials used in this study are presented in Figure 4-5. Rubber, anti-vibration pad (AVP); AVP is a commercially available material made of ethylene-vinyl acetate (EVA) rubber, acrylic form, and polyurethane (PU) foam exhibit viscoelastic properties and generate soft impacts. On the other hand, the hard impact is achieved by removing the viscoelastic materials from the walls of cavity, so that the particle mass hits the metallic walls.

In general, the mechanical properties of viscoelastic materials are dependent on the vibration frequency and temperature. However, the effect of temperature is assumed to be constant and therefore, the properties are determined in the frequency domain only. The viscoelastic properties (storage modulus E_s, loss modulus E_l, loss factor η) are determined by performing dynamic mechanical tests through a dynamic mechanical analyser (DMA- Mettler Toledo DMA1). The DMA testing machine has a limit for the sample size at (6 mm x 10 mm), therefore, the materials are cut according to the requirements. Additionally, the machine can apply a maximum force of 10 N and maximum displacement of 400 micrometres. It allows the user to choose the test type either by displacement or force; the one selected will be applied to the sample and the other one will be fixed. These tests are performed by displacement with a fixed force of 5 N.

The dynamic tests display the viscoelastic properties of the materials, as shown in Figure 4-6. The four viscoelastic materials evaluated are rubber, anti-vibration pad, acrylic foam, and polyurethane (PU) foam. Storage modulus, loss modulus, and loss factor are measured through DMA tests in the frequency domain at room temperature. Storage modulus is referred to as the elastic response of the material while the loss modulus is the viscous response of the material over the frequency span (Henriques et al., 2020). The loss factor is the measure of material damping and is defined as the ratio of loss modulus and storage modulus. Figure 6 shows that polyurethane (PU) foam has a lower magnitude of storage and loss modulus. On the other hand,

acrylic foam exhibits a higher loss factor with larger storage (elastic) and loss (viscous) moduli. It is worth noting that the elastic and viscous properties of the viscoelastic materials are interlinked and are not independent.
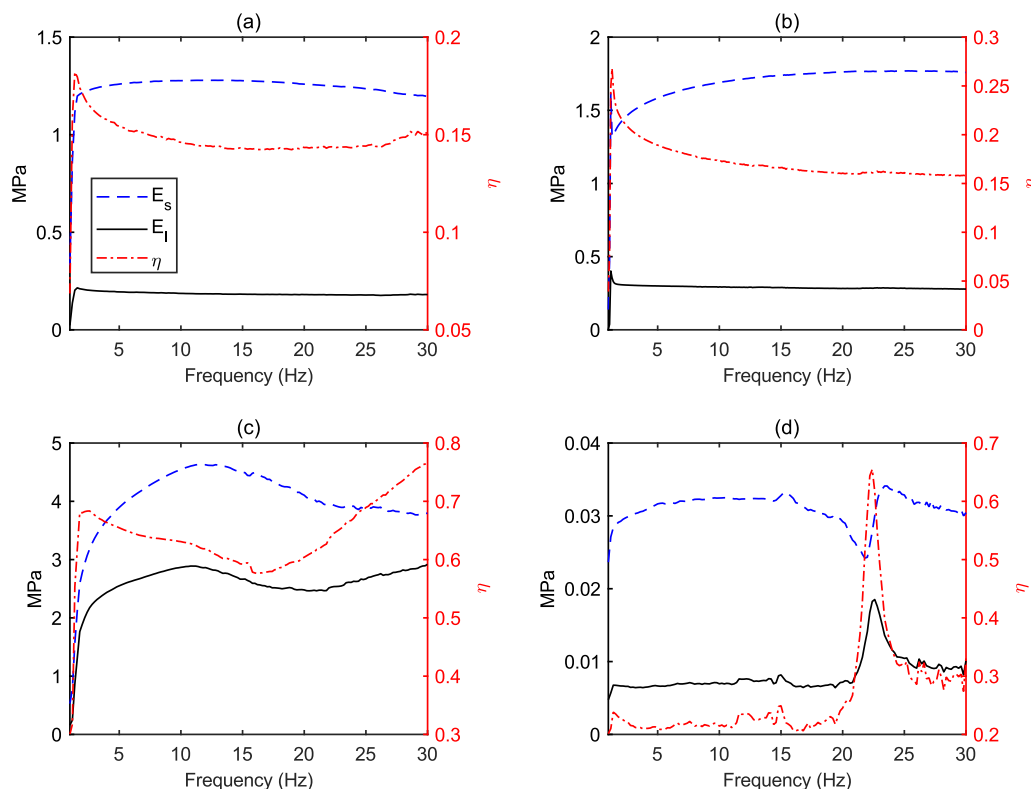
Figure 4-6. Viscoelastic properties from DMA tests; (a) Rubber; (b) Anti-vibration pad; (c) Acrylic Foam; (d) Polyurethane (PU) foam

Moreover, the change in the material properties in frequency domain is not very marked, especially at low frequency vibrations showing the system equivalent to a material with constant hysteretic damping, which is not frequency dependent. Hence Voigt model can approximate the material response very well. Therefore, Voigt model (Figure 4-2) describes the elastic effect with storage modulus and shape factor $(k_1 = \nu E_s)$, while the viscous part is represented by elastic part and loss factor $(c_1 = \nu E_s \eta / f = k_1 \eta / f)$. Here, the viscoelastic factors such as E_l and η are selected from Figure 6 according to the natural frequency of the system.

Furthermore, the shape factor (sometimes called the geometry factor) may directly influence the response of the viscoelastic materials. As the name states, the shape factor

depends on the geometry or shape of the viscoelastic material and it can be calculated as $\nu = \frac{A}{L}$ for rectangular shape and $\nu = \frac{\pi D^2}{4L}$ for cylindrical shape; Here L is the length, A is the area, and D is the diameter in the case of a round sample.

4.2. Results and discussion

In this section, the results are presented for both numerical and experimental analysis. The key observations are discussed from the numerical results and the conclusions drawn from numerical analysis are validated through experiments.

4.2.1. Numerical Analysis

The theoretical model of a single-degree-of-freedom structure with a SPID is presented in Section 4.1.1. The model is simulated with the Runge-Kutta 4th-order method. There are various important parameters that can affect the performance of a SPID such as viscoelastic properties, relative clearance magnitude and mass ratio. It has been identified that the relationships of these design parameters are inter-linked, therefore, a contour map is simulated to observe the effect over several combinations.

Figure 4-7 demonstrates how vibration amplitude changes across several combinations of important design parameters such as, relative clearance and properties of the viscoelastic materials. The first contour (Figure 4-7a) shows the resonant vibration amplitude over various combinations of relative clearance and storage modulus, while keeping the loss factor constant at 0.2. It can be observed from Figure 7 that the role of storage modulus of viscoelastic materials is minor in the damping performance of SPID. However, the clearance magnitude is observed to be the critical parameter for the design of SPID. On the other hand, Figure 4-7b shows the contour map between several combinations of relative clearance magnitude and loss factor while keeping the stiffness $[\nu E_s]$ constant at 1000 N/m. Similarly, it can be observed that the relative clearance magnitude is a critical parameter.
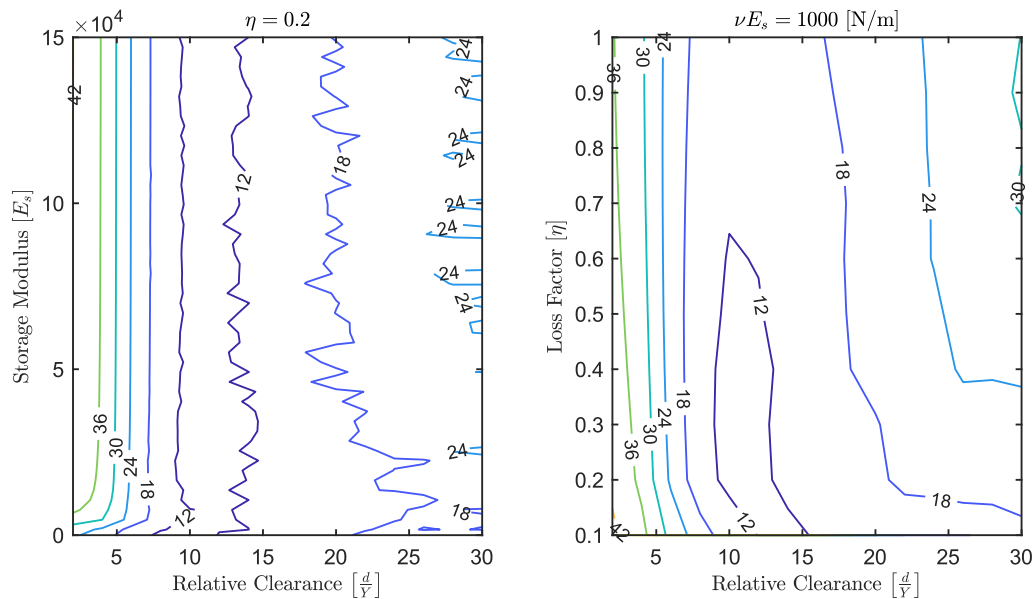
Figure 4-7. Contour of resonant vibration amplitude over various combinations of relative clearance $\left[\frac{d}{Y}\right]$, stiffness$[\nu E_s]$, and loss factor $[\eta]$.

As the influence of viscoelastic properties is minimal for the design of SPID, the impact force can be reduced with viscoelastic materials. The impact force depends on the viscoelastic properties (elastic + viscous). Therefore, the impact force and noise produced during the operation of a SPID can be reduced by introducing a soft material at the walls of the container without degrading the damping performance. Three different relative clearance magnitudes are assessed with the soft materials and compared with a hard impact. The selected parameters of each viscoelastic material for numerical analysis are presented in Table 4-5.

Table 4-5. Viscoelastic properties selected for numerical simulations for soft impact.

Material	νE_s [kN/m]	Loss Factor (η)
Rubber	43.436	0.164
Anti-Vibration Pad	51.636	0.209
Acrylic Foam	112.43	0.683
Polyurethane Foam	1.0249	0.224

Steel does not show viscoelastic behaviour; however, it should have an extremely high stiffness and small viscous effect in comparison with the viscoelastic properties of these soft materials. The numerical model described for viscoelastic materials cannot represent the behaviour of steel, therefore, the damping performance of steel in the SPID for hard impact is only measured through experiments and compared with the soft impacts.

Figure 4-8 illustrates the vibration response of the structure with different clearance magnitudes and various viscoelastic materials. The numerical results indicate that the choice of material for soft impact has a minimal impact on the vibration response. PU foam has the lowest stiffness (storage modulus) among all the tested materials, resulting in enhanced energy dissipation and slightly improved damping performance. Interestingly, the vibration response remains relatively consistent across all tested materials.
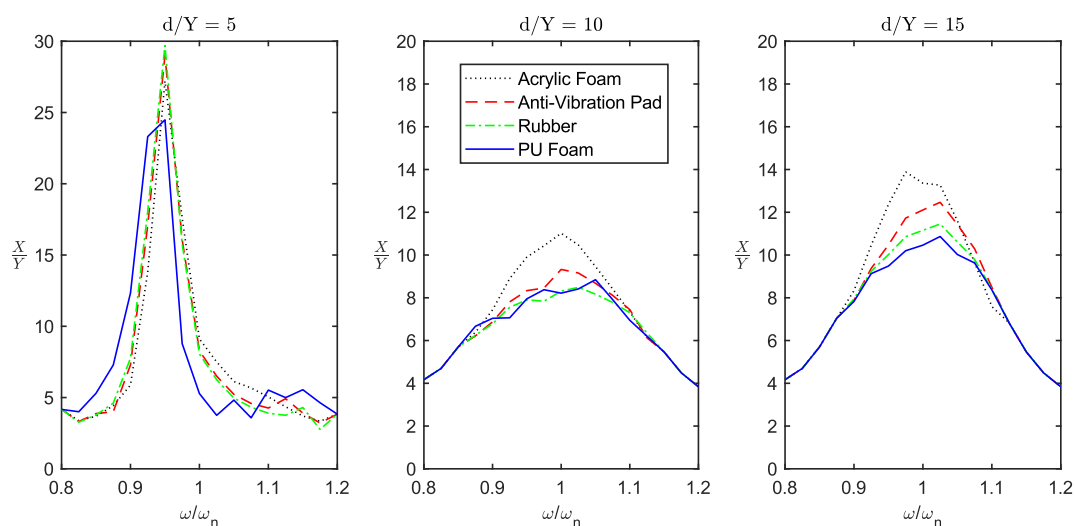
Figure 4-8. Simulated resonant vibration amplitude at different clearance magnitudes with soft materials.

The findings indicate that the choice of material has a minimal impact on the vibration response, except in the case of PU foam when the relative clearance magnitude is 5 or 15. PU foam exhibits the lowest stiffness (storage modulus) among all the tested materials, resulting in enhanced energy dissipation and improved damping performance. Interestingly, the vibration response remains relatively consistent across all tested materials, except for acrylic foam when the relative clearance magnitude is 10 and 15. The acrylic foam (AF) is relatively stiffer than the other tested materials.

Overall, it can be concluded that the choice of material for soft impact has less influence on the performance of a SPID. On the other hand, clearance magnitude is clearly the most influential and important design parameter for a SPID. The freedom in the choice of material in SPID allows for resolving other issues related to SPID in literature. High-intensity impact force and excessive noise are commonly mentioned problems associated with SPID. These problems can be resolved by employing a soft material (PU foam) at the walls of the cavity in

SPID without compromising the damping performance. The softer material enhances the damping performance as well.

4.3. Experimental validations

In order to further validate the conclusions from the numerical analysis, experiments are conducted on a single-degree-of-freedom structure with a SPID with different materials.
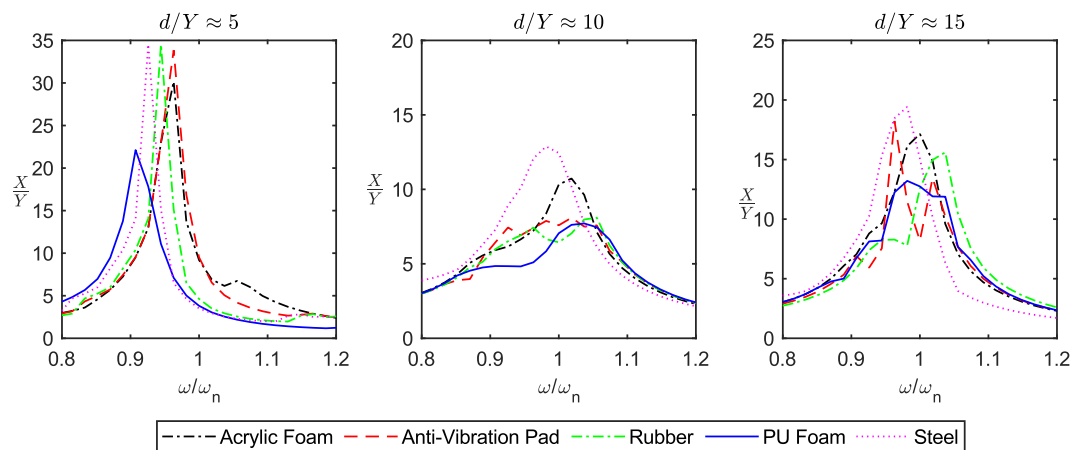
Figure 4-9. Resonant vibration amplitude recorded from experiments with soft and hard impact in SPID over different clearance magnitudes.

Figure 4-9 shows the vibration amplitude of the primary structure with different clearance magnitudes. In the experimental analysis, a rigid material (steel) is evaluated alongside viscoelastic materials for comparison of hard and soft impact features. The results show a similar trend found in the numerical analysis for viscoelastic materials shown in Figure 4-8. However, it can be observed that there is a difference in damping performance with soft and hard impacts. The soft impacts (PU foam) in the SPID reduce vibration amplitude by 36%, 40% and 32% compared with hard impact (Steel) for relative clearance magnitude of 5, 10, and 15, respectively.

Table 4-6. Comparison of experimentally recorded and simulated vibration amplitude ratio over different clearance magnitudes of SPID.

$\dfrac{d}{Y}$	Acrylic Foam		Anti-Vibration Pad		Rubber		PU Foam		Steel
	Exp.	Sim.	Exp.	Sim.	Exp.	Sim.	Exp.	Sim.	Exp.
5	30.16	27.19	33.84	28.99	34.52	29.70	22.11	24.48	34.52
10	10.73	11.01	8.09	9.32	8.09	8.41	7.71	8.84	12.87
15	17.15	13.88	18.46	12.46	15.60	11.45	13.21	10.86	19.41

These findings support the initial hypothesis that a hard impact enhances the momentum exchange between the primary mass and the particle with minimal energy dissipation. In contrast, a softer impact achieves a balance between momentum exchange and energy dissipation through material deformation and internal complex structure. It becomes apparent that when a hard impact occurs between the primary structure and the particle, the impact force and noise during operation will be higher. Conversely, a softer impact leads to minimal noise, lower impact force, and better damping performance. Furthermore, the vibration amplitude ratio of SDOF structure is compared in Figure 4-9 gathered from simulations and experimental data. The comparison shows that there is a good qualitative agreement between simulations and experimental data.
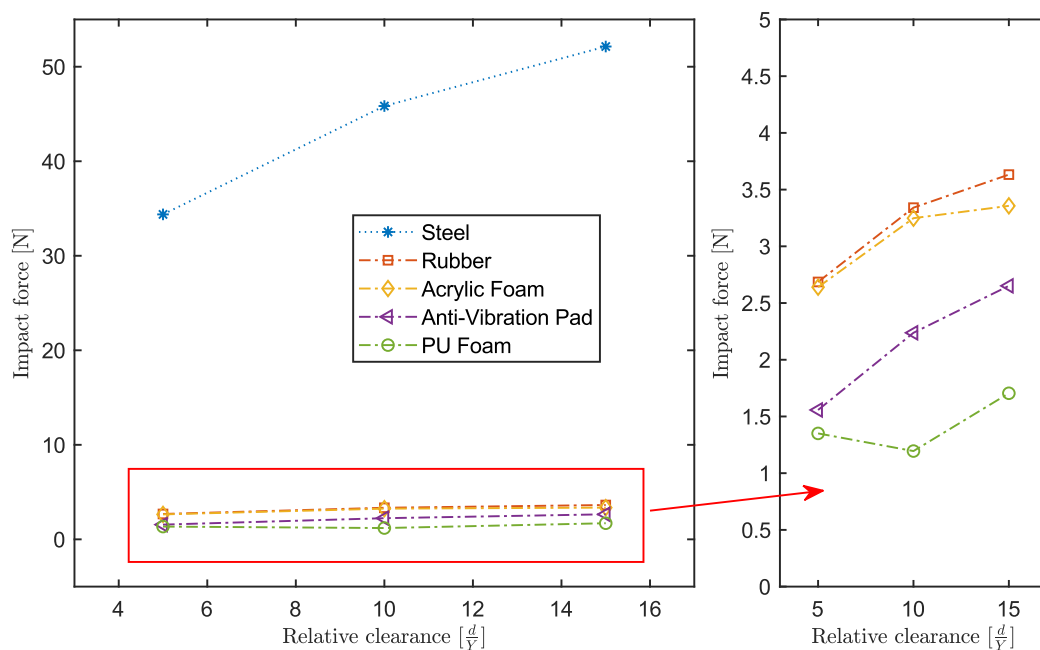
Figure 4-10. Impact force exerted on primary structure from SPID with different impact materials.

In order to verify the reduction in impact force exerted on primary structure, two force sensors are installed on either wall of the cavity in a SPID. The impact force data is recorded for each impact material and compared in Figure 4-10. Maximum impact force for a specific setting of SPID is determined from the dataset. The results show that the maximum impact force exerted on the primary structure is reduced significantly by installing a viscoelastic material in SPID. The impact force is reduced by 96%, 97%, and 96% for relative clearance magnitudes of 5, 10, and 15 respectively by using PU foam instead of rigid plastic. It shows

that a soft impact absorbs the impact force due to material deformation and the internal structure of the viscoelastic materials. However, a rigid material such as steel transfers the impact force to the primary structure and repeated intense impact force can be harmful for structures.
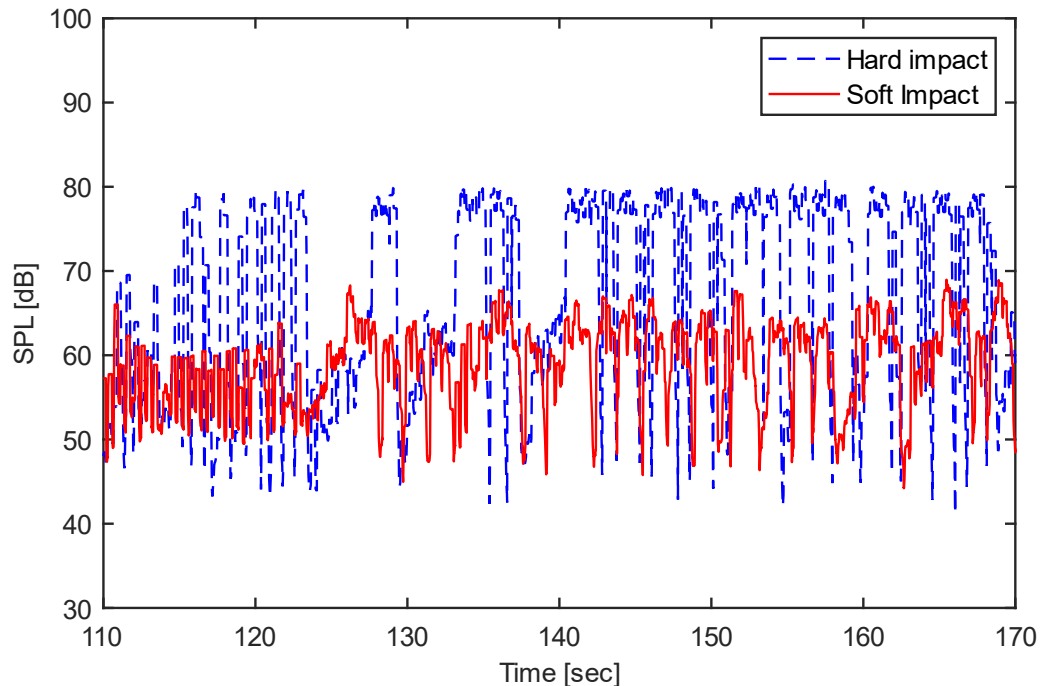
Figure 4-11. Recorded noise level [dB] during the operation of SPID at resonance with soft (PU foam) and hard impact (Steel).

One of the key problems associated with SPID is the high noise levels during operation. Apparently when a metallic particle is colliding with a metallic surface of cavity in SPID, it generates continuous high intensity noise, and this continuous hitting noise can be uncomfortable for the living beings around. In order to show the noise generated with the proposed SPID with soft impact, the noise during the experiments with soft and hard impact are recorded with a B&K free filed microphone (Type 4189). The audio data from microphone provides sound pressure levels in Pascal (Pa) units. This audio data is processed with a MATLAB Audio Toolbox to determine the sound pressure level (SPL) in decibel units at resonance. The results are presented in Figure 4-11, and it can be seen that the hard impact has peaks whenever there is an impact between particle and primary structure. The hard impact shows a maximum noise level of 80.88 dB, while the maximum noise level with soft impact is calculated as 69.33 dB. The results show that a SPID with soft impact does not generate any

significant noise to pollute the surroundings, while a SPID with hard impact can raise the noise levels by almost 11.55 dB.

4.4.   Conclusions

In conclusion, this chapter focused on addressing the challenges associated with the SPID by integrating soft-impact materials to mitigate larger impact forces and noise levels. The main findings of this chapter are:

1. The working principle of SPID is based on momentum transfer and energy dissipation through various impacts between primary structure and particle mass. Therefore, the nature of impact directly influences the momentum transfer and energy dissipation. A hard impact involving rigid surface has higher momentum transfer and less energy dissipation during impact. On the other hand, a soft impact provides increased energy dissipation due to the deformation of viscoelastic materials while momentum transfer is relatively decreased.

2. The numerical and experimental results show that a soft impact can reduce the vibration amplitude by 40 % compared with a hard impact. However, the difference in damping performance with tested viscoelastic materials is found to be minimum.

3. Integrating viscoelastic material resolves the common issues related with the SPID such as high-intensity impact force and noise levels. In order to observe the reduction in impact force, force sensors are installed at the walls if cavity in SPID. The results show a significant 96% reduction in impact force with a soft impact.

4. The experiments with soft and hard impacts are recorded and processed to determine the sound pressure levels (SPL). The results show that a SPID with soft impact does not generate any noise pollution during operation, while a SPID with hard impact increases the noise level by around 11.55 dB during operation.

These findings highlight the potential of viscoelastic materials in mitigating high-impact forces and noise levels in SPID, while improving the damping performance. Viscoelastic materials evaluated in this study are commercially available materials, therefore, an effective and safe SPID can be designed and installed easily. Compared with a multi-particle impact damper, a SPID is significantly easier to design and install as the design parameters are

consistent and the nonlinearities are less. However, high-intensity impact force and noise were the major issues related with SPID, but these results provide a basis for the SPID design and further advancements for optimal design and performance.

4.5.   Summary

In this chapter, the focus is on expanding the understanding and addressing the challenges associated with the single-particle impact damper (SPID). While SPID offers advantages such as simplicity in design and installation, it also presents critical issues that can impact the integrity of the primary structure. One prominent issue is the presence of larger impact forces resulting from the concentrated mass of the single particle. These impact forces transfer high-intensity stresses to the primary structure, which can be particularly problematic for weak or vulnerable structures. Additionally, the use of SPID can lead to higher levels of noise during operation, which can be undesirable in practical applications.

By introducing viscoelastic materials at the point of impact between the particle and the primary structure, the aim is to minimize the impact forces and reduce the noise levels while maintaining the damping performance of the SPID. To investigate the effects of hard and soft impacts on the damping performance, numerical simulations are conducted. A numerical model is developed, considering the viscoelastic behaviour of the soft materials. The dynamic mechanical properties of four different viscoelastic materials are characterized through dynamic mechanical analyser (DMA) tests. These properties, including frequency-dependent mechanical behaviour, are then used in numerical simulations.

The results of the numerical simulations indicate that the use of a softer impact material leads to an improvement in damping performance. These findings are further validated through experimental tests, where there is good agreement between the numerical and experimental results. To quantitatively measure the reduction in impact force, force sensors are installed at both ends of the cavity in the SPID. Forced vibration experiments are conducted to verify the impact force reduction achieved by utilizing soft materials. The results demonstrate a significant reduction of 96% in the impact force when employing a soft material in the single-particle impact damper. The results show that a SPID with soft impact does not generate any noise pollution during operation, while a SPID with hard impact increases the noise level by around 11.55 dB during operation.

Chapter 5

A hybrid damper with a tunable single-particle impact damper and Coulomb friction

This chapter presents a novel approach to improve the performance of a single-particle impact damper in structural vibration control applications. While a single-particle impact damper possesses advantages such as simpler design, easier installation, and a wider frequency range compared to a tuned mass damper (TMDs), they are often unable to achieve vibration suppression levels comparable to an optimally tuned mass damper. This limitation has stalled the general adoption of single-particle impact dampers in structural vibration control applications.

Friction dampers offer advantages such as a larger damping force-to-mass ratio compared to other commonly used passive dampers and cost-effectiveness. However, their design involves non-linear phenomena, with stick-slip behaviours and non-linearity being the main challenges to resolve. The stick-slip phenomenon occurs when the excitation force is insufficient to overcome static friction. Considering the various challenges associated with FD and ineffectiveness at resonance, it is usually combined with other dampers (Hundal, 1979; Mansour & Filho, 1974; Sun et al., 2022; Xia et al., 2021; Ziaee & Hejazi, 2023) to mitigate these challenges and enhance their effectiveness in vibration control applications.

The proposed hybrid damper supplements the advantages of both SPID and FD to improve their damping capacities. The FD contributes a larger damping force, which can be particularly useful for reducing vibration amplitudes in large structures. While friction dampers are theoretically considered ineffective at resonance, researchers have demonstrated in practical applications that they can reduce resonance peaks due to the presence of internal damping in structures.

This chapter presents a numerical model that simulates the response of a single-degree-of-freedom (SDOF) structure equipped with the hybrid damper in both free and forced vibrations. Additionally, a parametric analysis is conducted to establish an optimal design methodology for the hybrid damper in various vibration scenarios. Furthermore, a prototype of the hybrid damper is constructed to validate the numerical model and verify the efficacy of the

71

proposed design. By intelligently designing and implementing the hybrid damper, the chapter demonstrates how the combination of SPID and FD can overcome their respective constraints and improve the overall damping capacity and vibration suppression performance. This approach has the potential to enhance the effectiveness of a single-particle impact damper and make it a viable option for structural vibration control applications.

5.1. Methodology

5.1.1. Numerical model

The numerical models for both the single-particle impact damper (SPID) and the hybrid damper, which combines the SPID and FD are developed. Figure 5-1 illustrates the mechanical model of the single-degree-of-freedom (SDOF) structure equipped with a single-particle impact damper. In this model, the spring constant is denoted by k, representing the stiffness of the system, while c represents the viscous damping coefficient that characterizes the internal damping of the structure. The primary structure's mass is denoted as M, and the mass of the particle is represented by m. It is important to note that the particle has a maximum travel distance of $2d$, and when it reaches this boundary, it collides with the primary structure.
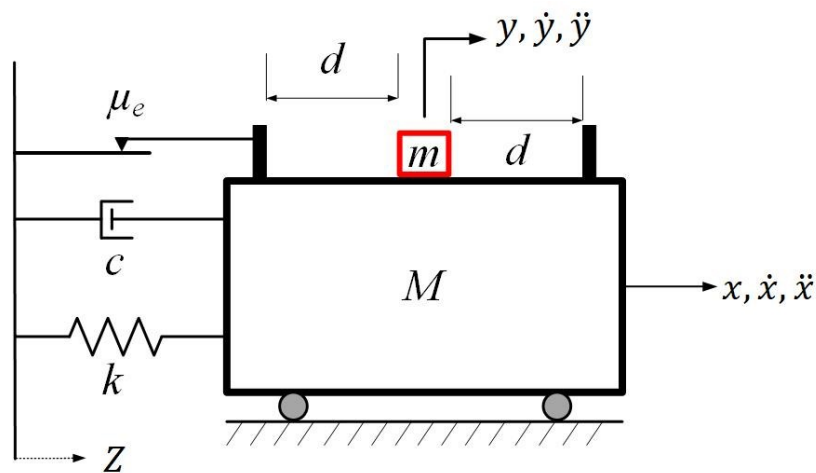
Figure 5-1. A model of a single-degree-of-freedom system with a hybrid damper.

Disregarding friction within the single-particle impact damper (SPID), the equation of motion for the primary structure, before any impact between the particle and the structure has occurred, can be expressed as follows,

$$M\ddot{x} + c(\dot{x} - \dot{z}) + k(x - z) + F_f \, \text{sgn}(\dot{x} - \dot{z}) = 0 \tag{5.1}$$

Here $F_f = \mu_e F_N$ is the friction force. The sgn is the signum function, which is defined as,

$$\text{sgn}(\dot{x} - \dot{z}) = \begin{cases} -1 & \text{if } \dot{x} - \dot{z} < 0 \\ 0 & \text{if } \dot{x} - \dot{z} = 0 \\ 1 & \text{if } \dot{x} - \dot{z} > 0 \end{cases} \tag{5.2}$$

The equation of motion of the particle can be written as

$$m\ddot{y} = 0 \tag{5.3}$$

A collision happens when the difference between the displacement of the primary mass and particle is equal to the clearance magnitude.

$$|x(t) - y(t)| \geq d \tag{5.4}$$

The numerical simulation method described in Chapter 3 is used in this chapter as well. However, the equation of motion of the primary structure is slightly different. The equation in Chapter 3 includes the internal friction (between primary mass and particle mass) while the equation of motion in this chapter includes the external friction (primary mass only). The remaining of the simulation method is similar to the one explained in Chapter 3.

5.1.2. Experiment setup

The experiment rig used in this Chapter is same as explained in Chapter 3. However, a friction damper is installed in addition to the experiment setup used in Chapter 3. A friction damper (FD) with tunable friction is integrated into the structure. Figure 5-2 shows the setup of the friction damper. The friction damper consists of a metal block that applies friction force to one side of the primary structure. To ensure the structure's shape remains unchanged when the friction force is applied, linear guide bearings are installed on the opposite side of the structure. These guide bearings prevent any distortion or torsional motion of the structure during the application of friction force. The normal force in the friction damper can be adjusted by loosening or tightening the spring using a bolt and lock nut, as depicted in Figure 5-2.

The friction force in the FD explained can be controlled with the spring extension or compression. The nut at the end can be loosened or tightened to control the friction force

exerted on the primary structure. Additionally, a force sensor is installed between the metallic block touching the primary structure and spring. This sensor records the compression force during the operation for the comparison of different compressions of the spring. It can be difficult to estimate the exact friction force or coefficient of friction between the block and primary structure due to many nonlinearities. Therefore, force sensor data is used only for the comparison of friction force for simplicity.
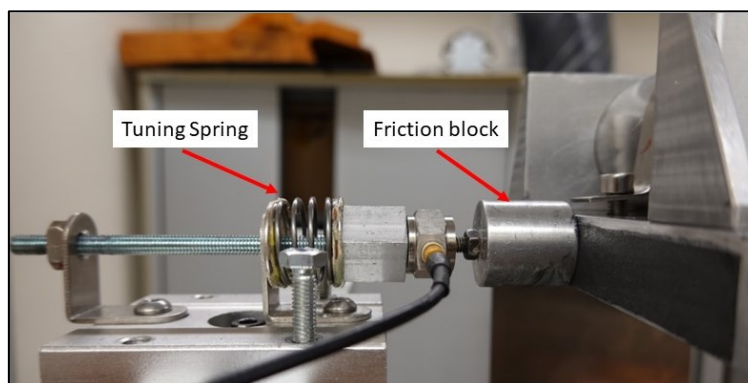
Figure 5-2. A model of a tunable friction damper (FD) connected to the structure.

5.2. Results and discussion

In this section, the results from both numerical and experimental analyses regarding the suppression of primary structure amplitude vibrations are presented and discussed. The performance of a single-particle impact damper (SPID) and a friction damper (FD) is examined separately, considering various design combinations. The numerical results are compared and validated against the experimental data obtained from the physical prototypes. Moreover, the performance of the proposed hybrid damper, which combines both SPID and FD designs, is investigated and compared to that of the traditional tuned mass damper (TMD). The hybrid damper's effectiveness in suppressing vibrations is assessed based on both numerical simulations and experimental testing.

5.2.1. Free Vibrations

Consider an SDOF structure with a single-particle impact damper (SPID) with $\mu_e = 0$, $c = 0$ and $Z = 0$, as shown in Figure 5-1. The mathematical model of free vibration of the mass M and m can be written as,

$$M\ddot{x} + kx = 0 \tag{5.10}$$

Solution for the free vibration response of the system due to an initial displacement x_0 or velocity $\dot{x}_0$ of mass M can be written as,

$$x(t) = x_0 \sin(\omega_n t) + \frac{\dot{x}_0}{\omega_n} \cos(\omega_n t) \tag{5.11}$$

Similarly, the equation of motion of a particle mass can be written as,

$$m\ddot{y} = 0 \tag{5.12}$$

The solution of the equation (5.12) for particles can be obtained as,

$$y(t) = \int_{t_n}^{t_{n+1}} \dot{y}_0 \, dt \tag{5.13}$$

where t_n and t_{n+1} is the time of the nth and $(n+1)^{th}$ impacts respectively between primary structure M and a particle m. Likewise, If the structure is excited by a base motion (z), the equation of motion of the primary mass and particle can be written as,

$$M\ddot{x} + k(x - z) = 0 \tag{5.14}$$

$$m\ddot{y} = 0 \tag{5.15}$$

The response of the SDOF structure to a ground impulse is investigated as well. This impulse refers to a sudden displacement input applied at the base of the structure, simulating an impulse function. The impulse is used to initiate free vibrations in the SDOF structure and observe its response behaviour. As the aim is to investigate the common scenarios for free vibration initiation and impulse is a sudden ground motion experienced by structures are machines due to a sudden bump or aftershocks during earthquakes, therefore impulse is studies as well here. Figure 5-3 displays the impulse provided to the SDOF structure. This figure illustrates the magnitude and duration of the impulse displacement that is applied to the base of the structure.
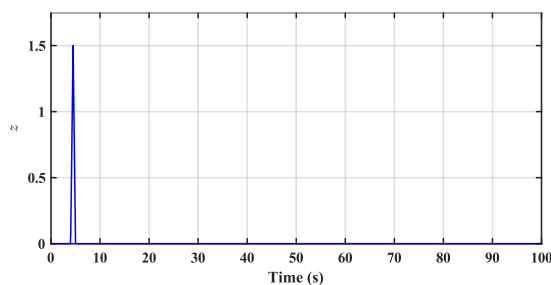
Figure 5-3. Impulse z (m) used as a base motion to excite the SDOF structure.

In Figure 5-4, the free vibration response of the SDOF system due to initial conditions and ground impulse is illustrated. The head-on collisions between the SDOF system and the single-particle impact damper (SPID) during the duration denoted as t_1 are observed to provide efficient energy dissipation. As a result, the amplitude of the mass M reduces significantly in both cases considered. The collisions occurring during t_1 contribute to a sharp decrease in the vibration amplitude of mass M. In contrast, during the duration denoted as t_2, the collisions between the primary mass and the particle resemble overtaking collisions. In this case, the energy dissipation of mass M slows down swiftly, resulting in a much smaller decrease in the vibration amplitude. The amplitude reduction achieved during t_2 is only a few percent compared to the 85% reduction observed during t_1.
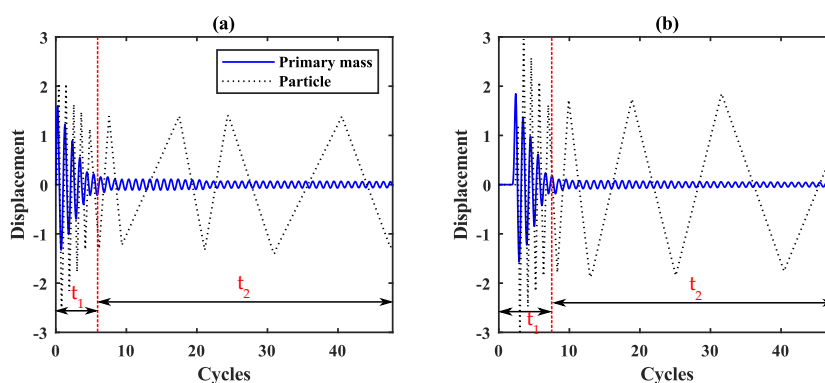
Figure 5-4. Displacement (m) of the primary structure and particle; (a) because of initial condition. $\dot{x}_0 = 5$ m/s, $d/x_{max} = 0.8$, $e = 0.3$; (b) due to base excitation $d/Z = 1.1$, $e = 0.4$

Figure 5-4 also reveals that there are approximately four highly damped cycles within t_1. After these cycles, the subsequent cycles exhibit extremely low damping within the simulated time limit. This observation suggests that energy dissipation during t_1 is highly effective initially but becomes less efficient over time. Another important parameter to consider is the

impact frequency. During t_1, the impact frequency in the SPID is close to the vibrating frequency of mass M, contributing to more effective damping. However, during t_2, the impact frequency significantly decreases, leading to less efficient damping.

In Figure 5-5, the addition of a small external friction damper combined with a single-particle impact damper to the primary system is shown as a means to eliminate the free vibrations of mass M.
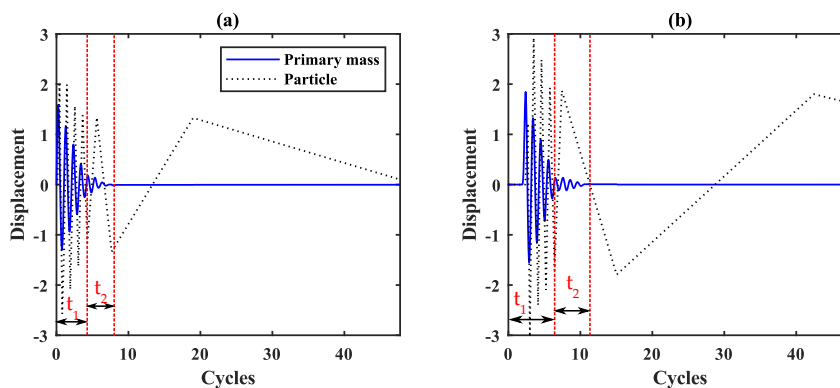
Figure 5-5. Displacement (m) of the primary structure and single particle with friction damper $\beta = 0.1$; (a) due to initial velocity. $\dot{x}_0 = 5$ m/s, $d/x_{max} = 0.8$, $e = 0.3$, $\mu_e = 0.01$; (b) $d/Z = 1.1$, $e = 0.4$, $\mu_e = 0.01$

The results indicate that the performance of the single-particle impact damper (SPID) can be enhanced by incorporating a small amount of friction in the system. However, it should be noted that a friction damper requires a larger friction force to function properly. When a larger friction force is applied, various nonlinear phenomena may occur. These nonlinear effects can introduce complexities in the system's behaviour. Additionally, a friction damper can be sensitive to environmental conditions. Factors such as temperature, humidity, and the presence of contaminants can affect the performance and reliability of friction dampers.

In the experimental model explained in Section 5.1.1, the free vibrations of the primary structure are initiated by an initial displacement (35 mm) to the primary mass similar to that used in Chapter 3. The resulting response of the primary mass, denoted as (x/x_0), is recorded. In Figure 5-6, the recorded displacement response of the primary mass with different damper settings is presented. The three tested configurations include the friction damper (FD) only, the single-particle impact damper (SPID) only, and the hybrid damper. The graph demonstrates that there is a large difference in damping when the SPID is combined with the external FD.

The addition of the friction damper to the system enhances the damping performance, resulting in a more rapid decay of the vibration amplitude of the primary mass. The friction force, denoted as F_{fe}, is measured from the force sensor added to the friction damper.
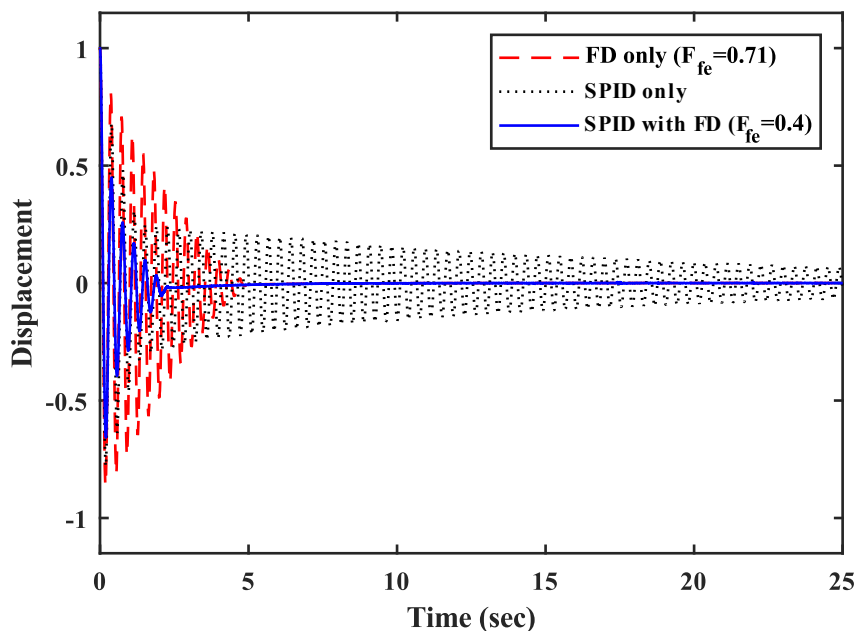
Figure 5-6. Normalized displacement (x/x_0) of the primary structure with different dampers.

Initially, the SPID shows superior damping in the few cycles due to its dependence on the vibration amplitude. As the vibration amplitude is higher, the damping provided by the SPID is also larger. However, as the vibration amplitude decreases to a certain level, the damping provided by the SPID becomes extremely low or non-existent. This can be attributed to the reduction in impacts between the primary mass and the single particle as the amplitude decreases. Consequently, the SPID becomes less effective in further reducing the vibration amplitude beyond a certain point.

In contrast, the FD provides a constant damping force regardless of the vibration amplitude. Therefore, it takes a longer time for the FD to reduce the vibration amplitude in the first phase compared to the SPID. The constant damping force of the FD ensures a consistent level of damping throughout the vibration response. The proposed combination of the SPID and the FD takes advantage of the complementary characteristics of both damping

technologies. By combining the SPID's initial high damping with the constant damping force of the FD, the overall damping performance is improved.

5.2.2. Forced vibrations.

This section focuses on the results acquired from numerical simulations and experiments, particularly regarding the performance of the single-particle impact damper (SPID), friction damper (FD) and hybrid damper in the time and frequency domains. During the experiments, a sinusoidal ground motion is applied at the base of the SDOF structure to excite the system. It is observed that the operation of the SPID varies with time, and the damping characteristics may change over the time domain. This behaviour is recognized because the damping of the SPID depends on the occurrence of impacts between the primary mass and the single particle. As a result, the damping provided by the SPID may vary throughout the response.

The time-history displacement response of the primary mass shows an initial increase in amplitude due to the absence of impacts, followed by a steady-state amplitude after the first peak when consistent impacts occur. This behaviour highlights the importance of allowing the system to vibrate for an appropriate number of cycles at each excitation frequency when evaluating the performance of the SPID. General frequency sweep tests may not accurately capture the damping properties of the SPID unless the system vibrates for a sufficient duration. To precisely measure the frequency response of the structure with a SPID, the experiments are conducted over a range of excitation frequencies around the natural frequency of the primary mass. Separate experiments are performed at each excitation frequency, and the steady-state vibration amplitude at each frequency is measured. The resulting data from all frequencies are then combined to form a frequency response curve.

The experiments are conducted on the SDOF primary structure with three different configurations: SPID only, FD only, and SPID combined with FD. By evaluating the frequency response of each configuration, the effectiveness of the SPID, FD, and their combination can be analysed.

5.2.2.1.   *Single-particle impact damper (SPID)*

In this section, the performance of the single-particle impact damper (SPID) is investigated with an SDOF structure through numerical simulations and experimental

validation. In the experiments, the total cavity length of the SPID varied at three different settings: 15mm, 45mm, and 75mm. These settings allow for investigating the influence of the cavity length on the damping performance of the SPID. To validate the accuracy of the numerical model used in the simulations, simulations are executed with similar parameters as those in the experiments.
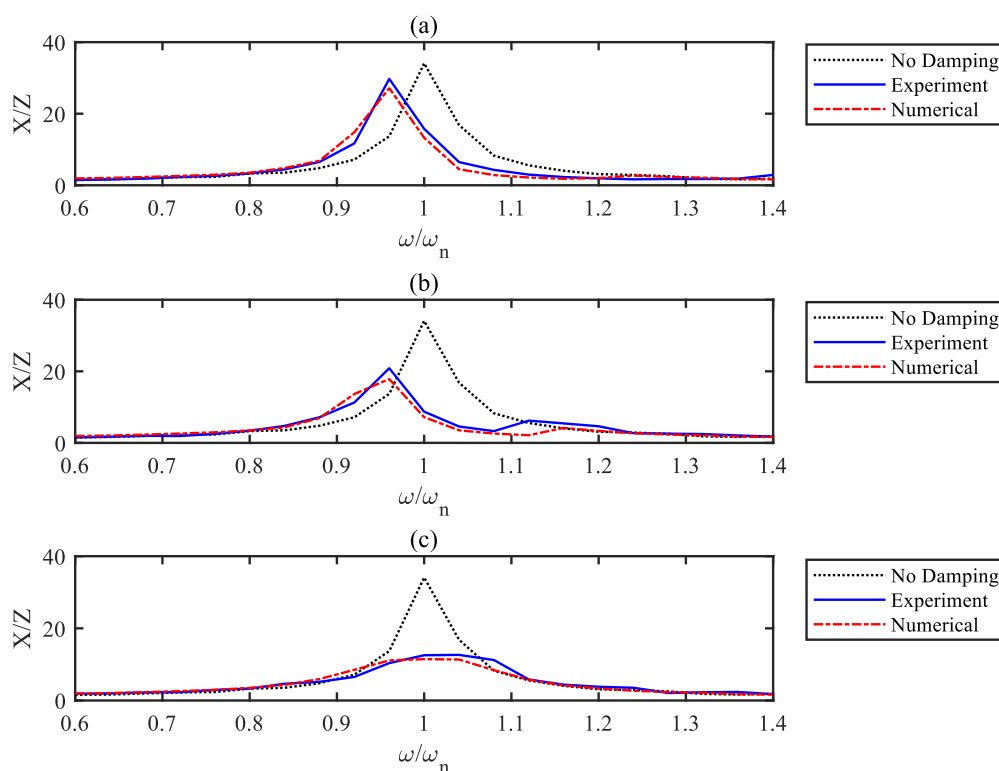
Figure 5-7. Experimental and computed response of the primary structure;
(a) d = 7.5 mm; (b) d = 22.5 mm; (c) d = 37.5 mm.

Figure 5-7 presents the frequency response of the primary system obtained from both experiments and simulations. The results highlight the influence of the clearance magnitude (d) in the single-particle impact damper (SPID) design on the damping characteristics. In Figure 5-7a, it is observed that a smaller clearance magnitude (d = 7.5 mm) leads to lower damping. This can be attributed to the limited space available for the particle to gather momentum before impact. As a result, the impact forces are reduced, leading to lower damping in the system. On the other hand, increasing the clearance magnitude in the SPID design improves the damping performance. Figure 5-7c demonstrates that the displacement ratio

(X/Z) is minimized at the resonance frequency when the SPID with a clearance magnitude of $d = 35.5$ mm is assessed. This indicates that the system achieves better vibration suppression and damping effectiveness at this particular clearance magnitude. These results highlight the presence of various nonlinear phenomena in the behaviour of the SPID, leading to differing opinions regarding its optimal design. The contradictory findings indicate the complexity of the SPID's behaviour and the challenges associated with determining an optimal design method.
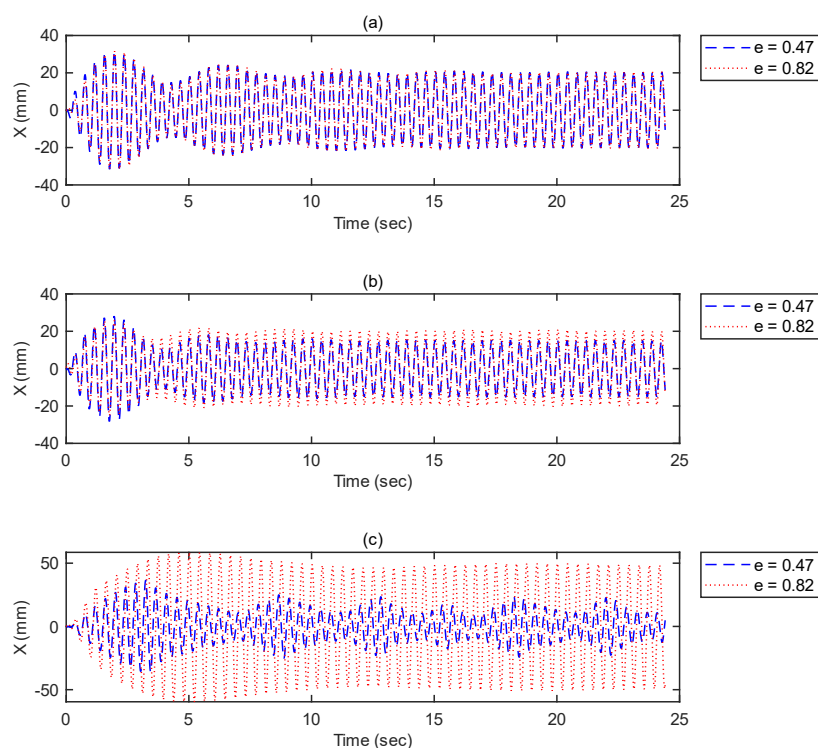
Figure 5-8. Response of the primary structure at resonance with various coefficients of restitution (Experiments); (a) $d = 7.5$ mm; (b) $d = 22.5$ mm; (c) $d = 37.5$ mm.

In addition to the analysis of clearance magnitude, the effect of the coefficient of restitution (COR) on the damping performance of the single-particle impact damper (SPID) is examined by varying the impact surfaces, as illustrated in Figure 5-8. The findings reveal important insights into the relationship between COR and SPID's performance.

Figure 5-8 demonstrates that increasing the coefficient of restitution reduces the damping performance of the SPID. This is due to the impacts between the primary mass and the particle having better momentum exchange but lesser energy dissipation. A higher COR allows for a

more efficient transfer of momentum during impacts, resulting in reduced energy dissipation and, consequently, lower damping in the system. This suggests that achieving higher damping levels with the SPID may require careful consideration and control of the coefficient of restitution. On the other hand, while larger clearance magnitudes can improve damping performance, they may lead to non-uniform displacement of the primary structure. This non-uniform displacement can raise concerns regarding the structural integrity of the system. It highlights the need to reach a balance between achieving higher damping levels and maintaining structural integrity when selecting the clearance magnitude for the SPID design.

5.2.2.2.   *Friction Damper*

In this section, the function of the friction damper (FD) in the resonant vibration of the single-degree-of-freedom (SDOF) structure is analysed. The analysis assumes that there is no single-particle impact damper (SPID) present in the system, as depicted in Figure 5-1. In this case, the equation of motion for the SDOF structure with only the friction damper (i.e., c = 0) can be written as,

$$M\ddot{x} + F_f \, \text{sgn}(\dot{x} - \dot{z}) + k(x - z) = 0 \tag{5.16}$$

where $F_f = \mu_e F_N$ is the friction force, μ_e is the coefficient of friction, and F_N is the normal force exerted on the primary structure.

The friction-force ratio (γ_F) is introduced as a measure to compare the effect of external friction on the dynamic response of the system. It is defined as the ratio of the friction force to the excitation force and can be expressed as,

$$\gamma_F = \frac{\mu_e F_N}{kZ} \tag{5.17}$$

To explore the effect of different magnitudes of γ_F on the dynamic response, the system's behaviour is recorded for a finite time through a range of excitation frequencies. The vibration response of the SDOF structure with the friction damper (FD) is presented in Figure 5-9. In this context, a study presented by Luca et al. (Marino et al., 2019) has shown that using a friction damper only is not efficient in suppressing vibration amplitudes at resonance. Similarly, Levitan et al. (Levitan, 1960) presented an analytical model for an SDOF structure

with Coulomb friction in base motions and demonstrated that a friction damper alone cannot effectively reduce resonant vibration amplitudes. When the friction force is relatively small, a structure shows a harmonic response. However, if the friction force is large, it can lead to discontinuous motion of the primary structure. This non-smooth behaviour poses challenges in achieving effective vibration control. Min et al. (Min et al., 2010) also derived a solution for a friction damper at resonance but concluded that the structure cannot demonstrate a steady-state response under such conditions.
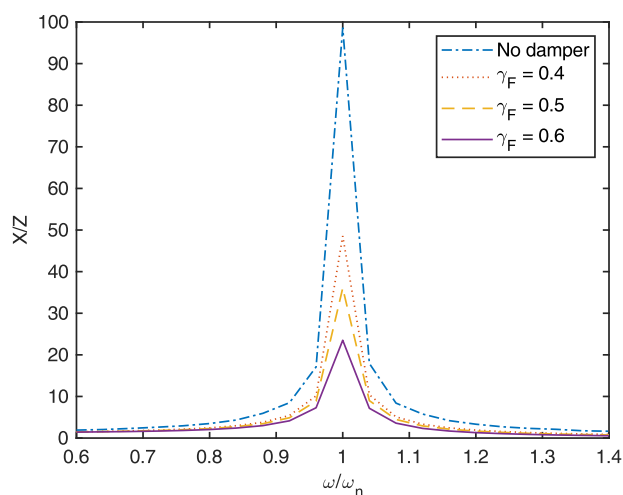
Figure 5-9. Computed displacement response of the structure with FD at different friction force ratios.

While friction dampers can generate significant friction forces, this introduces various challenges for dynamic structures. The high friction force can result in increased temperatures and excessive wear, raising concerns about the reliability and durability of the structure and damping system (López et al., 2004). Additionally, controlling a large friction force is complex, as it is not constant due to temperature rise and material wear or removal, which can alter the contact surfaces (Spencer & Nagarajaiah, 2003). Friction dampers have limited applications in vibration control because of phenomena like the stick-slip effect and non-linear damping forces, which can affect the stability of the structure and cause discomfort to occupants nearby (Ding & Chen, 2008). Considering the theory of structures with friction damper in base excitation (Jaisee et al., 2021) the representation of the relative response of the primary structure can be found in Appendix A.

$$\frac{A}{Z} = \left(\frac{(n^2)^2 - \left(\frac{4\mu_e F_N}{\pi k Z}\right)^2}{(1-n^2)^2}\right)^{\frac{1}{2}} \tag{5.18}$$

Here $A = X - Z$, and $n = \omega/\omega_n$. Equation (5.18) describes the relative displacement at resonance i.e., $(n = 1)$ turn into infinite with every level of the friction force. It indicates that the friction damper alone is not enough to restrict the vibration amplitude at resonance.

Experiments are conducted to discover the effect of different expansions of the spring in the friction damper (FD). F_N is determined by the stiffness of the spring (k_s) and the change in length (Δs), expressed as $F_N = k_s \Delta s$. In this context, both the external friction coefficient (μ_e) and the stiffness of the spring (k_s) are assumed as constants. Therefore, by altering the length of the spring, the friction force could be modified accordingly. The experimental procedure involved stretching the spring till the metallic block was closer to the primary mass, and the resulting extension of the spring was measured as zero-reading. Subsequently, the spring is further extended by loosening the nut to increase the normal force in the friction damper, consequently leading to a bigger friction force.
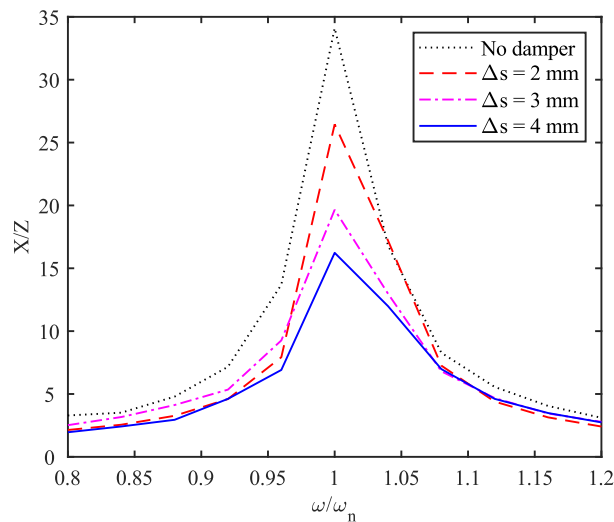
Figure 5-10. Recorded response of the primary structure with friction damper (FD) with different compressions of tuning spring.

Figure 5-10 illustrates the displacement response of the primary structure for different compressions of the spring in the FD. It is evident from the plot that the resonant vibration amplitude decreases as the deflection (Δs) of the spring increases, as shown in Figure 5-10.

Comparing Figure 5-9 and Figure 5-10, it is noteworthy that the curve for $\gamma_F = 0.6$ in Figure 5-9 exhibits a peak value of X/Z at approximately 20, which is similar to the curve for FD $\Delta s = 3$ mm. However, even with a friction force ratio of $\gamma_F = 0.6$, which is close to the theoretical limit of $\pi/4$; This is a limit from the theoretical expressions where the system still shows harmonic response and it is also revealed that the system goes into nonlinear behaviour such as stick-slip and other phenomena when the friction force ratio reached this limit or beyond, the vibration peak remains relatively high. This observation suggests that the FD alone is not sufficient to effectively suppress the resonant vibration of the single-degree-of-freedom (SDOF) primary system. Additional measures or damping techniques would be necessary to achieve more significant reductions in the vibration peak at resonance.

5.2.2.3.   *Hybrid Damper (SPID+FD)*

To investigate the behaviour of a combined hybrid damper consisting of a single-particle impact damper (SPID) and a friction damper (FD), a numerical model is developed. This model is used to simulate various combinations of the friction force ratio (γ_F) of the FD and the relative length of the cavity (d/Z) of the SPID. A program in MATLAB software is developed to efficiently manage the large amount of data generated by the simulations. This program systematically calculated the displacement response of the primary structure at resonance for each design combination considered.
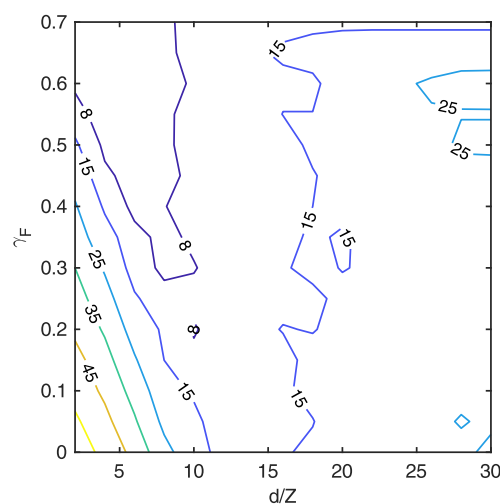
Figure 5-11. Simulated vibration amplitude ratio (X/Z) of the primary structure at resonance with the hybrid damper at different γ_F and d/Z.

Figure 5-11 presents a contour plot that visualizes the 2-dimensional dataset of resonant vibration amplitudes as a function of the relative clearance (d/Z) and the friction ratio (γ_F). This plot provides a comprehensive overview of how changes in these design parameters influence the vibration response of the primary structure. To validate the performance of the proposed hybrid damper, a series of experiments were conducted on a single-degree-of-freedom (SDOF) structure equipped with the combined SPID and FD system. The displacement response of the primary structure under varying conditions of friction forces and clearance values in the SPID is recorded from the experiments. Polyurethane (PU) cushions are installed into its design to provide a soft impact effect.
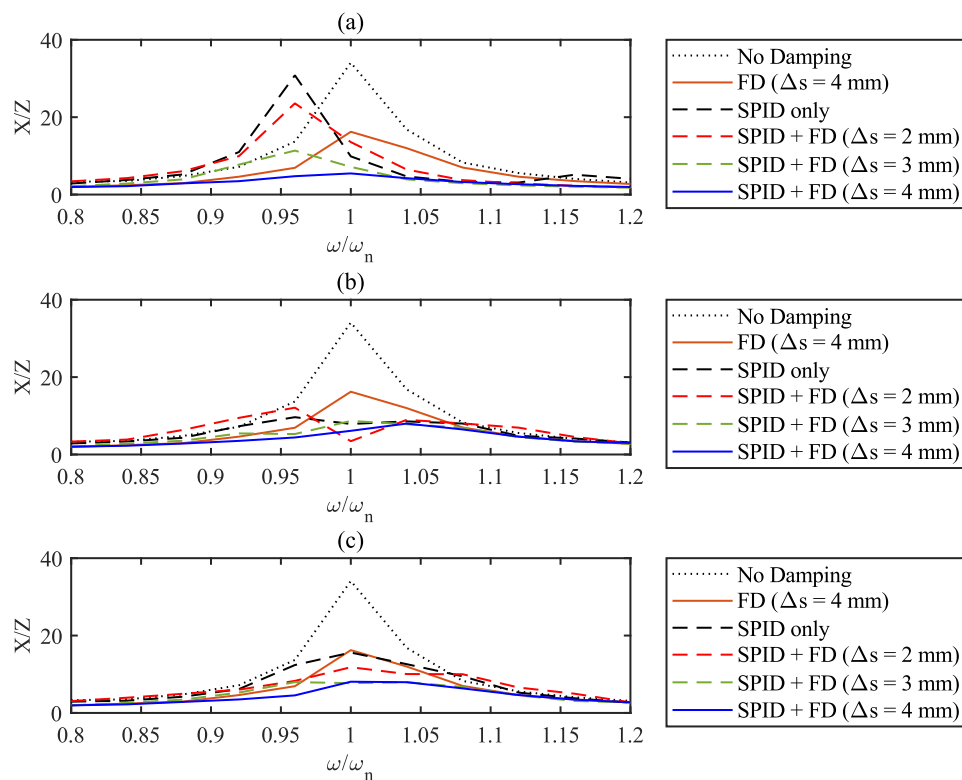
Figure 5-12. Recorded vibration amplitude of the primary system with different cavity lengths of SPID (a) $d = 7.5$ mm $(d/Z \approx 5)$; (b) $d = 22.5$ mm $(d/Z \approx 10)$; (c) $d = 37.5$ mm $(d/Z \approx 15)$

During the experiments, the displacement response of the primary structure was recorded while adjusting the spring deflections (Δs) in the FD and the relative clearance (d/Z) in the SPID. Figure 5-12 displays the recorded displacement response of the primary structure for different spring deflections and varying clearance magnitudes.

Table 5-1 demonstrates that the proposed hybrid damper achieves a minimum resonant vibration amplitude of $X/Z = 5.46$ when the clearance (d) value is set to 7.5 mm. This significant reduction in vibration amplitude highlights the effectiveness of the hybrid damper configuration in mitigating resonance-induced vibrations. Comparing the results to using the FD alone, the hybrid damper reduces the resonant vibration amplitude by 66%. This demonstrates the advantage of combining the SPID and FD, as the hybrid configuration provides superior vibration control capabilities compared to relying solely on the FD.

Table 5-1. Maximum vibration amplitude $\max(X/Z)$ with various dampers.

	d = 7.5 mm	d = 22.5 mm	d = 37.5 mm
SPID only	29.73	9.64	15.06
FD only (Δs = 4mm)	16.22	16.22	16.22
Hybrid (SPID+FD)	5.46	7.99	8.06

Furthermore, when comparing the hybrid damper to the use of the SPID alone with a clearance of 22.5 mm, a 43% reduction in the resonant vibration amplitude is achieved. This comparison highlights the added benefits of incorporating the FD into the hybrid damper system, as it yields further improvements in vibration suppression compared to using the SPID in isolation.

5.2.2.4. *Comparison with Tuned Mass Damper*

A traditional tuned mass damper (TMD) is a passive vibration-absorbing device commonly used for vibration control. It consists of a secondary mass attached to the primary structure through a spring and a damper as shown in Figure 5-13. TMD is typically pre-tuned to the natural frequency of the primary mass, allowing it to effectively reduce vibrations at that particular frequency. The design of TMDs has been extensively studied, and there is a wealth of knowledge regarding analytical methods to optimize their performance for maximum vibration suppression. The theoretical effectiveness of TMDs in reducing vibrations makes them an attractive solution for vibration control applications.

However, despite their theoretical advantages, TMDs are not widely used in many practical scenarios. One of the main challenges with TMDs is related to the exact damping conditions for the secondary mass. Achieving the optimal damping ratio for the TMD can be

challenging due to the variability in operating conditions and structural dynamics. Inaccurate damping settings can lead to worsening vibrations instead of attenuating them. Additionally, TMDs have limitations in their effectiveness beyond the tuned frequency. They are primarily designed to suppress vibrations at a specific natural frequency and may not be as effective in controlling vibrations at other frequencies. This limited bandwidth can restrict their applicability in systems with broad frequency ranges or varying excitation frequencies.

As a result of these practical challenges, alternative damping solutions, such as hybrid damper combining multiple techniques like the proposed hybrid damper with SPID and FD, have gained attention. These hybrid dampers offer a broader frequency response and can be more easily tuned or adjusted to adapt to changing operating conditions.
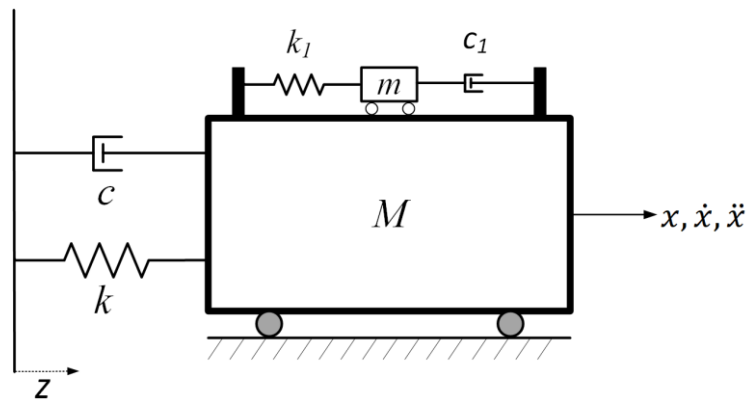
Figure 5-13. Representation of a Tuned mass damper (TMD) attached to an SDOF structure.

The response of the primary structure with a TMD can be derived (Wong, 2016),

$$\left|\frac{X}{X_{st}}\right| = \left|\frac{X}{Z}\right| = \sqrt{\frac{(\gamma^2 - \lambda^2)^2 + (2\gamma\lambda\zeta)^2}{[(1 - \lambda^2)(\gamma^2 - \lambda^2) - \mu_1\gamma^2\lambda^2]^2 + [2\gamma\lambda\zeta(1 - \lambda^2 - \mu_1\lambda^2)]^2}} \quad (5.19)$$

Here $\mu_1 = m/M$, $\gamma = \omega_a/\omega_n$, $\omega_a = \sqrt{(k_1/m)}$ and $\omega_n = \sqrt{k/M}$), $\lambda = \omega/\omega_n$, $\zeta = c/(2\sqrt{mk_1})$, and X is the vibration amplitude of the primary structure. The optimal parameters for a tuned mass damper are derived from the following equations (Wong, 2016),

$$\gamma_{opt} = \frac{1}{1 + \mu_1} \quad (5.20)$$

$$\zeta_{opt} = \sqrt{\frac{3\mu_1}{8(1 + \mu_1)}} \tag{5.21}$$

The vibration response of the primary structure with an optimized conventional tuned mass damper (TMD) is simulated and compared with the response obtained using the proposed hybrid damper experimentally. The design parameters for the optimized TMD and hybrid damper are given in Table 5-2.

Table 5-2. Optimum parameters of TMD and hybrid damper for comparison

TMD		
Mass-ratio (μ_1)	Optimum frequency ratio (γ_{opt})	Optimal damping ratio (ζ_{opt})
0.1	0.9091	0.1679

Hybrid Damper (SPID + FD)			
Mass-ratio (μ)	Clearance (d/Z)	Coefficient of restitution (e)	Spring compression (Δs)
0.1	5	0.47	4 mm

Additionally, Figure 5-14 illustrates the comparison between the response of the primary structure with the optimized TMD and the response achieved with the proposed hybrid damper. It is observed that the traditional TMD is effective in reducing vibrations at the resonance frequency, as expected. However, there are practical challenges associated with TMDs. To achieve optimum performance, the damping coefficient of the TMD needs to be accurately tuned. The range for tuning is typically narrow, making it difficult to find or design a damper with the exact required damping coefficient. If the damping coefficient is not accurately set, the TMD's performance can be negatively impacted, potentially leading to worsened vibration control.

In contrast, the proposed hybrid damper offers advantages over traditional TMDs. By combining the SPID and FD, the hybrid damper provides a broader frequency response and can effectively suppress vibrations over a wider range of frequencies. Additionally, the hybrid damper does not rely on precise damping coefficient tuning, making it more practical to implement.

The results obtained from Figure 5-14 demonstrate that the proposed hybrid damper, consisting of the SPID and FD, performs closely to the optimally tuned traditional mass damper (TMD). While the TMD exhibits a slightly lower resonance amplitude compared to the hybrid damper, the hybrid damper highlights efficiency over a wider frequency range. It is worth noting that the proposed hybrid damper offers several advantages over the TMD. Firstly, the design process for the hybrid damper is generally more straightforward compared to the precise tuning requirements of the TMD. Furthermore, the proposed hybrid damper can provide effective vibration control over a wider frequency range. This wider frequency response is advantageous in scenarios where the vibrations are not limited to a single excitation frequency or when the excitation frequencies vary. In contrast, the TMD's effectiveness is primarily confined to its tuned frequency, making it less versatile in applications with broader frequency ranges.
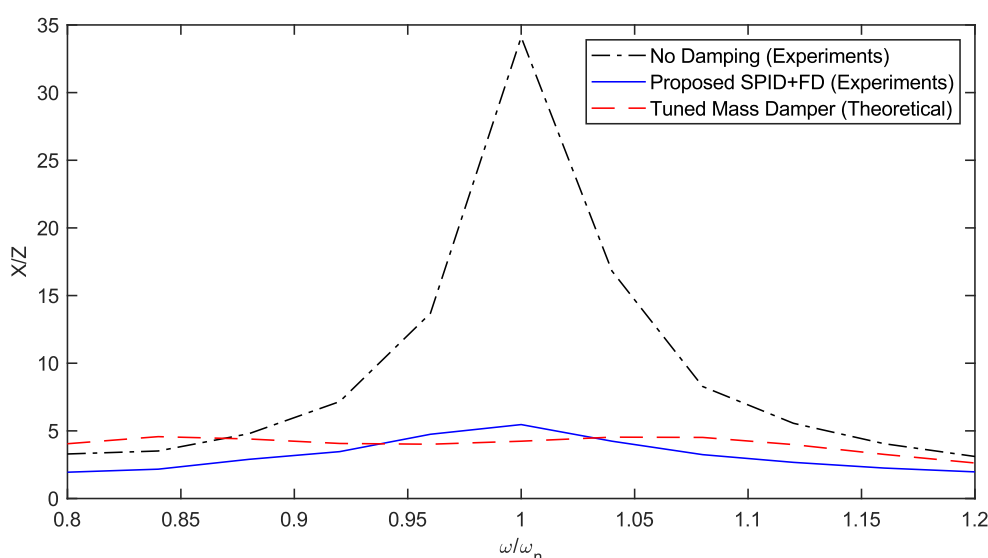
Figure 5-14. Response of the primary structure with a hybrid damper and TMD (Mass ratio = 0.1).

Considering these factors, the proposed hybrid damper can serve as a viable alternative to the TMD in passive vibration control applications. The hybrid damper offers comparable performance to the TMD while being easier to design and implement. This makes it a cost-effective and practical solution, especially in cases where the utilization of TMDs is challenging or costly.

5.2.2.5.   Random excitation case

In previous sections, the hybrid damper was designed and assessed under harmonic excitations. However, it is important to consider the potential applications of the damper in real-life scenarios, such as during earthquakes where the excitation is random. To evaluate the performance of the hybrid damper under earthquake conditions, it is investigated using random earthquake records. The earthquake input used for testing is extracted from the built-in MATLAB example data called "quake." This example data contains seismic data from the Loma Prieta earthquake that occurred on October 17, 1989, in the Santa Cruz Mountains. Numerical simulations are conducted to analyse the response of the hybrid damper under random earthquake data. The results of these simulations are then compared with the performance of an optimally tuned mass damper (TMD) with a similar mass ratio, in the identical excitation situation. This comparison allows for an assessment of how well the proposed hybrid damper performs in mitigating vibrations during earthquake events when compared to the TMD.
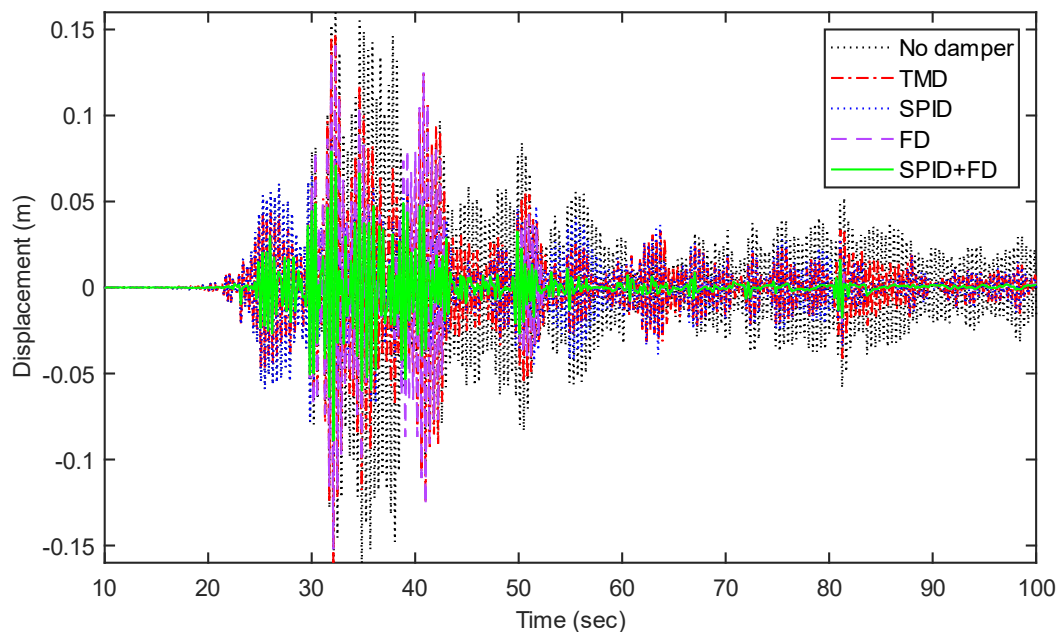
Figure 5-15. Response of the primary structure in earthquake excitation with different dampers.

Figure 5-15 illustrates an example case of a random earthquake scenario, comparing the performance of the proposed hybrid damper with the other damper assessed. The results

91

demonstrate that the proposed damper exhibits superior damping characteristics in the presence of random excitations. This advantage can be attributed to the wider frequency band of the hybrid damper, which allows it to effectively dampen vibrations over a range of frequencies. In contrast, the tuned mass damper (TMD) is designed to operate optimally at a specific frequency and may not be as effective when faced with random excitations that span various frequencies.

Furthermore, Table 5-3 provides the RMS and maximum vibration amplitude values for the primary structure in random earthquakes, considering various dampers. The RMS amplitude reflects the overall performance of the damper throughout the entire excitation period, indicating its effectiveness over a sustained duration. When comparing the RMS and maximum vibration amplitude of the structure with separate dampers, it is evident that the proposed hybrid damper exhibits the most effective vibration suppression. Specifically, the hybrid damper lowers the maximum displacement amplitude by 46% compared with a Tuned Mass Damper (TMD).

Table 5-3. RMS and maximum vibration amplitude of primary structure in earthquake excitation with different dampers.

	No Damping	TMD	SPID	FD	SPID + FD
Max. amplitude (m)	0.1671	0.1473	0.0851	0.1400	0.0790
RMS amplitude (m)	0.0335	0.0238	0.0168	0.0200	0.0106

5.3. Conclusion

The single-particle impact damper (SPID) is a developing passive vibration absorber that offers several advantages over other systems. Numerical and experimental findings reveal that the SPID exhibits two distinct damping phases when applied to an SDOF structure in free vibrations. The first phase demonstrates significant damping with numerous intense collisions, while the second phase begins when the amplitude of the primary system decreases to a particular level. In this second phase, the SPID shows negligible damping over a prolonged period with only a few ineffective impacts. To address this limitation, it is proposed to merge the SPID with a small friction damper (FD) to shrink the duration of the second ineffective damping phase. Experimental verification confirms the effectiveness of this approach. The

combination of the friction damper with the single-particle impact damper reduces the time required to reduce the vibration amplitude to zero compared to using either damper alone.

The single-particle impact damper exhibits high damping rates initially but decreases as the amplitude decreases. This is because the damping performance of the single-particle impact damper depends on the vibration levels, resulting in a smaller damping rate as the amplitude reduces. In contrast, the friction damper offers a constant damping force, taking longer than the single-particle impact damper to decrease the vibration amplitude in the initial phase. Conversely, overall, the friction damper outperforms the single-particle impact damper in reducing the vibration amplitude to zero. Merging a single-particle impact damper with a friction damper complement both dampers and achieves a relatively superior damping performance throughout the entire vibration suppression process. The results demonstrate that the vibration amplitude decreases to zero in half the time compared to using the friction damper alone, indicating robust and efficient vibration reduction with the proposed combination.

Furthermore, both numerical and experimental analyses on a hybrid-damper comprising a single-particle impact damper (SPID) and a friction damper (FD) are conducted to study its effects on forced vibrations. The FD is found to be ineffective in mitigating the resonant vibration amplitude of the primary structure, while the SPID displayed low damping. However, the proposed hybrid damper, combining the SPID and FD exhibited effectiveness in controlling resonant structural vibrations. A numerical model for the hybrid damper is created and numerical simulations are conducted on a single-degree-of-freedom (SDOF) structure. Experimental tests on a prototype are conducted to further validate the conclusions. Through a parametric analysis of the hybrid damper, the optimal design combinations are derived for the SPID and FD, which are subsequently validated through experiments. Compared to using the FD alone, the proposed hybrid damper reduced the maximum vibration amplitude of the SDOF primary structure by an additional 66%, and compared to using the SPID alone, it achieved a 43% reduction. It delivered a vibration suppression performance similar to that of a tuned mass damper (TMD) with the same mass ratio but without the issue of detuning associated with TMD. Additionally, the hybrid damper demonstrated excellent performance across a wide range of excitation frequencies. When subjected to random earthquake excitation data, the hybrid damper exhibited significantly superior damping capabilities compared to the TMD due

to its broad frequency band. It reduced the maximum vibration amplitude by approximately 46% during earthquakes, surpassing the performance of the TMD.

5.4. Summary

The Chapter presents a hybrid damper (FD + SPID) that combines a single-particle impact damper (SPID) and a friction damper (FD) for vibration control. The SPID dissipates energy through impacts, while the FD provides a higher damping force-to-mass ratio. The research aims to address the limitations of each damper individually and utilize their advantages in combination. A numerical model of the hybrid damper is developed and validated through numerical simulations on a single-degree-of-freedom (SDOF) structure. Experimental tests are conducted on a prototype to validate the predicted results. Parametric analysis is performed to determine the optimal design combination of SPID and FD.

The findings demonstrate that the proposed hybrid damper outperforms using either the FD or SPID alone, reducing the vibration amplitude of the SDOF primary structure by about 66% compared to FD and 43% compared to SPID alone. The hybrid damper accomplishes a vibration control performance similar to an optimally tuned mass damper (TMD) of the same mass ratio while avoiding the detuning problem associated with TMD. Moreover, the hybrid damper exhibits effectiveness across a wide range of excitation frequencies, making it suitable for various applications. In testing with random earthquake excitation data, the hybrid damper demonstrates significantly better damping than the TMD, lowering the maximum vibration amplitude by approximately 46% during earthquakes.

Chapter 6
Conclusions and Future Works

In this chapter, the conclusions drawn from this research are demonstrated and a further suggestion for future work is provided.

6.1. Conclusions

Particle impact dampers, such as single-particle impact dampers (SPID) and multi-particle impact dampers (MPID), are relatively underdeveloped passive vibration control devices when it comes to optimal design and effectiveness, similar to other well-known passive vibration absorbers like the tuned mass damper (TMD). However, despite the lack of understanding and available analytical models, particle impact dampers show exciting potential due to their simplicity and ease of installation. This research aims to provide a comprehensive understanding of SPID and its potential as a simple yet effective solution for structural vibration control.

A brief experimental study conducted in Chapter 2 highlighted the challenges associated with SPID and MPID, clarifying certain ambiguities related to SPID. The conclusions drawn from this chapter emphasize that a single-particle impact damper exhibits a slightly higher damping rate due to its significant mass. This characteristic makes it easier to formulate design methodologies and installation processes.

Chapter 3 presents a comprehensive methodology for designing and optimizing the performance of a single-particle impact damper (SPID). The methodology includes a parametric analysis of fundamental design parameters, which is conducted numerically and validated through experiments. It is observed that the design parameters of SPID are interconnected and exhibit a nonlinear relationship. Thus, analysing the combined effect of these parameters is necessary to understand their impact on the damper's behaviour. Furthermore, the study concludes that internal friction in the SPID design diminishes the kinetic energy of the particle, resulting in reduced momentum exchange. As a result, internal friction generally degrades the performance of SPID. By employing a combination of numerical analysis and experimental validation, the study identifies optimal design parameters

such as the relative clearance magnitude and coefficient of restitution. These parameters play a crucial role in ensuring effective damping in both free and forced vibration scenarios.

Chapter 4 addresses concerns regarding high-impact forces, noise levels, and induced stresses by a single-particle impact damper (SPID) by studying the impact of soft and hard materials on their performance. The study introduces viscoelastic materials into SPID and develops a new numerical model that considers the viscoelastic behaviour of these materials. Four different materials are selected, and their dynamic mechanical properties are determined through DMA (Dynamic Mechanical Analysis) tests. These measured properties are then included in numerical simulations, and the results are validated through experiments. Based on the numerical and experimental findings, it is concluded that the impact material used in SPID does not have a significant effect on damping performance. Instead, the clearance magnitude between the particles is identified as a highly influential factor. However, the inclusion of soft materials in the SPID design does lead to a slight improvement in damping performance. Through the combination of numerical simulations and experimental results, it is demonstrated that the integration of softer materials can reduce impact forces by 96% while maintaining effective damping performance with minimal noise. This finding not only enhances the overall functionality of a single-particle impact damper but also helps mitigate potential issues associated with their implementation.

After developing an optimal design methodology for single-particle impact damper (SPID) and recognizing their advantages over traditional tuned mass damper (TMDs) in terms of simplicity of installation and design process, it became apparent that SPID alone cannot achieve vibration suppression rates comparable to TMDs. To address this limitation, Chapter 5 proposes a hybrid damper that combines the high damping force of a friction damper (FD) with the simplicity of a SPID. The application of the hybrid damper (SPID+FD) is explored in both free and forced vibrations. The behaviour of a single-particle impact damper in free vibrations reveals two distinct damping phases. Recognizing the limitations of the second phase, which is less effective, the addition of a small friction damper is proposed. Numerical simulations and experimental validations are conducted to assess the effectiveness of the hybrid damper, demonstrating its ability to reduce vibration amplitudes more rapidly than either damper alone. Furthermore, the hybrid damper proves highly effective in suppressing resonant structural vibrations, surpassing the performance of a SPID or friction damper alone. It is

shown that the friction damper alone is insufficient at resonance, thus the combination with a SPID allows the friction damper to be utilized in structural vibration control applications. Notably, the hybrid damper achieves similar performance to an optimally tuned mass damper (TMD) without the detuning issue often encountered with TMDs. The hybrid damper exhibits strong damping performance across a wide range of excitation frequencies, including during seismic events. This underscores the effectiveness of the hybrid approach in providing vibration control in various scenarios. Overall, Chapter 5 demonstrates the potential and advantages of the hybrid damper (SPID+FD) in achieving superior damping performance and mitigating resonant vibrations compared to individual damper.

In summary, this research has contributed to the understanding of a single-particle impact damper, presenting practical design strategies for achieving optimal performance. The advantages of a single-particle impact damper, such as its simplicity, ease of installation, and effectiveness across a wide frequency band, have been highlighted. The findings of this study provide valuable insights and open new possibilities for further exploration and practical applications of a single-particle impact damper in the field of structural vibration control.

6.2. Future works

Particle impact dampers are currently less developed compared to other passive vibration absorbers. As a result, several aspects deserve further investigation beyond the conclusions drawn from this research. Presented below are some potential areas of future work,

1. First, as a potential vibration absorber in structural vibration control, a single-particle impact damper is required to be studied with a multi-degree-of-freedom structure. A comprehensive numerical model of MDOF with a single-particle impact damper can provide further insights into the potential of SPID in structural vibration control applications.

2. The research concluded that the impact surface does not significantly affect damping performance in a single-particle impact damper (SPID). However, a hard impact results in higher impact forces, which can be utilized for energy harvesting. Replacing the impact surface with energy-harvesting materials, such as piezoelectric materials,

allows for the generation of energy during SPID operation. This energy can be used to power sensors for structural health monitoring alongside vibration absorption.

3. The hybrid damper (FD + SPID) showed comparable damping performance to a TMD and better vibration suppression across a wider frequency range. Future research can examine the performance of the hybrid damper in multi-degree-of-freedom structures through numerical and experimental studies, focusing on optimal design considerations.

4. There is further research required about the proposed hybrid damper. The friction force in the proposed hybrid damper is kept within a defined boundary where it is not significantly large. However, a large friction force may influence the overall dynamics of the system with SPID. Therefore, further investigation is required to analyse the performance of a hybrid damper with a larger friction force.

Appendix A

The steady-state response of an SDOF structure with friction damper excited by sinusoidal base excitation

A single-degree-of-freedom structure (SDOF) excited by the sinusoidal motion of a base as presented in Figure A1.
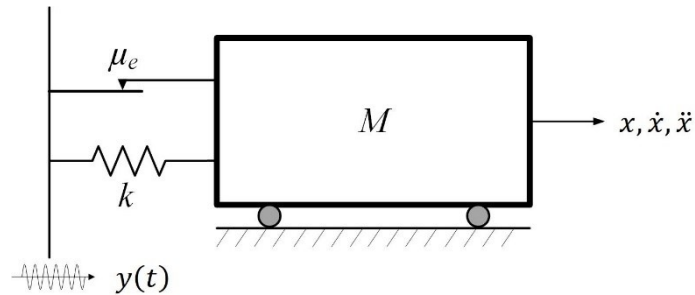
Figure A1. Mechanical model of an SDOF structure with a friction damper (FD).

The equation of motion of the presented system might be written as,

$$M\ddot{x} + kx + \mu_e N_M \, \text{sgn}(\dot{x} - \dot{y}) = 0 \tag{A1}$$

μ_e is the friction coefficient, $N_M = Mg$ is the normal force exerted by mass M, and "sgn" is the signum function to determine the direction of the friction force, which is defined as,

$$\text{sgn} \, (\dot{x} - \dot{y}) = \begin{cases} -1 & \text{if } \dot{x} - \dot{y} < 0 \\ 0 & \text{if } \dot{x} - \dot{y} = 0 \\ 1 & \text{if } \dot{x} - \dot{y} > 0 \end{cases} \tag{A2}$$

The solution of equation (A1) is challenging to attain due to the non-linear terms. Nonetheless, the FD can be considered as an equivalent viscous damper $\left(c_{eq}\right)$ to express an estimated analytical solution. In order to determine the viscous damping, the energy dissipated by an equivalent viscous damper and the energy dissipation by a friction damper can be compared. The energy dissipated by the friction damper in one cycle of vibration is determined as,

$$\Delta W = 4\mu_e N_M \, (X - Y) \tag{A3}$$

Here $(X - Y)$ is the relative displacement of the primary structure and base motion. The energy dissipated through a viscous damper in one cycle might be defined as,

$$\Delta W = \pi c_{eq} \omega \, (X - Y)^2 \tag{A4}$$

where ω is the frequency of base. Through comparing eqns. A3 and A4,

$$c_{eq} = \frac{4\mu_e N_M}{\pi\omega(X - Y)} \tag{A5}$$

Eqn. (A1) can be modified as,

$$M\ddot{x} + c_{eq}(\dot{x} - \dot{y}) + k(x - y) = 0 \tag{A6}$$

If the motion of (M) comparative to the base is considered,

$$M\ddot{z} + c_{eq}(\dot{z}) + kz = M\ddot{y} \tag{A7}$$

Here $z = (x - y)$. If the ground has sinusoidal motion i.e., $(y = Y\sin(\omega t))$, where Y is the amplitude of the base. Equation (A7) can be reorganized as,

$$M\ddot{z} + c_{eq}\dot{z} + kz = M\omega^2 Y\sin(\omega t) \tag{A8}$$

The solution of equation A8 is given by,

$$Z = \frac{M\omega^2 Y}{((k - m\omega^2)^2 + (c\omega)^2)^{\frac{1}{2}}} \tag{A9}$$

or

$$Z = \frac{Yn^2}{\left((1 - n^2)^2 + \left(2\zeta_{eq}n\right)^2\right)^{\frac{1}{2}}} \tag{A10}$$

Here $n = \omega/\omega_n$, and $\zeta_{eq} = \frac{c_{eq}}{c_c}$.

$$\zeta_{eq} = \frac{c_{eq}}{c_c} = \frac{\frac{4\mu_e N_M}{\pi\omega Z}}{2M\omega_n} = \frac{4\mu_e N_M}{2\pi M\omega_n\omega Z} \tag{A11}$$

And $Z = X - Y$, substituting equation A11 into equation A10,

$$Z = \frac{Yn^2}{\left((1-n^2)^2 + \left(\left(\frac{4\mu_e N_M}{\pi k Z}\right)\right)^2\right)^{\frac{1}{2}}} \qquad \text{(A12)}$$

Squaring both sides and rearranging,

$$Z^2\left((1-n^2)^2 + \left(\left(\frac{4\mu_e N_M}{\pi k Z}\right)\right)^2\right) = (Yn^2)^2$$

$$Z^2(1-n^2)^2 + \left(\frac{4\mu_e N_M}{\pi k}\right)^2 = (Yn^2)^2$$

$$Z^2(1-n^2)^2 = (Yn^2)^2 - \left(\frac{4\mu_e N_M}{\pi k}\right)^2$$

Multiplying with $\frac{1}{Y^2}$

$$\frac{1}{Y^2}(Z^2(1-n^2)^2) = \frac{1}{Y^2}\left((Yn^2)^2 - \left(\frac{4\mu_e N_M}{\pi k}\right)^2\right)$$

$$\frac{Z^2}{Y^2}((1-n^2)^2) = \frac{Y^2 n^4}{Y^2} - \left(\left(\frac{4\mu_e N_M}{\pi k}\right)^2\right)\frac{1}{Y^2}$$

$$\frac{Z^2}{Y^2}((1-n^2)^2) = n^4 - \left(\left(\frac{4\mu_e N_M}{\pi k Y}\right)^2\right)$$

$$\frac{Z^2}{Y^2} = \frac{n^4 - \left(\frac{4\mu_e N_M}{\pi k Y}\right)^2}{(1-n^2)^2}$$

Take the square root of both sides,

$$\frac{Z}{Y} = \left(\frac{(n^2)^2 - \left(\frac{4\mu_e N_M}{\pi k Y}\right)^2}{(1-n^2)^2}\right)^{\frac{1}{2}} \qquad \text{(A13)}$$

References

Araki, Y., Yokomichi, I., & Jinnnouchi, Y. (1986). Impact Damper with Granular Materials : 4th Report Frequency Response in a Horizontal System. *Bulletin of JSME*, *29*(258), 4334-4338. https://doi.org/10.1299/jsme1958.29.4334

Bannerman, M. N., Kollmer, J. E., Sack, A., Heckel, M., Mueller, P., & Poschel, T. (2011). Movers and shakers: granular damping in microgravity [Article]. *Phys Rev E Stat Nonlin Soft Matter Phys*, *84*, 011301, Article 011301. https://doi.org/10.1103/PhysRevE.84.011301

Bapat, C. N., & Sankar, S. (1985). Single Unit Impact Damper in Free and Forced Vibration. *JOURNAL OF SOUND AND VIBRATION*, *99*(1), 85-94. https://doi.org/Doi 10.1016/0022-460x(85)90446-8

Butt, A. S. (1995). *Dynamics of impact-damped continuous systems* (Publication Number 9535118) [D.Eng. , Louisiana Tech University]. United States -- Louisiana.

Butt, A. S., & Akl, F. A. (1997). Experimental analysis of impact-damped flexible beams [Article]. *Journal of Engineering Mechanics*, *123*(4), 376-383. https://doi.org/Doi 10.1061/(Asce)0733-9399(1997)123:4(376)

Casciati, F., & Faravelli, L. (2009). A passive control device with SMA components: from the prototype to the model. *Structural Control and Health Monitoring*, n/a-n/a. https://doi.org/10.1002/stc.328

Chatterjee, S., Mallik, A. K., & Ghosh, A. (1995). On Impact Dampers for Non-Linear Vibrating Systems. *JOURNAL OF SOUND AND VIBRATION*, *187*(3), 403-420. https://doi.org/10.1006/jsvi.1995.0532

Chehaibi, K., Mrad, C., & Nasri, R. (2019). Collision Modeling of Single Unit Impact Absorber for Mechanical Systems Vibration Attenuation. *Journal of Theoretical and Applied Mechanics*, *57*(4), 947-956. https://doi.org/10.15632/jtam-pl/112417

Chen, J. L., & Georgakis, C. T. (2013). Tuned rolling-ball dampers for vibration control in wind turbines. *JOURNAL OF SOUND AND VIBRATION*, *332*(21), 5271-5282. https://doi.org/10.1016/j.jsv.2013.05.019

Den Hartog, J. P. (1934). *Mechanical Vibrations: 4th Ed*. McGraw-Hill. https://books.google.com.hk/books?id=DBRLxQEACAAJ

Ding, Q., & Chen, Y. (2008). Analyzing resonant response of a system with dry friction damper using an analytical method. *JOURNAL OF VIBRATION AND CONTROL*, *14*(8), 1111-1123. https://doi.org/10.1177/1077546307080246

Djemal, F., Chaari, R., Gafsi, W., Chaari, F., & Haddar, M. (2019). Passive vibration suppression using ball impact damper absorber. *Applied Acoustics*, *147*, 72-76. https://doi.org/10.1016/j.apacoust.2017.09.011

Du, Y. C., & Wang, S. L. (2010). Modeling the fine particle impact damper. *INTERNATIONAL JOURNAL OF MECHANICAL SCIENCES*, *52*(7), 1015-1022. https://doi.org/10.1016/j.ijmecsci.2010.04.004

Duncan, M. R., Wassgren, C. R., & Krousgrill, C. M. (2005). The damping performance of a single particle impact damper. *JOURNAL OF SOUND AND VIBRATION*, *286*(1-2), 123-144. https://doi.org/10.1016/j.jsv.2004.09.028

Ekwaro-Osire, S., & Desen, I. C. (2001). Experimental study on an impact vibration absorber. *JOURNAL OF VIBRATION AND CONTROL*, *7*(4), 475-493. https://doi.org/Doi 10.1177/107754630100700401

Ekwaro-Osire, S., & Desen, I. C. (2016). Experimental Study on an Impact Vibration Absorber. *Journal of Vibration and Control*, *7*, 475-493. https://doi.org/10.1177/107754630100700401

Fang, X., & Tang, J. (2006). Granular damping in forced vibration: Qualitative and quantitative analyses. *Journal of Vibration and Acoustics-Transactions of the Asme*, *128*(4), 489-500. https://doi.org/10.1115/1.2203339

Fang, X., Tang, J., & Luo, H. (2007). Granular damping analysis using an improved discrete element approach [Article]. *JOURNAL OF SOUND AND VIBRATION*, *308*(1-2), 112-131. https://doi.org/10.1016/j.jsv.2007.07.034

Feeny, B. (1992). A Nonsmooth Coulomb-Friction Oscillator. *Physica D-Nonlinear Phenomena*, *59*(1-3), 25-38. https://doi.org/Doi 10.1016/0167-2789(92)90204-Z

Friend, R. D., & Kinra, V. K. (2000). Particle impact damping. *JOURNAL OF SOUND AND VIBRATION*, *233*(1), 93-118. https://doi.org/DOI 10.1006/jsvi.1999.2795

Gagnon, L., Morandini, M., & Ghiringhelli, G. L. (2019). A review of particle damping modeling and testing. *Journal of Sound and Vibration*, *459*, 114865. https://doi.org/10.1016/j.jsv.2019.114865

Grubin, C. (1956). On the Theory of the Acceleration Damper. *Journal of Applied Mechanics*, *23*(3), 373-378. https://doi.org/10.1115/1.4011339

He, H. X., Wang, B. S., & Yan, W. M. (2021). Mechanical Model and Optimization Analysis of Multiple Unidirectional Single-Particle Damper. *Journal of Engineering Mechanics*, *147*(7), 04021040. https://doi.org/Artn 04021040

10.1061/(Asce)Em.1943-7889.0001950

Henriques, I. R., Rouleau, L., Castello, D. A., Borges, L. A., & Deü, J. F. (2020). Viscoelastic behavior of polymeric foams: Experiments and modeling. *Mechanics of Materials*, *148*, 103506. https://doi.org/ARTN 103506

10.1016/j.mechmat.2020.103506

Hirsch, M. W., Smale, S., & Devaney, R. L. (2013). Closed Orbits and Limit Sets. In M. W. Hirsch, S. Smale, & R. L. Devaney (Eds.), *Differential Equations, Dynamical Systems, and an Introduction to Chaos* (pp. 213-232). Academic Press. https://doi.org/10.1016/b978-0-12-382010-5.00010-5

Hollkamp, J., & Gordon, R. (1998). *Experiments with particle damping* (Vol. 3327). SPIE. https://doi.org/10.1117/12.310675

Huang, X. H., Xu, W. B., Wang, J., Yan, W. M., & Chen, Y. J. (2021). Equivalent model of a multi-particle damper considering particle rolling and its analytical solution. *STRUCTURAL CONTROL & HEALTH MONITORING*, *28*(6), e2718. https://doi.org/ARTN e2718

10.1002/stc.2718

Hundal, M. S. (1979). Response of a Base Excited System with Coulomb and Viscous Friction. *JOURNAL OF SOUND AND VIBRATION*, *64*(3), 371-378. https://doi.org/Doi 10.1016/0022-460x(79)90583-2

IHSAN, C. D. (2000). *Experimental study on an impact vibration absorber* [Masters, Texas Tech University].

Jaisee, S., Yue, F., & Ooi, Y. H. (2021). A state-of-the-art review on passive friction dampers and their applications. *Engineering Structures*, *235*, 112022. https://doi.org/ARTN 112022

10.1016/j.engstruct.2021.112022

Johnson, C. D., & Simonian, S. S. (1995). *<title>Particle beam damper</title>* Smart Structures and Materials 1995: Passive Damping, https://doi.org/10.1117/12.208884

Kaul, S. (2021). Viscoelastic modeling—passive vibration isolators. In *Modeling and Analysis of Passive Vibration Isolation Systems* (pp. 27-61). https://doi.org/10.1016/b978-0-12-819420-1.00003-0

Lee, J. H., Berger, E., & Kim, J. H. (2005). Feasibility study of a tunable friction damper. *JOURNAL OF SOUND AND VIBRATION*, *283*(3-5), 707-722. https://doi.org/10.1016/j.jsv.2004.05.022

Leine, R. I., Van Campen, D. H., De Kraker, A., & Van den Steen, L. (1998). Stick-slip vibrations induced by alternate friction models. *Nonlinear Dynamics*, *16*(1), 41-54. https://doi.org/Doi 10.1023/A:1008289604683

Levitan, E. S. (1960). Forced Oscillation of a Spring-Mass System having Combined Coulomb and Viscous Damping. *The Journal of the Acoustical Society of America*, *32*(10), 1265-1269. https://doi.org/10.1121/1.1907893

Li, A. (2020). Viscoelastic Damper. In *Vibration Control for Building Structures* (pp. 129-160). Springer International Publishing. https://doi.org/10.1007/978-3-030-40790-2_6

Li, K., & Darby, A. P. (2006). Experiments on the effect of an impact damper on a multiple-degree-of-freedom system. *JOURNAL OF VIBRATION AND CONTROL*, *12*(5), 445-464. https://doi.org/10.1177/1077546306063504

Lieber, P., & Jensen, D. P. (1945). An Acceleration Damper: Development, Design, and Some Applications. *Journal of Fluids Engineering*, *67*(7), 523-530. https://doi.org/10.1115/1.4018316

López, I., Busturia, J. M., & Nijmeijer, H. (2004). Energy dissipation of a friction damper. *JOURNAL OF SOUND AND VIBRATION*, *278*(3), 539-561. https://doi.org/10.1016/j.jsv.2003.10.051

Lu, Z., Chen, X. Y., Zhang, D. C., & Dai, K. S. (2017). Experimental and analytical study on the performance of particle tuned mass dampers under seismic excitation. *EARTHQUAKE ENGINEERING & STRUCTURAL DYNAMICS*, *46*(5), 697-714. https://doi.org/10.1002/eqe.2826

Lu, Z., Lu, X. L., Lu, W. S., & Masri, S. F. (2012). Shaking table test of the effects of multi-unit particle dampers attached to an MDOF system under earthquake excitation. *EARTHQUAKE ENGINEERING & STRUCTURAL DYNAMICS*, *41*(5), 987-1000. https://doi.org/10.1002/eqe.1170

Lu, Z., Lu, X. L., & Masri, S. F. (2010). Studies of the performance of particle dampers under dynamic loads. *JOURNAL OF SOUND AND VIBRATION*, *329*(26), 5415-5433. https://doi.org/10.1016/j.jsv.2010.06.027

Lu, Z., Masri, S. F., & Lu, X. L. (2011). Parametric studies of the performance of particle dampers under harmonic excitation. *STRUCTURAL CONTROL & HEALTH MONITORING*, *18*(1), 79-98. https://doi.org/10.1002/stc.359

Lu, Z., Wang, Z. X., Masri, S. F., & Lu, X. L. (2018). Particle impact dampers: Past, present, and future. *Structural Control & Health Monitoring*, *25*, e2058. https://doi.org/10.1002/stc.2058

Mansour, W. M., & Filho, D. R. T. (1974). Impact Dampers with Coulomb Friction. *JOURNAL OF SOUND AND VIBRATION*, *33*(3), 247-265. https://doi.org/Doi 10.1016/S0022-460x(74)80001-5

Mao, K. M., Wang, M. Y., Xu, Z. W., & Chen, T. N. (2004). Simulation and characterization of particle damping in transient vibrations. *Journal of Vibration and Acoustics-Transactions of the Asme*, *126*(2), 202-211. https://doi.org/10.1115/1.1687401

Marhadi, K. S., & Kinra, V. K. (2005). Particle impact damping: effect of mass ratio, material, and shape. *Journal of Sound and Vibration*, *283*, 433-448. https://doi.org/10.1016/j.jsv.2004.04.013

Marino, L., Cicirello, A., & Hills, D. A. (2019). Displacement transmissibility of a Coulomb friction oscillator subject to joined base-wall motion. *Nonlinear Dynamics*, *98*(4), 2595-2612. https://doi.org/10.1007/s11071-019-04983-x

Masri, S. F. (1969). Analytical and Experimental Studies of Multiple-Unit Impact Dampers. *The Journal of the Acoustical Society of America*, *45*(5), 1111-1117. https://doi.org/10.1121/1.1911581

Masri, S. F. (1970). General Motion of Impact Dampers. *Journal of the Acoustical Society of America*, *47*(1p2), 229-237. https://doi.org/10.1121/1.1911470

Masri, S. F. (1973). Steady-State Response of a Multidegree System with an Impact Damper. *Journal of Applied Mechanics-Transactions of the Asme*, *40*(1), 127-132. https://doi.org/Doi 10.1115/1.3422910

Masri, S. F., & Caughey, T. K. (1966). On the Stability of the Impact Damper. *Journal of Applied Mechanics*, *33*(3), 586-592. https://doi.org/10.1115/1.3625125

Mead, D. J., & Mead, D. J. (1999). *Passive Vibration Control*.

Meyer, N., & Seifried, R. (2021). Toward a design methodology for particle dampers by analyzing their energy dissipation. *Computational particle mechanics*, *8*(4), 681-699. https://doi.org/10.1007/s40571-020-00363-0

Michon, G., Almajid, A., & Aridon, G. (2013). Soft hollow particle damping identification in honeycomb structures. *JOURNAL OF SOUND AND VIBRATION*, *332*(3), 536-544. https://doi.org/10.1016/j.jsv.2012.09.024

Min, K. W., Seong, J. Y., & Kim, J. (2010). Simple design procedure of a friction damper for reducing seismic responses of a single-story structure. *Engineering Structures*, *32*(11), 3539-3547. https://doi.org/10.1016/j.engstruct.2010.07.022

Momani, L., Alsakarneh, A., Tabaza, T. A., Joureyeha, M., & Barrett, J. (2021). Impact dynamics modelling of viscoelastic materials. *Materials Today-Proceedings*, *38*, 2968-2974. https://doi.org/10.1016/j.matpr.2020.09.316

Moore, J. J., Palazzolo, A. B., Gadangi, R., Nale, T. A., Klusman, S. A., Brown, G. V., & Kascak, A. F. (1995). A Forced Response Analysis and Application of Impact Dampers to Rotordynamic Vibration Suppression in a Cryogenic Environment. *Journal of Vibration and Acoustics-Transactions of the Asme*, *117*(3), 300-310. https://doi.org/Doi 10.1115/1.2874452

Oyadiji, S. O. (1996). Damping of vibrations of hollow beams using viscoelastic spheres.*Proceedings of the Society of Photo-Optical Instrumentation Engineers (Spie)* [Passive damping and isolation - smart structures and materials 1996]. Smart Structures and Materials 1996 Conference - Passive Damping and Isolation, San Diego, California.

Paget, A. (1937). Vibration in steam turbine buckets and damping by impacts. *Engineering*, *143*, 305-307.

Panossian, H. (2002). Non-Obstructive Particle Damping: New Experiences and Capabilities. In *49th AIAA/ASME/ASCE/AHS/ASC Structures, Structural Dynamics, and Materials Conference, 16th AIAA/ASME/AHS Adaptive Structures Conference,10th AIAA Non-Deterministic Approaches Conference, 9th AIAA Gossamer Spacecraft Forum, 4th AIAA Multidisciplinary Design Optimization Specialists Conference*. https://doi.org/10.2514/6.2008-2102

Panossian, H. V. (1992). Structural Damping Enhancement Via Nonobstructive Particle Damping Technique [Article]. *Journal of Vibration and Acoustics-Transactions of the Asme*, *114*(1), 101-105. https://doi.org/Doi 10.1115/1.2930221

Papalou, A., & Masri, S. F. (1998). An experimental investigation of particle dampers under harmonic excitation [Article]. *JOURNAL OF VIBRATION AND CONTROL*, *4*(4), 361-379. https://doi.org/Doi 10.1177/107754639800400402

Papalou, A., Strepelias, E., Roubien, D., Bousias, S., & Triantafillou, T. (2015). Seismic protection of monuments using particle dampers in multi-drum columns. *SOIL DYNAMICS AND EARTHQUAKE ENGINEERING*, *77*, 360-368. https://doi.org/10.1016/j.soildyn.2015.06.004

Sack, A., Heckel, M., Kollmer, J. E., Zimber, F., & Poschel, T. (2013). Energy dissipation in driven granular matter in the absence of gravity. *Phys Rev Lett*, *111*(1), 018001. https://doi.org/10.1103/PhysRevLett.111.018001

Saeki, M. (2002). Impact damping with granular materials in a horizontally vibrating system. *JOURNAL OF SOUND AND VIBRATION*, *251*(1), 153-161. https://doi.org/10.1006/jsvi.2001.3985

Salvi, J., Rizzi, E., Rustighi, E., & Ferguson, N. S. (2018). Optimum Tuning of Passive Tuned Mass Dampers for the Mitigation of Pulse-Like Responses. *Journal of Vibration and Acoustics-Transactions of the Asme*, *140*(6), 061014. https://doi.org/Artn 061014

10.1115/1.4040475

Sami Faiz, M. (1965). *Analytical and experimental studies of impact dampers* [Dissertation (Ph.D.), California Institute of Technology]. https://resolver.caltech.edu/CaltechETD:etd-04172003-091816

Sánchez, M., Carlevaro, M., & Pugnaloni, L. A. (2014). Effect of particle shape and fragmentation on the response of particle dampers [Article]. *JOURNAL OF VIBRATION AND CONTROL*, *20*(12), 1846-1854. https://doi.org/10.1177/1077546313480544

Sánchez, M., & Manuel Carlevaro, C. (2013). Nonlinear dynamic analysis of an optimal particle damper. *JOURNAL OF SOUND AND VIBRATION*, *332*(8), 2070-2080. https://doi.org/10.1016/j.jsv.2012.09.042

Sánchez, M., & Pugnaloni, L. A. (2011). Effective mass overshoot in single degree of freedom mechanical systems with a particle damper [Article]. *JOURNAL OF SOUND AND VIBRATION*, *330*(24), 5812-5819. https://doi.org/10.1016/j.jsv.2011.07.016

Sánchez, M., Rosenthal, G., & Pugnaloni, L. A. (2012). Universal response of optimal granular damping devices. *JOURNAL OF SOUND AND VIBRATION*, *331*(20), 4389-4394. https://doi.org/10.1016/j.jsv.2012.05.001

Sinha, A., & Trikutam, K. T. (2018). Optimal Vibration Absorber With a Friction Damper. *Journal of Vibration and Acoustics-Transactions of the Asme*, *140*(2). https://doi.org/Artn 021015

10.1115/1.4038272

Snoun, C., & Trigui, M. (2018). Design parameters optimization of a particles impact damper. *International Journal of Interactive Design and Manufacturing - Ijidem*, *12*(4), 1283-1297. https://doi.org/10.1007/s12008-018-0463-y

Spencer, B. F., & Nagarajaiah, S. (2003). State of the art of structural control [Review]. *Journal of Structural Engineering*, *129*(7), 845-856. https://doi.org/Doi 10.1061/(Asce)0733-9445(2003)129:7(845)

Sun, R. Q., Wong, W. O., & Cheng, L. (2022). A tunable hybrid damper with Coulomb friction and electromagnetic shunt damping. *JOURNAL OF SOUND AND VIBRATION*, *524*, 116778. https://doi.org/ARTN 116778

10.1016/j.jsv.2022.116778

Titirla, M. D. (2023). A State-of-the-Art Review of Passive Energy Dissipation Systems in Steel Braces. *Buildings*, *13*(4), 851. https://doi.org/10.3390/buildings13040851

Wang, D. Q., & Wu, C. J. (2015). Vibration Response Prediction of Plate with Particle Dampers Using Cosimulation Method. *Shock and Vibration*, *2015*, 1-14. https://doi.org/10.1155/2015/270398

Wang, Q., & Dan, D. (2022). A simplified modeling method for multi-particle damper: Validation and application in energy dissipation analysis. *JOURNAL OF SOUND AND VIBRATION*, *517*. https://doi.org/10.1016/j.jsv.2021.116528

Wang, W., Hua, X., Wang, X., Chen, Z., & Song, G. (2017). Numerical modeling and experimental study on a novel pounding tuned mass damper. *JOURNAL OF VIBRATION AND CONTROL*, *24*(17), 4023-4036. https://doi.org/10.1177/1077546317718714

Wang, Y. R., Liu, B., Tian, A. M., & Tang, W. (2016). Experimental and numerical investigations on the performance of particle dampers attached to a primary structure undergoing free vibration in the horizontal and vertical directions. *JOURNAL OF SOUND AND VIBRATION*, *371*, 35-55. https://doi.org/10.1016/j.jsv.2016.01.056

Wei-ming, Y., Bao-shun, W., & Hao-xiang, H. (2019). Research of mechanical model of particle damper with friction effect and its experimental verification. *JOURNAL OF SOUND AND VIBRATION*, *460*, 114898. https://doi.org/10.1016/j.jsv.2019.114898

Wong, C. X., Daniel, M. C., & Rongong, J. A. (2009). Energy dissipation prediction of particle dampers. *Journal of Sound and Vibration*, *319*, 91-118. https://doi.org/10.1016/j.jsv.2008.06.027

Wong, W. O. (2016). Optimal design of a hysteretic vibration absorber using fixed-points theory. *J Acoust Soc Am*, *139*(6), 3110. https://doi.org/10.1121/1.4953069

Wong, W. O., Fan, R. P., & Cheng, F. (2018). Design optimization of a viscoelastic dynamic vibration absorber using a modified fixed-points theory. *J Acoust Soc Am*, *143*(2), 1064. https://doi.org/10.1121/1.5024506

Wouw, N. V. D., Bosch, H. L. A. V. D., Kraker, A. D., & Campen, D. H. V. (1998). Experimental and Numerical Analysis of Nonlinear Phenomena in a Stochastically Excited Beam System with Impact. *Chaos, Solitons & Fractals*, *9*(8), 1409-1428. https://doi.org/10.1016/s0960-0779(98)00073-3

Xia, X. J., Zheng, M. Y., Liu, P. F., Zhang, N., Ning, D. H., & Du, H. P. (2021). Friction observer-based hybrid controller for a seat suspension with semi-active electromagnetic damper. *Mechatronics*, *76*, 102568. https://doi.org/ARTN 102568

10.1016/j.mechatronics.2021.102568

Xu, Z. W., Wang, M. Y., & Chen, T. N. (2004). An experimental study of particle damping for beams and plates. *Journal of Vibration and Acoustics-Transactions of the Asme*, *126*(1), 141-148. https://doi.org/10.1115/1.1640354

Yang, M. Y., Lesieutre, G. A., Hambric, S. A., & Koopmann, G. H. (2005). Development of a design curve for particle impact dampers [Article]. *Noise Control Engineering Journal*, *53*(1), 5-13. https://doi.org/Doi 10.3397/1.2839240

Younes, M. (2017). Numerical Modelling and Experimental Investigation of a Single and a Compound Pendulum Impact Dynamic Vibration Absorbers. *International Conference on Aerospace Sciences and Aviation Technology*, *17*(AEROSPACE SCIENCES), 1-14. https://doi.org/10.21608/asat.2017.22479

Zhou, X. Q., Yu, D. Y., Shao, X. Y., Zhang, S. Q., & Wang, S. (2016). Research and applications of viscoelastic vibration damping materials: A review. *Composite Structures*, *136*, 460-480. https://doi.org/10.1016/j.compstruct.2015.10.014

Ziaee, M., & Hejazi, F. (2023). Development of Non-sticking Steady-State solution for structures with hybrid damping mechanism. *Structures*, *47*, 233-245. https://doi.org/10.1016/j.istruc.2022.10.118